INVESTIGATIONS OF PHASE TRANSITIONS IN SELECTED HIGH Tc SUPERCONDUCTORS AND FERROELECTRICS USING ULTRASONIC TECHNIQUE

THESIS SUBMITTED TO
THE COCHIN UNIVERSITY OF SCIENCE AND TECHNOLOGY
FOR THE AWARD OF THE DEGREE OF
DOCTOR OF PHILOSOPHY

R. SREEKUMAR

DEPARTMENT OF PHYSICS
COCHIN UNIVERSITY OF SCIENCE AND TECHNOLOGY
COCHIN - 682 022
INDIA

1993

CERTIFICATE

Certified that the work presented in this thesis is based on the bona fide work done by Mr. R.Sreekumar under my guidance in the Department of Physics, Cochin University of Science and Technology, and has not been included in any other thesis submited previously for the award of any degree.

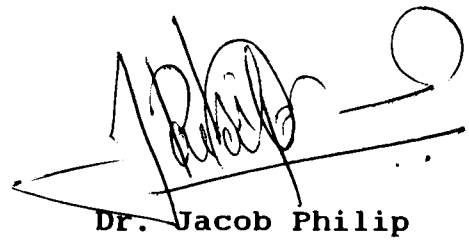

Cochin - 682 022
December 14, 1993

Dr. Jacob Philip
Supervising Guide

DECLARATION

Certified that the work presented in this thesis is based on the original work done by me under the guidance of Dr. Jacob Philip, Professor and Head, University Science Instrumentation Centre, Cochin University of Science and Technology, and has not been included in any other thesis submitted previously for the award of any degree.

Cochin - 682 022
December 14, 1993

R. Sreekumar

PREFACE

Ultrasonics is a widely employed tool in characterising the lattice dynamical properties of solids near phase transitions and critical points. The main advantage of ultrasonic measurements is that the static and dynamic properties can be investigated simultaneously. Low frequency acoustic velocities provide precise information about the equilibrium adiabatic properties of the system and the effects of temperature, pressure and external fields can be readily studied. Measurement of elastic response is extremely important to the study of phase transitions because a lot of information about the nature of the transition and the order parameter involved can be obtained. Measurement of elastic constants is a very sensitive method to locate transition points, to determine phase diagrams and in some cases to make statements about the order of the phase transition. The temperature dependence of elastic response functions help to deduce the type of coupling between strain and the order parameter involved. Ultrasonic attenuation measurements can give direct information about the dynamic behaviour of the system, and by studying its temperature as well as frequency dependence a great deal of information about the critical exponent and fluctuations near critical points can be obtained. Thus ultrasonics is an attractive method to be used in the field of phase transition studies in solids.

This thesis is the result of our attempts to probe the elastic properties of selected solid materials by measuring the ultrasonic velocity and attenuation in them. Temperature dependence of velocity and attenuation have been measured in all the samples investigated. The materials investigated include high Tc superconductors like Bi-Sr-Ca-Cu-O, Gd-Ba-Cu-O, a substrate material for 1-2-3 superconductor viz. Y-Ba-Zr-O and the ferroelectric crystal

TGS with different levels of phosphate doping (TGSP). The whole thesis is presented in seven chapters as outlined below.

Chapter 1 gives an overall introduction to the work presented in the thesis. Theory of elastic wave propagation in crystalline solids is described here. Wave propagation in anisotropic as well as isotropic media based on the tensor relation between stress and strain in solids are discussed. Determination of elastic constants using ultrasonic technique and the deduction of the elastic constants from the measured velocity data are briefly outlined. The description includes application of ultrasonics in determining the different elastic coefficients in crystals of different symmetry classes. The study of phase transitions using ultrasonic technique and the way in which the coupling between the order parameter and elastic strain gets reflected in these measurements are discussed. The elastic as well as thermal properties of high Tc superconductors and variation of the elastic properties of ferroelectric crystals like TGS around the phase transition points are also outlined in this chapter.

The second chapter deals with the experimental techniques involved and instrumentation employed for the investigations carried out in this thesis. Different experimental methods for studying ultrasonic properties are discussed briefly. The Pulse Echo Overlap (PEO) technique which is the method used for the velocity measurements and the pulse comparison technique used for attenuation measurements are explained in detail. The experimental setup needed for these investigations are discussed with the help of necessary block diagrams. Different experimental techniques like transducer bond corrections employed and temperature control techniques used are also discussed. It also describes the different mechanisms that contribute to errors in determining the ultrasonic parameters. One of the main parts of the experimental setup is the low temperature cryostat which can go down to liquid nitrogen temperature. Fabrication and

calibration of this cryostat is discussed in detail here. Also it deals with the setup for the high temperature ultrasonic measurements.

Chapter 3 discusses the result of the measurement of the ultrasonic velocity in Pb doped high temperature superconductor Bi-Sr-Ca-Cu-O. The temperature dependence of the ultrasonic velocity in the range 80-300K is discussed. The preparation and characterisation of these materials are also briefly discussed in this chapter. The anomalies observed near Tc in the ultrasonic measurements are discussed in the light of the existing models for high Tc superconductors.

Chapter 4 deals with the study of the ultrasonic properties of the 1-2-3 superconductor $GdBa_2Cu_3O_{7-\delta}$. Investigations have been carried out in samples having different Ag doping levels. The preparation of these samples is also discussed. Interesting results are obtained on the structural transition which the sample undergoes due to metastability of the system and its dependence on Ag doping. The electrical measurements and oxygen content studies also support these findings. Variation of the ultrasonic velocity and attenuation in the vicinity of Tc are also discussed in detail.

Details of the study of ultrasonic as well as thermal properties of a new substrate material YBa_2ZrO_6 (YBZO) for the preparation of 1-2-3 superconducting thin films and the results obtained form the fifth chapter of the thesis. From a technological point of view, high Tc superconducting materials prepared in the thin film form are very important and it is necessary to have a suitable material as the substrate to prepare the thin films. Since YBCO reacts with almost all materials, conventional substrates are unsuitable for preparing thin films. Moreover, it should have stable elastic and thermal properties while the temperature is varied. In this chapter the results of the measurements of the temperature dependence of elastic constants of YBZO is

discussed. In addition to the elastic properties, the thermal properties like specific heat and thermal conductivity of this material have also been measured and discussed. Calculation of thermal conductivity by measuring the thermal diffusivity by photoacoustic technique and specific heat from DSC data on the material forms a section of this chapter.

Chapter 6 describes the ultrasonic studies carried out on Triglycine Sulphate (TGS) single crystals which is an important ferroelectric material. TGS is also important due to its pyroelectric nature which enables it to be used as IR detectors. Replacing some of the sulphate groups in TGS by limited phosphate groups enhances pyroelectric coefficient and hence is very advantageous from technological point of view. In this chapter a systematic study of the elastic properties of phosphate doped TGS crystal (TGSP) is given. The sample preparation techniques used to grow large single crystals of TGSP are outlined. Variation of ultrasonic velocity as well as attenuation as a function of temperature around the ferroelectric-paraelectric transition in TGSP single crystals are discussed in detail in this chapter. The results are discussed and interpreted in detail.

Chapter 7 is the concluding chapter in which the overall conclusions drawn from the work presented in the previous chapters are discussed. It also outlines future scope of this type of experimentation.

The following papers have been published/ communicated for publication in different journals during the course of the work.

1. A simple microprocessor based ampoule lowering unit for Bridgeman technique
   R. Sreekumar, K. Remashan and Jacob Philip
   J. Instrum. Soc. India. **19**, 112 (1989).

2. Investigation of phase transitions using photoacoustic technique
   K.N.Madhusoodanan, R.Sreekumar and Jacob Philip
   J. Acoust. Soc. India. **XVII(3&4),** 347 (1989).

3. Elastic and thermal properties of Yttrium Barium Zirconate
   R.Sreekumar, J.Isaac, J.Philip, K.V.Paulose, M.T.Sebastian and A.D.Damodaran
   Physica Status Solidi (a) **133,** 341 (1992).

4. Ultrasonic velocity and attenuation in Ag doped $GdBa_2Cu_3O_{7-\delta}$ superconductors
   R.Sreekumar, J.Philip, D.Behera, H.P.Mohapatra, S.Misra and N.C.Mishra
   Proceedings of the Third National Conference on Phonon Physics (Wiley Eastern Ltd.). (To appear shortly)

5. Ultrasonic studies on TGS single crystals with different levels of phosphate doping
   R.Sreekumar and J.Philip
   Ferroelectrics. (Communicated)

Some of the results have been presented in various conferences/ symposia listed below.

1. A microprocessor controlled crystal pulling unit
   R.Sreekumar, K.Remashan and Jacob Philip
   Symposium on Current Trends in Pure and Applied Physics, October 24-25, 1988, Cochin University of Science & Technology, Cochin-22.

2. A simple stepper motor controller employing microprocessor 8085 for autoscanning monochromators
   R.Sreekumar and Jacob Philip
   National Symposium on Instrumentation (NSI-14), October 3-6, 1989, Indian Institute of Science, Bangalore-12.

3. Investigation of phase transitions using photoacoustic technique
   K.N.Madhusoodanan, R.Sreekumar and Jacob Philip
   National Symposium on Acoustics, November 7-10, 1989, Birla Industrial and technological Museum, Calcutta.

4. A bath type cryostat designed for ultrasonic measurements in solids
   R.Sreekumar and Jacob Philip
   National Symposium on Instrumentation (NSI-16), November 26-29, 1991, Cochin University of Science & Technology, Cochin-22.

5. Temperature dependence of the thermal and elastic properties of YBa_2ZrO_6
   R.Sreekumar and J.Philip
   Solid State Physics Symposium, December 21-24, 1991, Banaras Hindu University, Varanasi.

6. Ultrasonic velocity and attenuation in Ag doped $GdBa_2Cu_3O_{7-\delta}$ superconductors
   R.Sreekumar, J.Philip, D.Behera, H.P.Mohapatra, S.Misra and N.C.Mishra
   Third National Conference on Phonon Physics, January 20-23, 1993, Cochin University of Science & Technology, Cochin-22.

7. Ultrasonic study of the effect of Ag doping on the metastability of Gd-Ba-Cu-O superconductors (accepted)
   R.Sreekumar, J.Philip and N.C.Mishra
   10^{th} International Conference on Internal Friction and Ultrasonic Attenuation in Solids-ICIFUAS 10, September 6-9, 1993, University of Rome "La Sapienza", Roma, Italy.

8. Ultrasonic investigation of phase transition in phosphate doped TGS crystals (accepted)
   R.Sreekumar and J.Philip
   Solid State Physics Symposium, December 27-31, 1993, Bhabha Atomic Research Centre, Bombay.

9. Investigations of phase transitions in selected high Tc superconductors and ferroelectric using ultrasonic technique (thesis presentation accepted)
   R. Sreekumar
   Soild State Physics Symposium, December 27-31, 1993, Bhabha Atomic Research Centre, Bombay.

CONTENTS

Chapter 1
INTRODUCTION

1. Introductory remarks

Acoustics is the study of fine varying deformations or vibrations in material media. Determination of acoustic propagation properties of solid materials is very valuable from scientific as well as technological point of view as it enables one to probe the bulk elastic properties. Occurance of phase transitions is one of the most interesting properties exhibited by several solids. The ultrasonic velocity and attenuation measurements give very valuable information about the static and dynamic properties of solid matter. Measurement of elastic response as a function of temperature gives very important information about phase transitions occuring in a material and helps to locate transition points. Moreover, it helps to deduce the nature of coupling between the strain and the order parameter involved in such transition.

In this introductory chapter the different aspects of ultrasonic studies in solids are discussed. This chapter has two parts. In the first part elastic wave propagation in anisotropic as well as isotropic media are discussed. The elastic properties and the elastic constant matrices for different materials are discussed. Then the method of determining the elastic constant by measuring ultrasonic velocity along different directions in a material is discussed.

In the second part the necessary theory of ultrasonic studies of phase transition is discussed. First it gives a general introduction to the phenomena of phase transitions in solids. Then ultrasonic studies of phase transition are discussed in the frame work of Landau theory and later the fluctuation effects are discussed. Finally

ferroelectric and antiferroelectric transition are briefly discussed.

1.2. Elastic wave propagation in anisotropic solids.

1.2.1 Stress and strain

The elastic coefficients of a solid may be obtained from the wave velocities and the density, and the elastic coefficients are in turn connected to the binding forces between atoms [1]. The elastic constants are defined in terms of the response of a medium to an applied stress. We can connect the stress which is applied to a crystal, and the strain produced under the stress.

We can define the components of stress for an anisotropic medium [2], which is the most general case. Consider Fig.1.1. We can define the stress parallel and normal to an orthogonal axial reference system. Considering the generalised forces on the face of a unit cube within the stressed body, these can be resolved in to stress parallel and normal to an orthogonal axial reference frame. The stress components can be written in tensor notation as σ_{ij} , which is a second rank tensor. Here i is the direction of the normal to the plane on which stress acts and j is the direction of stress component. Since this is a second rank tensor there will be nine components. Components in which $i=j$ are the normal components of stress and $i\neq j$ give rise to the shear components of stress.

The deformation occuring in the material body due to the application of stress is called the strain. The strain tensor is defined in terms of the coordinates of a point $\mathbf{x}(x_i)$ and $\mathbf{x}'(x_i)$ before and after deformation, with displacement $\mathbf{u}(u_i)$ [1] *i.e.*,

$$\mathbf{u} = \mathbf{x}' - \mathbf{x} \qquad (1)$$

The coordinates x_i' of the displaced points are functions of the coordinates x_i of the initial position *i.e.*,

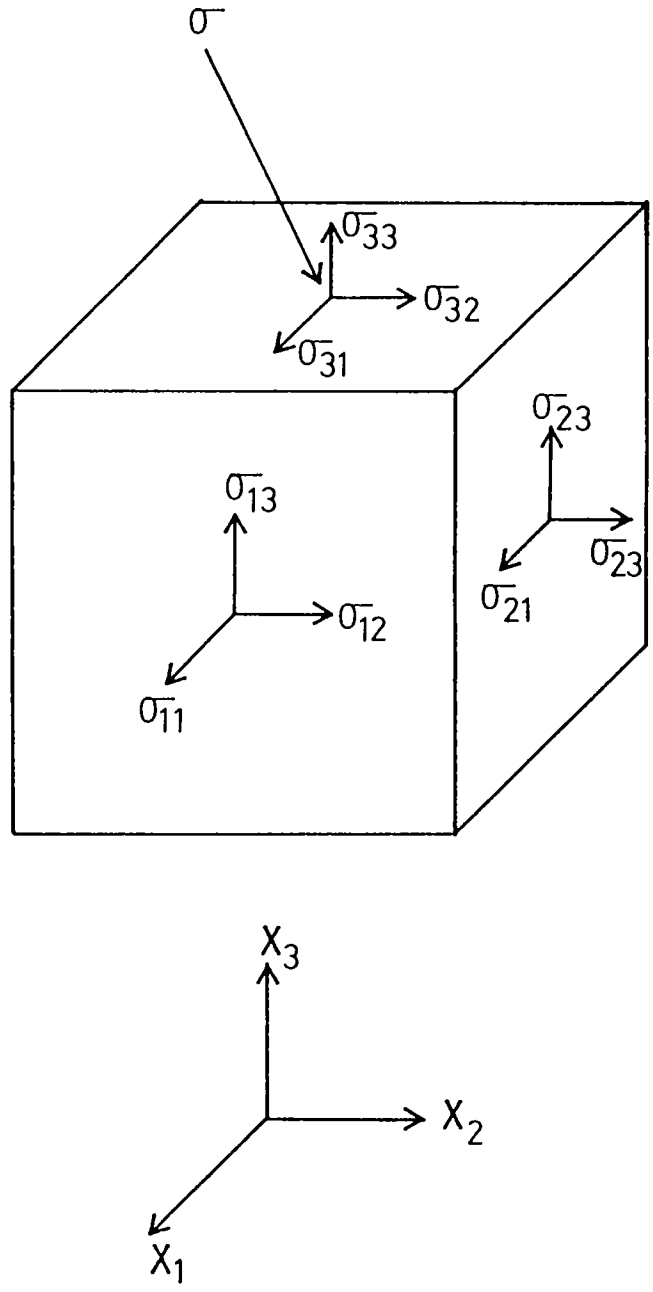

Fig.1.1 Stress components arising from generalised stress σ (shown on one face only); the right-hand axial system is also shown.

$\mathbf{u} = \mathbf{u}(x_i)$.

The displacement $\mathbf{u}(u_1, u_2, u_3)$ may be considered to be made up of three parts;

$$\mathbf{u} = \mathbf{u}_o + \mathbf{u}' + \mathbf{u}'' \tag{2}$$

where $\mathbf{u}_o$ is the rigid body translation, $\mathbf{u}'$ the rigid body rotation and $\mathbf{u}''$ the total deformation. In this the term contributing to the strain is the local deformation part since this is the only term denoting a relative displacement of the particles within the medium. The other two terms describe the motiom of the body as a whole. Then the strain can be written as

$$\varepsilon_{ij} = \frac{\partial u_i}{\partial x_j} \qquad i,j \rightarrow 1,2,3 \tag{3}$$

where u_i is the displacement of a point within the body and x_j is a coordinate of the reference frame. Thus there are nine strain components in three dimensional case, depending upon i and j. Among these, three are compressional strains ($i = j$) and six are shear strains ($i \neq j$). So strain also has nine components. Stress and strain are second rank tensors and may be represented by following arrays.

The stress tensor is

$$\begin{bmatrix} \sigma_{11} & \sigma_{12} & \sigma_{13} \\ \sigma_{21} & \sigma_{22} & \sigma_{23} \\ \sigma_{31} & \sigma_{32} & \sigma_{33} \end{bmatrix} \tag{4}$$

In the absence of any body torque, the stress tensor is symmetric *i.e.*,

$$\sigma_{ij} = \sigma_{ji} \tag{5}$$

and by this the array gets simplified to six independent stress components.

The strain tensor is

$$\begin{bmatrix} e_{11} & \frac{1}{2}(e_{12}+e_{21}) & \frac{1}{2}(e_{13}+e_{31}) \\ \frac{1}{2}(e_{12}+e_{21}) & e_{22} & \frac{1}{2}(e_{23}+e_{32}) \\ \frac{1}{2}(e_{13}+e_{31}) & \frac{1}{2}(e_{23}+e_{32}) & e_{33} \end{bmatrix} \quad (6)$$

$$= \begin{bmatrix} \varepsilon_{11} & \varepsilon_{12} & \varepsilon_{13} \\ \varepsilon_{21} & \varepsilon_{22} & \varepsilon_{23} \\ \varepsilon_{31} & \varepsilon_{32} & \varepsilon_{33} \end{bmatrix} \quad (7)$$

where $\varepsilon_{ij} = 1/2(e_{ij}+e_{ji})$ which represents the symmetric part that corresponds to the deformation. This matrix is also symmetric *i.e.*, $\varepsilon_{ij} = \varepsilon_{ji}$

Thus we can conclude that there can be six independent stress components and six strain components.

1.2.2 Elastic constants

According to Hooke's law, for small deformations, strain is linearly proportional to the applied stress [3]. When the deformation is increased the relation between strain and stress becomes nonlinear, but the body will reach its original state on removal of stress. There are linear and nonlinear elastic deformations. When the strain is increased beyond a certain limit the deformation will not be elastic. This limit is called elastic limit and beyond this limit the medium deforms permanently; ie, it cannot regain its original state after the removal of stress. This is called plastic deformation. All these are depicted in Fig.2.2. So according to Hooke's law, for small strains stress is linearly

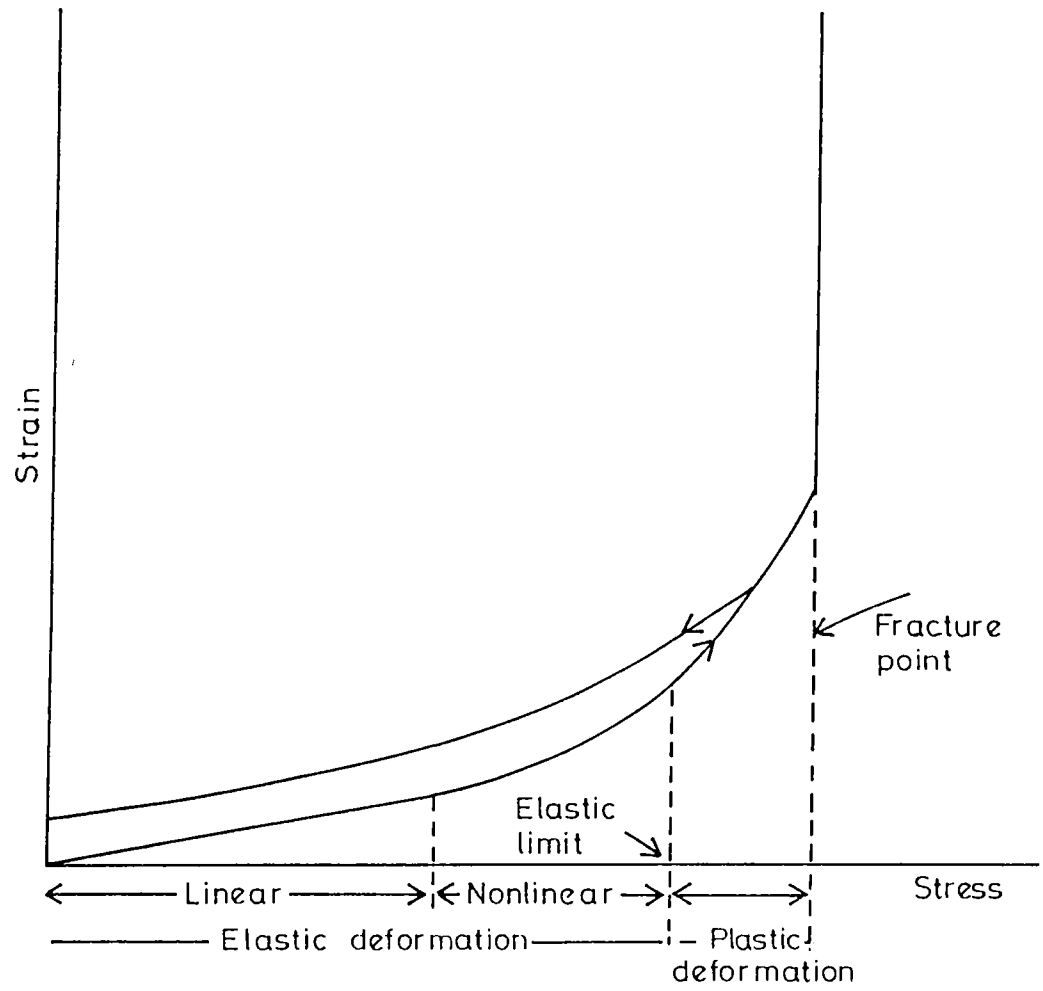

Fig.1.2 Typical stress-strain relation for a solid material

proportional to strain. *i.e.*,

$$\sigma_{ij} \propto \varepsilon_{kl}$$

The stress and strain are tensors of rank two. So the proportionality constant connecting them is a tensor of fourth rank. We can write this tensor as elastic stiffness c_{ijkl}. Its inverse is elastic compliance s_{ijkl} which relates the strain to stress. Hence

$$\sigma_{ij} = \sum c_{ijkl}\, \varepsilon_{kl} \tag{8}$$

$$\varepsilon_{ij} = \sum s_{ijkl}\, \sigma_{kl} \tag{9}$$

Here $i,j,k,l \rightarrow 1,2,3$. Elastic stiffnesses or compliances are a measure of the elastic behaviour of solids.

We can write,

$$\begin{aligned} \sigma_{11} = {} & c_{1111}\,\varepsilon_{11} + c_{1112}\,\varepsilon_{12} + c_{1113}\,\varepsilon_{13} \\ & + c_{1121}\,\varepsilon_{21} + c_{1122}\,\varepsilon_{22} + c_{1123}\,\varepsilon_{23} \\ & + c_{1131}\,\varepsilon_{31} + c_{1132}\,\varepsilon_{32} + c_{1133}\,\varepsilon_{33} \end{aligned} \tag{10}$$

We can see from the above equation that since there are nine similar equations there are 81 elastic constants altogether. These elastic constants are also symmetric [1]; *i.e.*, $c_{ijkl} = c_{jikl} = c_{ijlk} = c_{klij}$

In order to avoid the difficulty in using this full subscript notation we can use the Voigt notation which is an abbreviated form following the rule ij → m = i if i = j and ij → n = 9-(i+j) if i ≠ j which gives the matrix form as given below [1,2].

Tensor	11	22	33	23,32	31,13	12,21
Matrix	1	2	3	4	5	6

Using this compressed notation the stress and strain components can be written in tensor form as

$$\sigma_i = \sum_{j=1}^{6} c_{ij}\, \varepsilon_j \qquad i \to 1,2 \ldots 6 \qquad (11)$$

$$\varepsilon_i = \sum_{j=1}^{6} s_{ij}\, \sigma_j \qquad i \to 1,2 \ldots 6 \qquad (12)$$

and in matrix form we can write this as

$$\begin{bmatrix} \sigma_1 \\ \sigma_2 \\ \sigma_3 \\ \sigma_4 \\ \sigma_5 \\ \sigma_6 \end{bmatrix} = \begin{bmatrix} c_{11} & c_{12} & c_{13} & c_{14} & c_{15} & c_{16} \\ c_{12} & c_{22} & c_{23} & c_{24} & c_{25} & c_{26} \\ c_{13} & c_{23} & c_{33} & c_{34} & c_{35} & c_{36} \\ c_{14} & c_{24} & c_{34} & c_{44} & c_{45} & c_{46} \\ c_{15} & c_{25} & c_{35} & c_{45} & c_{55} & c_{56} \\ c_{16} & c_{26} & c_{36} & c_{46} & c_{56} & c_{66} \end{bmatrix} \begin{bmatrix} \varepsilon_1 \\ \varepsilon_2 \\ \varepsilon_3 \\ \varepsilon_4 \\ \varepsilon_5 \\ \varepsilon_6 \end{bmatrix} \qquad (13)$$

Hence considering all the symmetries the total number of elastic constants reduce to 21. This is the case for the most anisotropic system; *i.e.*, the least symmetric crystal which is triclinic. Again there will be reduction in the number of independent elastic constants depending upon the symmetry class of the particular system under consideration. As the symmetry is increased the total number of elastic constants get reduced.

Table 1.1 gives the number of elastic constants for different symmetry systems.

Table 1.1

System	No. of elastic constants
1. Triclinic	21
2. Monoclinic	13
3. Orthorhombic	9
4. Trigonal	7 or 6*
5. Tetragonal	5 or 6*
6. Hexagonal	5
7. Cubic	3

* depending on the point group of the crystal.

For example, in the case of a cubic system the symmetry finally leads to

$$\left.\begin{aligned} c_{11} &= c_{22} = c_{33} \\ c_{12} &= c_{13} = c_{23} \\ c_{44} &= c_{55} = c_{66} \end{aligned}\right\} \tag{14}$$

All other coefficients are zero. Then the elastic constant matrix for a cubic crystal reduces to

$$\begin{bmatrix} c_{11} & c_{12} & c_{12} & 0 & 0 & 0 \\ c_{12} & c_{11} & c_{12} & 0 & 0 & 0 \\ c_{12} & c_{12} & c_{11} & 0 & 0 & 0 \\ 0 & 0 & 0 & c_{44} & 0 & 0 \\ 0 & 0 & 0 & 0 & c_{44} & 0 \\ 0 & 0 & 0 & 0 & 0 & c_{44} \end{bmatrix} \tag{15}$$

1.2.3 Plane wave propagation in anisotropic media

In ultrasonic measurements the parameter that we measure is the velocity of the ultrasonic wave propagating through the sample and we can deduce the elastic constants from this measured parameter. For this we need a method to find the elastic constants by measuring the ultrasonic velocities in different directions.

Consider a plane stress wave propagating through a semi-infinite medium. Since the medium is semi-infinite there are no perturbations due to boundary effects. We can consider the equation of motion for such a wave and can relate the velocity to the elastic constants.

Consider the orthogonal coordinate system X_1, X_2, X_3. From eqn (13) we have [2]

$$\sigma_1 = C_{11}\varepsilon_1 + C_{12}\varepsilon_2 + C_{13}\varepsilon_3 + C_{14}\varepsilon_4 + C_{15}\varepsilon_5 + C_{16}\varepsilon_6 \quad (16)$$

and so on for σ_1, σ_2 etc.

Here we know that $\varepsilon_{ij} = \dfrac{\partial u_i}{\partial x_j}$ ie

$$\sigma_1 = C_{11}\frac{\partial u_1}{\partial x_1} + C_{12}\frac{\partial u_2}{\partial x_2} + C_{13}\frac{\partial u_3}{\partial x_3} + C_{14}\left(\frac{\partial u_2}{\partial x_3} + \frac{\partial u_3}{\partial x_2}\right)$$

$$+ C_{15}\left(\frac{\partial u_3}{\partial x_1} + \frac{\partial u_1}{\partial x_3}\right) + C_{16}\left(\frac{\partial u_2}{\partial x_1} + \frac{\partial u_1}{\partial x_2}\right) \quad (17)$$

and so on for σ_1, σ_2 etc.

where u_1, u_2 and u_3 are the components of displacements referred to the X_1, X_2, X_3 directions. Since the material is in dynamic equilibrium we can apply Newton's second law of motion and get the following expressions.

$$\frac{\partial \sigma_{11}}{\partial x_1} + \frac{\partial \sigma_{12}}{\partial x_2} + \frac{\partial \sigma_{13}}{\partial x_3} = \rho \frac{\partial^2 u_1}{\partial t^2}$$

$$\frac{\partial \sigma_{21}}{\partial x_1} + \frac{\partial \sigma_{22}}{\partial x_2} + \frac{\partial \sigma_{23}}{\partial x_3} = \rho \frac{\partial^2 u_2}{\partial t^2} \qquad (18)$$

$$\frac{\partial \sigma_{31}}{\partial x_1} + \frac{\partial \sigma_{32}}{\partial x_2} + \frac{\partial \sigma_{33}}{\partial x_3} = \rho \frac{\partial^2 u_3}{\partial t^2}$$

Since $\sigma_{ij} = \sigma_{ji}$ the LHS of eqns. (18) is symmetric. So the eqns.(18) contain the equations of motion for displacements u_1, u_2, u_3 of particles in the mutually orthogonal directions X_1, X_2, X_3 resulting from the corresponding stress components.

We can consider plane wave solution to eqns.(18) as

$$\begin{aligned} u_1 &= u_{10} \text{ Sin } (lX_1 + mX_2 + nX_3 - vt) \\ u_2 &= u_{20} \text{ Sin } (lX_1 + mX_2 + nX_3 - vt) \qquad (19) \\ u_3 &= u_{30} \text{ Sin } (lX_1 + mX_2 + nX_3 - vt) \end{aligned}$$

where l, m, n are the direction cosines of the wave normal to X_1, X_2, X_3 directions as shown in Fig.1.3 and v is the phase velocity.

Taking the nontrivial solution; *i.e.*, solution at which amplitudes are nonzero we get the following equation for waves of any amplitude as [4]

$$\begin{vmatrix} (\lambda_{11} - \rho v^2) & \lambda_{11} & \lambda_{11} \\ \lambda_{12} & (\lambda_{22} - \rho v^2) & \lambda_{23} \\ \lambda_{13} & \lambda_{23} & (\lambda_{33} - \rho v^2) \end{vmatrix} = 0 \qquad (20)$$

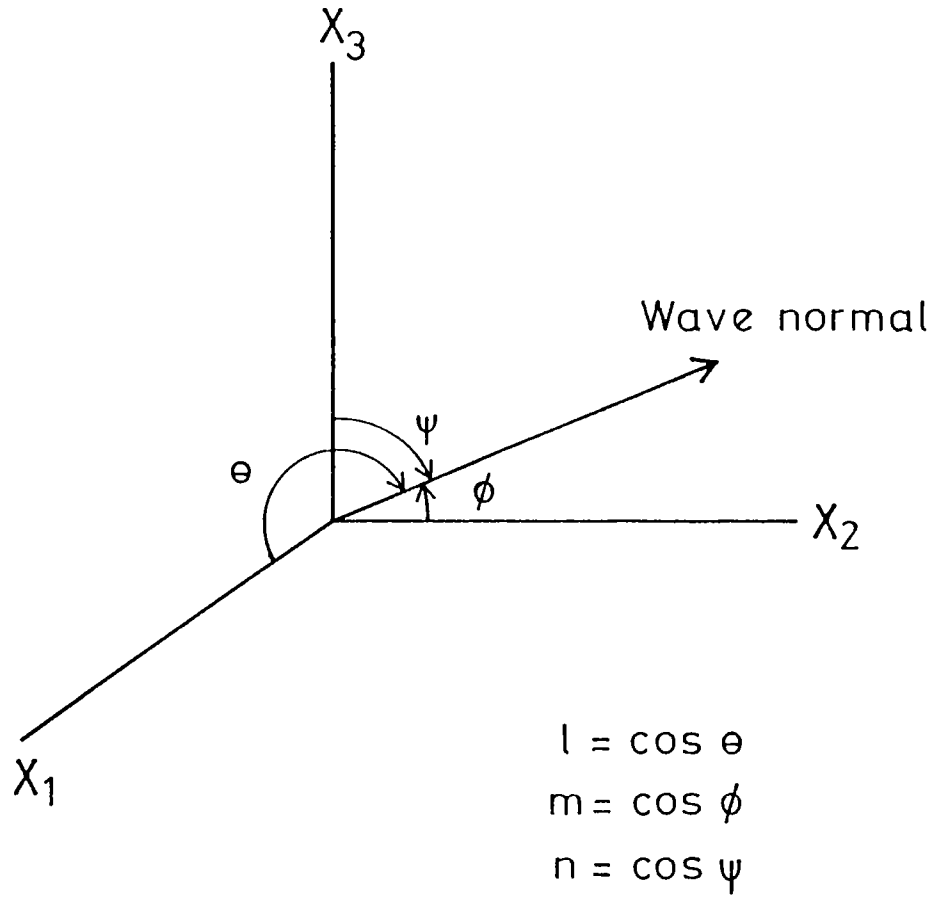

Fig.1.3 Direction numbers and direction cosines, referred to reference axes X_1, X_2, X_3.

where

$$\lambda_{11} = l^2c_{11} + m^2c_{66} + n^2c_{55} + 2mnc_{56} + 2nlc_{15} + 2lmc_{16}$$

$$\lambda_{12} = l^2c_{16} + m^2c_{26} + n^2c_{45} + mn(c_{46}+c_{25}) + nl(c_{14}+c_{56}) + lm(c_{12}+c_{66})$$

$$\lambda_{13} = l^2c_{15} + m^2c_{46} + n^2c_{35} + mn(c_{45}+c_{36}) + nl(c_{13}+c_{55}) + lm(c_{14}+c_{56})$$

$$\lambda_{22} = l^2c_{66} + m^2c_{22} + n^2c_{44} + 2mnc_{24} + 2nlc_{46} + 2lmc_{26}$$

$$\lambda_{23} = l^2c_{56} + m^2c_{24} + n^2c_{34} + mn(c_{44}+c_{23}) + nl(c_{36}+c_{45}) + lm(c_{25}+c_{46})$$

$$\lambda_{33} = l^2c_{55} + m^2c_{44} + n^2c_{33} + 2mnc_{34} + 2nlc_{35} + 2lmc_{45} \qquad (21)$$

Eqn.(20) is known as the Christoffel's equation. Putting appropriate values for l, m, n depending on the direction of propagation and considering the symmetry conditions we can find the elastic constant of a crystal from the measured phase velocities and density. The above equation has three solutions. One of these corresponds to the longitudinal wave and the other two to the two mutually perpendicular transverse waves.

Consider a wave propagating along the X_1 direction of a cubic crystal which is having the highest symmetry; ie wave propagating along [100] direction.

For a cubic crystal, we have

$$c_{11} = c_{22} = c_{33}$$
$$c_{12} = c_{23} = c_{13} \qquad (22)$$
$$c_{44} = c_{55} = c_{66}$$

All other constants are zero.

For [100] direction l = 1, m = 0, n = 0. Putting these values in Christoffel's equation we get the following three solutions in which one is for longitudinal and two for

transverse waves *i.e.*,

$$\rho V_{long}^2 = C_{11}$$
$$\rho V_{trans}^2 = C_{44} \qquad (23)$$
$$\rho V_{trans}^2 = C_{44}$$

This will be the case for direction [010] and [001] also in the case of cubic symmetry. For the [110] direction, we have

$$l = m = 1/\sqrt{2}$$
$$n = 0$$

Then we get

$$\rho V_{trans}^2 = C_{44} \quad \text{polarisation in [001]}$$
$$\rho V_{trans}^2 = \tfrac{1}{2}(C_{11} - C_{12}) \quad \text{polarisation in [110]} \qquad (24)$$
$$\rho V_{long}^2 = \tfrac{1}{2}(C_{11} + C_{12} + 2C_{44})$$

For the [111] direction, we have $l = m = n = 1/\sqrt{2}$

Then we get

$$\rho V_{long}^2 = \tfrac{1}{3}(C_{11} + 2C_{12} + 4C_{44})$$
$$\rho V_{trans}^2 = \tfrac{1}{3}(C_{11} - C_{12} + C_{44}) \qquad (25)$$
$$\rho V_{trans}^2 = \tfrac{1}{3}(C_{11} - C_{12} + C_{44})$$

In the case of a crystal with lower symmetry these calculations are more tedious. But it can be deduced using the above procedure.

1.3. Wave propagation in isotropic solids

1.3.1 Elastic constants of isotropic solids

In the case of isotropic solids, there is a further reduction in the number of independent elastic constants. In this case since there is no direction dependence for the velocity and the number of independent elastic constants

reduce to two. They are c_{11} and c_{12}. Then the elastic constant matrix simplifies to [2]

$$\begin{bmatrix} c_{11} & c_{12} & c_{12} & 0 & 0 & 0 \\ c_{12} & c_{11} & c_{12} & 0 & 0 & 0 \\ c_{12} & c_{12} & c_{11} & 0 & 0 & 0 \\ 0 & 0 & 0 & \frac{1}{2}(c_{11}-c_{12}) & 0 & 0 \\ 0 & 0 & 0 & 0 & \frac{1}{2}(c_{11}-c_{12}) & 0 \\ 0 & 0 & 0 & 0 & 0 & \frac{1}{2}(c_{11}-c_{12}) \end{bmatrix} \tag{26}$$

Here we can define two constants known as Lamé constants λ and G as

$$\lambda = c_{12}$$
$$G = \frac{1}{2}(c_{11} - c_{12}) \tag{27}$$

G is the shear modulus and $\lambda + 2G$ is the longitudinal modulus. Then the matrix in terms of λ and G becomes

$$\begin{bmatrix} \lambda+2G & \lambda & \lambda & 0 & 0 & 0 \\ & \lambda+2G & \lambda & 0 & 0 & 0 \\ & & \lambda+2G & 0 & 0 & 0 \\ & & & G & 0 & 0 \\ & & & & G & 0 \\ & & & & & G \end{bmatrix} \tag{28}$$

All the important constants related to the elasticity of isotropic solids can be expressed in terms of λ and G as follows.

$$\begin{aligned}
\text{Longitudinal Modulus} &= \lambda + 2G \\
\text{Young's Modulus} &= G\,\frac{3\lambda+2G}{\lambda + G} \\
\text{Bulk modulus} &= \lambda + 2G/3 \\
\text{Poisson's Ratio} &= \frac{\lambda}{2(\lambda+G)}
\end{aligned} \tag{29}$$

Considering plane elastic wave propagation in isotropic media and considering the symmetry conditions we get the Christoffel's equation for isotropic solid as

$$\begin{vmatrix} c_{11} - \rho V^2 & 0 & 0 \\ 0 & \frac{1}{2}(c_{11}-c_{12}) - \rho V^2 & 0 \\ 0 & 0 & \frac{1}{2}(c_{11}-c_{12}) - \rho V^2 \end{vmatrix} = 0 \tag{30}$$

We get three solutions in which one is for longitudinal and two are for transverse modes. But in the case of an isotropic sample direction of polarisation does not have any significance and so we get the elastic constants as

$$\begin{aligned}
\rho V_{long}^2 &= c_{11} \\
\rho V_{trans}^2 &= \frac{1}{2}(c_{11}-c_{12})
\end{aligned} \tag{31}$$

From this we can calculate c_{11} and c_{12}.

1.4. Study of phase transitions using ultrasonic technique

1.4.1 Introductory remarks

Various types of phase transitions occurring in solids are the one of the most interesting phenomena in condensed matter physics. This cross disciplinary subject is not only of academic interest but also of technological relevance. A great deal of work has been done in theoretical and experimental studies of phase transitions in solids and the subject continues to grow with the discovery of newer

kinds of phase transition in newer systems. Basic features of phase transitions have been discussed by several authors [5-7]. The basic ideas regarding phase transitions are outlined in the following section and the use of Ultrasonics to study structural phase transitions in solids is discussed in subsequent sections.

1.4.2 Phase transitions in solids

The homogeneous parts of a given assembly of atoms or molecules are called phases and they are characterised by the thermodynamic properties like volume, pressure, temperature and energy [5]. An isolated phase is stable only when its energy - or more generally its free energy - is a minimum for the specified thermodynamic conditions. If the phase is present in a local minimum of free energy instead of a unique minimum and is separated from still lower minima (under the same thermodynamic conditions) by energy barriers, the system is said to be in a metastable state. If the barriers do not exist, the state of the system becomes unstable and the system moves in to a stable or equilibrium state characterised by the lowest possible free energy. As the thermodynamic parameters like temperature, pressure or any other variables like an electric or a magnetic field acting on the system is varied, the free energy of the system changes smoothly and continuously. Whenever such variations of free energy are associated with changes in structural details of the phase - atomic or electronic configurations - a phase transition is said to occur. Hence a solid undergoes a phase transition [8] when a particular phase of the solid becomes unstable under a given set of thermodynamic conditions and changes occur discontinuously in structure and/or composition. The variation in free energy at the transition is associated with structural or compositional changes.

During a phase transition, whereas the free energy

of the system remains continuous, thermodynamic quantities like entropy, volume, specific heat capacity etc. undergo discontinuous change. Ehrenfest [9] classified phase transitions depending on the relation between the thermodynamic quantity undergoing discontinuity and the Gibb's free energy function. According to this, a transition is said to be of the same order as the derivative of the Gibb's free energy which shows a discontinuous change at the transition. The first order derivatives of Gibb's free energy are volume, entropy etc. and the transition in which these quantities show a discontinuity at transition point is called first order or discontinous transition. If specific heat, compressibility, thermal expansivity etc. are the quantities undergoing discontinuity, which are second order derivatives of Gibb's free energy function, then the transition is said to be of second order and so on. In general, according to Ehrenfest's definition an nth order transition is a transition where the $(n-1)^{th}$ derivative of Gibb's free energy is continuous while the nth derivative shows discontinuity at the transition temperature. However, several of the known transitions do not strictly belong to any of the above classes. There is superposition of second order behaviour in many first order transitions and vice versa. It is possible that many transitions are really of mixed order.

Ubbelohde [12] has preferred to classify transitions simply as thermodynamically continuous (or gradual) and thermodynamically discontinuous transitions. A systematic classification of phase transitions is desirable for clarity and a better appreciation of the phenomena. Existence of a measurable latent heat or a discontinuous volume change or, more precisely, formation of an interface with positive surface energy at the transition may be taken as characteristic of a first order transition. Phase transitions of the first order generally exhibit hysteresis which may also

be taken as a characteristic of these transitions. In first order transitions, the high temperature phases having high internal energy and low density will also have higher entropy. In fact the high temperature structures are generally of higher symmetry and higher disorder than the low temperature structures. In second order transition there is always some randomization in the structure. Randomization can be in position or orientation [5].

Phase transitions are always associated with configurational changes within the system. Magnetic phase transitions are driven by the alignment of unpaired spins in a specific direction and one does not observe any changes in the atomic configuration. On the other hand, several other types of phase transitions like the para-ferroelectric transitions are generally associated with atomic rearrangements or structural changes. These type of transitions, in which the material changes its crysatllographic structure are called structural phase transitions. The structural phase transitions can occur in two distinct ways. Firstly, there are transitions where the atoms of a solid reconstruct a new lattice as in the case of an amorphous solid changing to the crystalline state. Secondly, there are transitions where a regular lattice is distorted slightly without in any way disrupting the linkage of the network. This can occur as a result of small displacements in the lattice position of single atoms or molecular groups, or the ordering of atoms or molecules among various equivalent positions. Most of the ferroelectric transitions belong to the second group. The displacive type transitions are often driven by the freezing out of a vibrational mode called soft mode. In the case of a ferroelectric transition the soft mode is an optical phonon belonging to the centre of the Brillouin zone while in the case of an antiferroelectric transition it is a zone boundary phonon. At an elastic phase transition - also called

ferroelastic - the unit cell undergoes an elastic deformation. In the majority of cases this elastic deformation is a shear deformation and then the soft mode is the corresponding transverse acoustic phonon [13].

Since all phase transitions involve configurational changes, one can always identify a physical quantity that is characteristic of the new ordered phase. Hence the phase transition results in the development of long range order in some physical property [14]. This property may be utilised as a quantitative measure of the development of the new phase and is called the order parameter. Such a concept of an order parameter was introduced by Landau [15] in his thermodynamic theory of phase transitions. The order parameter has a nonzero value in the ordered phase below the transition temperature Tc and is zero above Tc. Thus in a ferroelectric transition the order parameter is the spontaneous polarisation while in a ferromagnetic transition it is the magnetisation. In the case of a ferroelastic transition, the spontaneous strain is the order parameter. If the order parameter increases continuously from zero in the new phase, the transition is said to be continuous or second order whereas if it increases discontinuously, it is said to be discontinuous or first order type. The appearance of order can be viewed as the breaking of a symmetry. For example, a structural phase transition between a non-piezoelectric and a ferroelectric state in a crystal represents the breaking of inversion symmetry. In group theoretical language, the ordered (or lower symmetry) phase is then viewed as a sub group of the parent (or higher symmetry) phase, with the reduced set of symmetry operations being represented by the order parameter. Landau expanded the Gibb's free energy in powers of the order parameter in the vicinity of a phase transition where the value of the order parameter is very small. The results of Landau theory supports Ehrenfest's classification and reveals many basic features of

phase transitions. Derivations from Landau theory near Tc can be understood using the Renormalisation group theory approach [16]. This theory has had remarkable success in providing insight and quantitative predictions of critical behavior near the transition temperature of most phase transitions.

Since phase transitions are often accompanied by interesting changes in their physical properties, several techniques are employed to investigate phase transitions depending on the nature of the solid and the properties of interest. Practically all experimental investigations deal with the order parameter either measuring it directly, or a generalised susceptibility, which describes its response in space and time, or its effects upon other measurable quantities. The pertinent experimental methods can be classified into two groups [17].

(a) The system to be studied is exposed to an external influence and the response of the whole system is measured.

(b) The variation of local properties is probed locally within the system.

To the first group belong all the scattering experiments, where the external influence is, for example, a beam of light or X-rays or thermal neutrons and also measurement of material properties such as the dielectric constant, refractive index, specific heat, thermal conductivity, electrical conductivity etc.. Examples for the second group are electron and nuclear magnetic resonance experiments. Common to the methods in the first category is that they determine a correlation function of physical quantities that are related to the order parameter. Literature abounds in studies of phase transitions using a wide range of techniques [11,13,17-27].

Ultrasonic experiments belong, in general, to the first group, the only exception being acoustic spin resonance.

The external influence is an elastic strain field ε_i (i = 1,2...6) varying sinusoidally in space and time. Quantities measured are the velocity v_s and the attenuation α_s of sound. The experimental investigation of sound propagation near distortive structural transitions picked up momentum during the late sixties [28-30]. Since Ultrasonics is a very good tool to probe the bulk properties and elastic response of condensed matter, a large amount of work has been done using ultrasonics to probe different types of phase transitions [13,17,22-30].

1.4.3 Ultrasonics as a tool to study phase transitions

Ultrasonic studies are very helpful in characterising the elastic behaviour of systems near phase transitions and critical points [26]. Sound attenuation and dispersion have long been recognised as important means for studying static and dynamic properties of matter and are very helpful in investigating phase transitions [22,31]. Since the coupling of a sound wave to the order parameter of phase transitions is quite different from that of neutron or light, the acoustic experiments provide information about the aspects of order parameter dynamics somewhat different from those of scattering experiments [31].

Ultrasonic experiments overlap with other techniques both at higher and lower frequencies. At the high frequency end they overlap with Brillouin scattering. Such an experiment mainly determines sound velocities, but has the advantage that it can be performed with a small volume of the material in contrast to ultrasonic measurements. At the other end of the frequency scale there are pressure or more generally stress experiments. They can in many cases give the same information as ultrasonic experiments regarding static interaction between strain and the order parameter, but they do not give any information about the dynamics [17].

Several review articles on ultrasonic effects at phase transitions have appeared in literature. The most extensive one by Garland [26] treats the whole spectrum of phase transitions ranging from the liquid-gas transition through binary liquid mixtures to solids. Ultrasonic effects, especially at magnetic transformations, are discussed by Lüthi *et al.* [32]. In his article on ferroelectric phase transitions, Nettleton [33] has devoted a chapter to ultrasonic experiments. The effect of intermediate and high frequency sound wave in the critical region is discussed by Kawasaki [22]. There is a shorter review paper by Joffrin [34] stressing more general aspects. The elastic properties of different solids having different types of structural phase transitions are extensively reviewed with necessary theory and experimental results by Lüthi and Rehwald [35].

In the following paragraphs the effects of structural phase transitions upon sound propagation are discussed with necessary theoretical formulations. Since we are dealing with structural changes in solids, two concepts are of importance: symmetry as an inherent property of crystalline matter and soft modes of lattice vibrations. The role of the latter was first demonstrated by Cochran [36] and Anderson [37] for a ferroelectric phase transition and has since then proved important for a vast number of other structural transitions.

Thus ultrasonics can be used as an effective tool to probe phase transitions if we can relate the order parameter with the elastic response function, *i.e.*, if there is a coupling between the order parameter and lattice strain. In the next section the interaction between the strain and the order parameter is discussed. Static effects determine the variations in sound velocity. Dynamic effects, ie order parameter fluctuations, which are important for the ultrasonic attenuation, but which can also give contributions to the

sound velocity are also discussed.

1.4.4 Landau Theory

If G is the Gibb's free energy of a lattice, according to Landau it can be written as an expansion of powers in Q where Q is the order parameter. Then the mean field (or Landau) expansion for this free energy G may be written in terms of the order parameter as [7,15,38-40].

$$G(Q,T) = Go(T) + (1/2)a(T)Q^2 + (1/4)bQ^4 + \ldots \quad (32)$$

Here we have considered a case where symmetry forbids odd powers. The equilibrium value Qo is determined from the condition $\partial G/\partial Q=0$ and Qo should vanish above critical temperature Tc and non-zero below Tc. Then $a>0$ for $T>Tc$ and $a<0$ for $T<Tc$ where T and Tc are the temperature and transition temperature respectively. Thus according to Landau theory we can write

$$a = a'(T-Tc) \text{ near } Tc. \quad (33)$$

Thus from the stability criteria, $\partial G/\partial Q = 0$, we get the equilibrium value for order parameter Q as

$$\begin{aligned} Qo &= 0 \quad \text{when } T > Tc \\ Qo^2 &= (a'/4b)(Tc-T) \quad \text{when } T < Tc \\ &= a/4b \end{aligned} \quad (34)$$

The susceptibility $\chi\ (K=0) = (\partial^2 G/\partial Q^2)^{-1}$ is then

$$\begin{aligned} \chi(0) &= 1/a \qquad T > Tc \\ &= 1/2a \qquad T < Tc \end{aligned} \quad (35)$$

These results are given under the assumption that the exponents describing the critical behaviour are $\beta = 1/2$ and $\gamma = 1$.

In all structural phase transitions the order parameter is coupled to the elastic strains or possibly other

secondary order parameters by terms in the free energy. If ε is the strain, the elastic energy contribution by this strain is [35]

$$\frac{1}{2} C_o \varepsilon^2 \qquad (36)$$

where Co is the background elastic constant *i.e.*, elastic constant taken at zero order parameter. Due to the coupling of the strain to the order parameter an interaction energy also has to be taken into account. The free coupling energy density is usually written in terms of increasing powers of ε_i and Q_k, *i.e.*, $G_c(\varepsilon_i, Q_k) = g_{ij} Q_i \varepsilon_j + h_{ijk} Q_i Q_j \varepsilon_k + i_{ijk} Q_i \varepsilon_j \varepsilon_k +$

$$j_{ijkl} Q_i Q_j \varepsilon_k \varepsilon_l + \qquad (37)$$

Symmetry determines which of the coupling coefficients g, h etc. are different from zero. In order to keep the exposition simple we can take the case of only one component of ε and Q. Then

$$G_c = g\varepsilon Q + h\varepsilon Q^2 + i\varepsilon^2 Q + j\varepsilon^2 Q^2 + \ldots\ldots \qquad (38)$$

According to relaxation theory as applied to a sound wave travelling through condensed media [41] and for a low amplitude sound wave of angular frequency $\omega = 2\pi f$, the stress, strain and the characteristic order parameter, if it is coupled to the strain, will vary as exp $i(\omega t - \mathbf{q}^* . \mathbf{r})$ where $\mathbf{q}^*$ is the complex wave vector. Then the ordering quantity plays the role of an internal degree of freedom. It can move more or less freely under the action of forces exerted by the ultrasonic strain field and described by Gc. The ordering quantity responds to these forces and reacts back on the elastic system. Then the effect of this will be a change, generally a decrease in the elastic stiffness. Thus the most important information about structural phase transition is obtained from the temperature dependence of the elastic

stiffness functions.

Consider the case of bilinear coupling *i.e.*, strain is directly coupled to the order parameter *i.e.*, Gc = gεQ. Then the free energy given by eqn.(32) is then extended to include the strain as

$$G = Go + \frac{1}{2}a(T)Q^2 + bQ^4 + g\varepsilon Q + \frac{1}{2}Co\varepsilon^2 \qquad (39)$$

The condition for the material to be stress free is that $\partial G/\partial\varepsilon = 0$, from which we can find out the expression for ε as

$$\varepsilon = -gQ/Co \qquad (40)$$

Since the interaction forces are proportional to strain only and no other forces are present

$$\frac{\partial G}{\partial Q} = g\varepsilon + \left[\frac{\partial^2 G}{\partial Q^2}\right]_\varepsilon \delta Q$$

$$= g\varepsilon + \frac{\delta Q}{\chi Q} = 0 \qquad (41)$$

and the ordering quantity can in general follow freely the applied varying strain $\delta Q = -\chi_Q g\varepsilon$; where χ_Q is the unrenormalised order parameter susceptibility $\left[\partial^2 G/\partial Q^2\right]_\varepsilon^{-1}$ and this determines the response of this varying order parameter δQ. This moving ordering quantity δQ adds a contribution to the stress σ acting within the sound wave.

$$\sigma = \partial F/\partial\varepsilon = Co\varepsilon + g\delta Q$$

$$= (Co - g^2\chi_Q)\varepsilon \qquad (42)$$

From the above equation it is clear that the result is a diminished elastic constant and in the static limit it is equal to

$$C_T = Co - g^2\chi_Q = Co\,\frac{T-Tc-g^2/a'Co}{T-Tc} \qquad (43)$$

In this equation $Tc = T_c^{\varepsilon}$, in the case of a continuous transition, is the transition temperature for zero strain (clamped state) and in the absence of strain interaction,

$$T^{\sigma} = Tc + g^2/a'Co \qquad (44)$$

is the transition temperature in the free state (zero stress). For discontinuous transitions Tc denotes the lower stability limit.

Thus taking the case of bilinear coupling of strain and order parameter, the elastic stiffness probes directly the order parameter susceptibility. This is the case for static or lower frequency response as well as for general dynamic response throughout the whole frequency range.

The source for critical attenuation can be obtained from the imaginary part of χ_Q^{ε}.

Taking the case of linear coupling and if the order parameter decays exponentially in time with a single relaxation time τ (non-dispersive relaxation) [22], the real part of the elastic constant is obtained as

$$C_T(\omega) - C_T(\omega=0) = g^2\chi_Q^{\varepsilon}(0)\,\frac{\omega^2\tau^2}{1+\omega^2\tau^2} \qquad (45)$$

and for attenuation the imaginary part as

$$\alpha(\omega) = \frac{g^2\chi_Q^{\varepsilon}(0)}{\rho V^3}\,\frac{\omega^2\tau}{(1+\omega^2\tau^2)} \qquad (46)$$

For $\omega\tau >> 1$, $C_T(\omega) \rightarrow C_T(\omega = 0) + g^2\chi_Q^{\varepsilon}(0)$. According to eq.(43) this is the background elastic constant C_0.

For the specified direction of propagation, the complex wave vector $\mathbf{q}^*$ or the equivalent complex sound

velocity $\mathbf{v}^*$ can be related to the real velocity V and attenuation α by

$$\mathbf{q}^* = \omega/\mathbf{v}^* = (\omega/V) - i\alpha \qquad (47)$$

Thus $V = \omega/\mathrm{Re}(\mathbf{q}^*)$ and $\alpha = -\mathrm{Im}\ \mathbf{q}^*$

Taking $C^* = \rho(V^*)^2$ as the frequency dependant elastic constant for the medium characterised by the relaxation time τ involving long range ordering,

$$(V^*)^2 = V_\alpha^2 - \frac{V_\alpha^2 - V_0^2}{1 + i\omega\tau} \qquad (48)$$

where $V_\alpha = V(\omega = \alpha)$ is the infinite frequency velocity which describes any variation of the stress which is so rapid that the order parameter cannot follow and $V_0 = V(\omega = 0)$ is the zero frequency velocity, which pertains to the propagation of any sound wave which varies slowly enough that the system is in equilibrium at all times. When $(\alpha V/\omega)^2 = \left(\frac{\alpha_\lambda}{2\pi}\right)^2 << 1$ (which is usually valid) we get $C = \rho V^2 = \mathrm{Re}(C^*)$ and $2\rho V^3\alpha/\omega = \mathrm{Im}(C^*)$. The resulting expressions for V^2 and α are

$$V^2 = V_\alpha^2 - \frac{V_\alpha^2 - V_0^2}{1 + \omega^2\tau^2}$$

$$= V_0^2 + \frac{(V_\alpha^2 - V_0^2)\ \omega^2\tau^2}{1 + \omega^2\tau^2} \qquad (49)$$

$$\alpha = \frac{V_\alpha^2 - V_0^2}{2V^3}\ \frac{\omega^2\tau}{1 + \omega^2\tau^2} \qquad (50)$$

in these representations both the order parameter susceptibility and the relaxation time are taken at constant strain (χ_Q^ε, τ^ε).

As there is a coupling such that Q changes during the passage of sound wave, the rate of approach of Q to its equilibrium value Q_0 is determined by the transport equation [26].

$$\frac{dQ}{dt} = - L \frac{\partial G}{\partial Q} \qquad (51)$$

where L is the kinetic coefficient which in its simplest form is a constant in the vicinity of Tc. According to Landau and Khalatnikov [42], the relaxation time associated with long range ordering below Tc is given by

$$\tau^{\varepsilon} = \frac{1}{La'(Tc-T)} \text{ , and} \qquad (52)$$

in terms of the order parameter susceptibility

$$\tau^{\varepsilon} = \frac{\chi_Q^{\varepsilon}(T)}{L} \qquad (53)$$

Thus in the case of bilinear coupling of strain and order parameter, there is an elastic instability $C_T \rightarrow 0$ at T_c^{σ} and an increase in ultrasonic attenuation towards T_c^{σ}. The condition $\omega\tau = 1$ is practically not reached in ultrasonic experiments at structural transitions, but Brillouin scattering can show dispersive effects.

In the case when strain couples with the square of the order parameter *i.e.*,

$$G_c = h\varepsilon Q^2$$

there is no effect on the elasticity above Tc except for fluctuations. Below Tc the developing order parameter <Q> generates a force from the strain upon Q that increases with <Q>. This results in a decrease of elastic constants [43] given by

$$C(T<Tc) = C_0 - 4h^2<Q>^2\chi_Q(T)$$

$$= C_0 - 2h^2/V \qquad (54)$$

which is a constant in the framework of Landau theory. This variation can be related to a step in the specific heat ΔC [35], as

$$C(T) = C_0 - \frac{4h^2 \Delta C(T)}{a'^2 T} \qquad (55)$$

Assuming a single relaxation time for <Q>, formulae similar to (45) and (46) can be written for the dynamic case [39] and for T<Tc. For $T>T_0$ the strain couples to order parameter fluctuations only and more sophisticated transport theory like mode-mode coupling have to be applied.

Taking the higher orders in the expansion of G_c, we get anharmonic terms like

$$G_c = i\varepsilon^2 Q + j\varepsilon^2 Q^2 \qquad (56)$$

The corresponding contributions to the elastic constants in the ordered phase are proportional to <Q> and $<Q^2>$. In favorable cases where domain effects are absent, a measurement of such elastic constants can give the temperature dependence of the order parameter.

A type of coupling which connects the strain to the spatial derivative of the order parameter has also been proposed [45].

In the low frequency region variation of elastic constant C^Z with temperature around Tc for different types of coupling has been discussed by Rehwald [17] and it is shown in Fig.1.4.

1.4.5 Fluctuation damping

Landau theory in its simplest form neglects completely the fluctuations of the order parameter $\delta Qi = Qi(t) - <Q>$. These fluctuations can give important contributions to C_{ij} and α, the elastic coefficients and attenuation

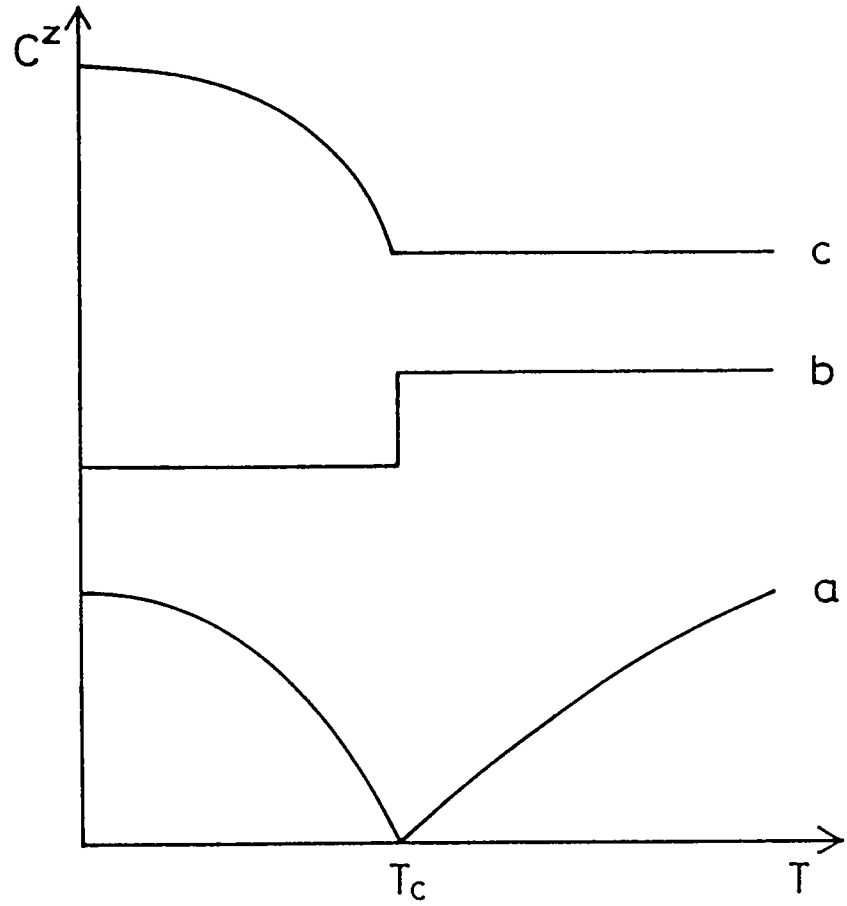

Fig.1.4 General behaviour of low frequency elastic constant (when order parameter moves freely under the applied ultrasonic strain) for a continuous phase transition (a) - Linear coupling, (b) - Coupling linear in strain but quadratic in the order parameter and (c) - Coupling linear in the order parameter but quadratic in the strain.

respectively. Eventhough Landau and Khalatnikov suggest an increase in the attenuation in the vicinity of phase transition due to the increased relaxation time of the order parameter, in the absence of bilinear coupling their theory is not a success [17]. For this Levayuk [46] developed a theory accounting for interaction of sound wave with thermal fluctuations in the order parameter. Theoretical treatments of transport coefficients incorporating these fluctuations are known as mode-mode coupling theories [47]. The fluctuation dissipation theorem [48] states that the linear response of a given system to an external perturbation can be expressed in terms of internal fluctuations of the system when it is in equilibrium. In the case of ultrasonic experiments the important dynamic property is the ultrasonic attenuation α or the sound wave damping constant D_s ($\alpha = \omega^2 D_s / 2V^3$). In the absence of a linear coupling between strain and order parameter this mechanism would play a dominant role [26,46]. It is assumed that the free energy density can be expanded in terms of the deviation $\Delta Q = Q - Q_0$ in the order parameter and the deviation $\Delta V = V - V_0$ is the volume strain and a term $(\text{Grad}\ \Delta Q)^2$ is included to take into account approximately the correlation between values of ΔQ at different points in space. The Levanyuk equations of motion do not include inertial terms (thus Q approaches its equilibrium value with a relaxation character), but they do include a random force which accounts for the fluctuations in Q. For T>Tc this theory reduces to the propagation of sound in medium with random inhomogeneities of a known statistical character. Below Tc the results can be represented as a sum of two terms, one due to the random thermal fluctuations and one which correspond directly to the Landau-Khalatnikov result. Another physical picture behind this fluctuation effects, according to Lüthi and Rehwald [35], is that there is a whole spectrum of fluctuations $\delta Q_1(q)$ with different wave vectors q, centred around q_0, the wave vector

of the order parameter. In displacive phase transitions, for example, these fluctuations are formed by the soft part of the optical phonon branch. In order-disorder transitions these modes belong to collective tunneling motions.

Assuming a coupling of the form $G_c = h_{ijm} Q_i Q_j \varepsilon_m$ two fluctuations δQ of nearly opposite wave vectors combine and produce by anharmonic interaction a stress fluctuation of nearly zero wave vector. The total stress is the sum over the whole fluctuation spectrum and is given by

$$\delta\sigma_m = \sum_{\underline{q}, i, j} h_{ijm} \quad \delta Q_i(\underline{q}) \delta Q_j(-\underline{q}) \tag{57}$$

The easy way to calculate the elastic functions is to write these quantities as correlation functions; according to fluctuation-dissipation theorem and equipartition theorem [15,48]

$$C_m(T) = C_m^0 - \frac{V}{K_B T} < \left| \delta\sigma_m \right|^2 > \tag{58}$$

$$\alpha_m(T) = \frac{\omega^2 V}{2\rho V_s^3 K_B T} \int_0^{\alpha} e^{i\omega t} <\delta\sigma_m(T) . \delta\sigma_m^*(0)> dt \tag{59}$$

The above equation for attenuation means that, as in Brownian motion, the sound attenuation coefficient can be expressed as Fourier transform of time dependant correlation functions of random stresses originating from the interaction energy G_c due to the coupling between the order parameter and strain.

The latest work in this area to remove the drawbacks of these theories, is the renormalisation group analysis. The success of the Renormalisation Group approach to critical phenomena was to distinguish between relevant and irrelevant

parameters and to give a formal procedure to calculate certain critical exponents for static and dynamic problems [16,49,50].

In general it is easy to see that in the case of bilinear coupling between strain and order parameter the elastic instability occurs at Tc. Then the elastic constant C $\rightarrow$ 0 at Tc and attenuation $\alpha \rightarrow \infty$ Symmetry of the material determines which of the coefficients C_{ij} will become zero. If strain is not the order parameter *i.e.*, it couples to a power of the order parameter equal to or higher than two the effects of the elastic stiffness functions near the phase transition points are weaker than that in the case of linear coupling. Even if it is weaker it is observable in the velocity and attenuation curves. In this case the fluctuation effects are more predominant. So ultrasonic technique can be used as an efficient tool to study the static as well as the dynamic aspects of structural phase transitions.

1.4.6. Ferroelectric and antiferroelectric transitions.

In all ferroelectric materials there is a strong coupling between mechanical and dielectric behaviour due to piezoelectric or electrostrictive effects [26]. There are several papers dealing with theories of the anomalies in sound velocity and attenuation in different types of ferroelectrics [17,26,35,51-55]. In ferroelectric crystals which are piezoelectric the influence of the long range forces have been considered by Geguzina and Krivoglaz [56]. The original application of the Landau theory to ferroelectrics was made by Yakovlev and Velichkina [26,58]. In this it is assumed that the relaxation rate $\partial P/\partial t$ at a given point depends only on the polarisation **P** at that point. However, if the acoustic wavelength is smaller than the Debye screening length, dipole-dipole interactions between the variations in P at different points in the crystal will become important. When this nonlocal coupling was included, Geguzina and Krivoglaz

found that the attenuation and velocity variation of ultrasonic waves have a very strong direction dependence. In the case of a uniaxial ferroelectric crystal the anomalous behaviour of ultrasonic waves can occur only when the acoustic wave vector is perpendicular to the polar axis. The frequency and wave vector dependence of velocity and attenuation are analysed for the case of Rochelle salt but treatment is equally valid for KDP and the ferroelectric phase of TGS. But this is valid only in the case of piezoelectric coupling becoming the dominant mechanism for the interaction between acoustic waves and polarisation. In the case of a uniaxial ferroelectric which is not piezoelectric in its paraelectric phase, Levanyuk *et al.* [58] have shown that there is still anomalous attenuation caused by the interaction of sound wave with thermal fluctuations in polarisation as explained in the last section. For biaxial and triaxial ferroelectric, the behaviour of the complex elastic modulus is given by the theory of Levanyuk which deals with fluctuations correlated only at short distances. Uniaxial ferroelectrics form a special class, since polarisation fluctuations are very strongly suppressed [26]. Only the fluctuations in components of polarisation parallel to the polar axis $P_{\parallel}(q)$ increase at $T \rightarrow Tc$ and then only for propagation vectors **q** which are perpendicular to the polar axis. Levanyuk *et al.* [53] predict that the largest anomalies in V and α for uniaxial nonpiezoelectric crystals are associated with acoustic waves generating strains which are coupled by electrostriction to $P_{\parallel}^2$. Such anomalies should be of observable magnitude within $\approx 0.2^{\circ}C$ of Tc and it is predicted that they should be independent of the direction of propagation of the sound wave. This electrostrictive fluctuation is in large contrast with piezoelectric relaxation result [56]. From these we can see that from direction dependence of α we can distinguish the two effects. Waves propagating parallel to the polar axis in a

uniaxial ferroelectric should have no anomaly due to piezoelectric coupling, but will have an electrostrictive anomaly due to the thermal fluctuations in P. But for waves propagating perpendicular to the polar axis, the piezoelectric effect will dominate below Tc due to the presence of spontaneous polarisation or even above Tc for crystals which are piezoelectric in the paraelectric phase.

Considering a case when an external electric field is applied for a crystal which is piezoelectric, the attenuation and velocity anomalies are appreciably reduced as the field is increased. For a crystal which is not piezoelectric, the case is more complicated above the Curie point. The relaxation strength $\frac{(V_\alpha^2 - V_0^2)}{2V^3}$ in eqn.(50) is proportional to P_0^2 where P_0 is the equilibrium polarisation [27]. In this case the acoustic attenuation is zero in the paraelectric phase [59] without the electric field. When the electric field is applied attenuation can occur due to the interaction of the waves with induced polarisation. As a result of the behaviour in the relaxation strength, Geguzina and Timan [59] predicts that TGS type ferroelectrics will show an increase in α when an electric field is applied in its paraelectric phase.

References

1. R.Truell, C.Elbaum and B.B.Chick in *Ultrasonic Methods in Solid State Physics*, Academic Press, New York (1969).

2. E.Schreiber, O.L.Anderson and N.Soga in *Elastic Constants and Their Measurements*, Mc.Graw-Hill, New York (1973).

3. B.A.Auld in *Acoustic Fields and Waves in Solids* Vol.II, John Wiley and Sons, New York (1973).

4. H.J.McSkimin in *Physical Acoustics* Vol.I,Pt.A (Ed. W.P.Mason) Academic Press, New York (1964).

5. C.N.R.Rao and K.J.Rao in *Phase Transitions in Solids*, Mc.Graw Hill, New York (1978).

6. H.E.Stanley in *Introduction to Phase Transitions and Critical Phenomena*, Clarendon Press, Oxford (1971).

7. P.A.Fleury, *Science*, **211,** 125 (1981).

8. R.Roy in *Phase Transitions* (Ed. H.K.Henisch, R.Roy and L.E.Cross) Pergamon Press, New York (1973).

9. P.Ehrenfest, *Proc. Amsterdam Acad.* **36**, 153 (1933).

10. K.J.Rao and C.N.R.Rao, *J. Mater. Sci* **1,** 238 (1966).

11. C.N.R.Rao and K.J.Rao, in *Progress in Solid State Chemistry* Vol.4 (Ed.H.Reiss) , Pergamon Press, Oxford (1967).

12. A.R.Ubbelohde, *Quart. Rev.* **11**, 246 (1957).

13. F.Schwabl, *J. Stat. Phys.* **39**, 719 (1985).

14. J.M.Kosterlitz and D.J.Thouless, *J. Phys.* **C6,** 118 (1973).

15. L.D.Landau and E.M.Lifshitz, in *Statistical Physics*, Pergamon Press, Oxford (1959).
16. K.G.Wilson, *Rev.Mod.Phys* **55,** 583 (1983).

17. W.Rehwald, *Advances in Physics* **22**, 721 (1974).

18. C.N.R.Rao and M.Natarajan in *Crystal Structure Transformation in Binary Halides*, NSRDS-NBS Monograph 41, National Bureau of Standards, Washington D.C. (1972).

19. C.N.R.Rao and G.V.Subba Rao in *Transition Metal Oxides: Crystal Chemistry, Phase Transition and Related Aspects*, NSRDS-NBS Monograph 49, National Bureau of Standards. Washington D.C. (1974).

20. C.N.R.Rao and K.P.R.Pisharody in *Transition Metal Sulphides, Progress in Solid State Chemistry*, Vol.10, Pergamon Press, Oxford (1975).

21. J.B.Goodenough and J.M.Longo in *Crystallographic and Magnetic Properties of Perovskite and Perovskite Related Compounds*, Landolt-Börnstein, New series, Group III, Vol 4a, Springer Verlag, Berlin (1970).

22. K.Kawasaki in *Dynamical Aspects of Critical Phenomena*, (Eds. J.I.Budnik and M.P.Kawatra) Gordon & Breach Science Publishers, New York (1972).

23. K.Parlinski, *Acta Physica Polonica* **A58**, 183 (1980).

24. K.Parlinski, *Acta Physica Polonica* **A58**, 197 (1980).

25. A.D.Bruce and R.A.Cowley in *Structural Phase Transitions*, Taylor and Francis Ltd., London (1981).

26. C.W.Garland in *Physical Acoustics*, Vol. **VII,** (Eds. W.P.Mason & R.N.Thurston) Academic press, New York (1970).

27. K.A.Müller and H.Thomas Eds. in *Structural phase transitions I*, Springer Verlag, Berlin (1981).

28. B.Berre, K.Fossheim and K.A.Müller, *Phys. Rev. Lett.* **23**, 589 (1969).

29. W.Rehwald, *Phys. Kondens. Mat.* **14**, 21 (1971).

30. J.M.Courdille and J.Dumas, *Solid State Commun.* **9**, 609 (1971).

31. K.F.Herzfeld and T.A.Litovitz in *Absorption and Dispersion of Ultrasonic Waves*, Academic press, New York (1959).

32. B.Lüthi, T.J.Moran and R.J.Pollina , *J. Phys. Chem. Solids* **31**, 1741 (1970).

33. R.E.Nettleton, *Ferroelectrics* **1**, 221 (1970).

34. J.Joffrin, *Ber. Bunsunges* **76,** 268 (1972).

35. B.Lüthi and W.Rehwald in *Structural Phase Transitions I* (Eds. K.A.Müller and H.Thomas) Springer Verlag, Berlin (1981).

36. W.Cochran, *Adv. Phys.* **9**, 387 (1960).

37. P.W.Anderson in *Fizica Dielektrov* (Ed. G.I.Skanavi) Moskow (1960).

38. L.P.Kandanoff, W.Götze, D.Hamblen, R.Hecht, E.A.S.Lewis, V.V.Palciauskas, M.Rayl, J.Swift, D.Aspnes and J.Kane, *Rev. Mod. Phys* **39,** 395 (1967).

39. M.E.Fisher, *Rev. Mod. Phys*.**46,** 597 (1974).

40. C.Domb and M.S.Green Eds., *Phase transitions and Critical Phenomena*, Vols. 5A & 6, Academic Press, New York (1976).

41. K.F.Herzfeld and T.A.Litovitz in *Absorption and Dispersion of Ultrasonic Waves*, Academic Press, New York, (1959).

42. L.D.Landau and I.M.Khalatnikov, *Dokl. Akad. Nauk SSSR*, **96**, 469 (1954).

43. J.C.Slonczewski and H.Thomas, *Phys.Rev*. **B1**, 3599 (1970).

44. E.Pytte, *Phys.Rev.* **B1**, 924 (1970).

45. A.Michelson, *Phys.Rev*. **B14**, 4121 (1976).

46. A.P.Levanyuk, *Sov. Phys. JETP* **22**, 901 (1966).

47. K.Kawasaki in *Phase transitions and Critical Phenomena*, Vol.**5a**, (Eds. C.Domb and M.S.Green) Academic, London (1976).

48. Kubo, *Rep. Prog. Phys*. **29,** 255 (1966).

49. M.E.Fisher, *Rev. Mod. Phys.* **46**, 597 (1974).

50. P.C.Hohenberg and B.I.Halperin, *Rev. Mod. Phys.* **49**, 435 (1977).

51. D.G.Sannikov, *Sov. Phys. Solid State* **4**, 1187 (1962).

52. V.Dvorak, *Phys.Rev.* **167**, 525 (1968).

53. I. Lefkowitz and Y.Hazony, *Phys.Rev.* **169,** 441 (1968).

54. K.Tani and N.Tsuda, *J. Phys. Soc. Jpn.* **26**, 113 (1969).

55. M.Inoue, *J. Phys. Soc. Jpn* **26**, 420 (1969).

56. S.Ya.Geguzina and M.A.Krivoglaz, *Sov. Phys. Solid State,* **9**, 2441 (1968).

57. I.A.Yakovlev and T.S.Velichkina, *Usp. Adv. Phys. Sci.* **63**, 552 (1957).

58. A.P.Levanyuk, K.A.Minaeva and B.A.Strukov, *Sov. Phys. Solid State*, **10,** 1919 (1969).

59. S.Ya.Geguzina and B.L.Timan, *Sov. Phys. Solid State* **9**, 1702 (1968).

Chapter 2
INSTRUMENTATION

2.1. Introduction

As ultrasonics is an important tool in materials science and technology, several techniques have been developed for the measurement of ultrasonic parameters like velocity, attenuation etc. in solids. Each of them has its own merits and demerits, and one has to select the most suitable one depending upon the application and requirement. In this chapter some of the important techniques to measure ultrasonic velocity and attenuation in solids are briefly discussed. In the present investigations a technique called Pulse Echo Overlap (PEO) method is used and this is discussed in detail in this chapter. The Mc Skimin Δt criterion for selecting properly overlapped echoes and the method of making bond corrections are outlined in this chapter. The actual experimental setup used for the present studies is also discussed in detail giving the features of the different electronic modules used. A well designed cryostat is essential for low temperature measurements. The design and fabrication of the cryostat used is also discussed in this chapter. Thus this chapter gives an overall picture of the techniques and instrumentation involved in the work presented in this thesis.

2.2. Ultrasonic velocity and attenuation measurements in solids

As the measurement of acoustic parameters is very important in characterising materials, several methods have been developed for the purpose. Experimentally one measures ultrasonic velocity and attenuation in the material. The methods of making these measurements can be classified as shown in Table 2.1 [1-5].

Table 2.1

Experimental methods for investigating elastic coefficients and attenuation.

Method	Frequency Range	Elastic Coefficient Measured	Loss
Torsion Pendulum	10^{-4} - 10Hz	C_{ij}	Quality
Resonance-antiresonance	10KHz - 1MHz	S_{ij}	Quality
Ultrasonics	1MHz - 1GHz	C_{ij}	Attenuation
Hypersonics	1GHz - 20GHz	C_{ij}	Attenuation
Brillouin Scattering	100MHz - 10GHz*	C_{ij}	Attenuation

* Depends on scattering geometry

With the methods listed in Table 2.1, a frequency range of 10^{-4} - 10^{10} Hz is possible. The ultrasonic and hypersonic methods have the largest frequency range among these acoustic methods and have the greatest variability. Among these the ultrasonic technique is the most suitable due to its higher range and sensitivity. Generally ultrasonic experiments overlap with other techniques both at higher and lower frequencies. At the high frequency end they overlap with Brillouin scattering and at the other end of the frequency scale these are pressure or more generally stress experiments. Ultrasonic techniques enable one to make velocity and attenuation measurements very accurately.

In ultrasonic experiments, travelling waves are introduced into the specimen by a piezoelectric or

magnetostrictive transducer in most cases, although other methods have also been deviced. The commonly used piezoelectric material is quartz and materials like $LiNbO_3$, $BaTiO_3$, $SrTiO_3$, PZT etc. are extensively used. For high frequency applications CdS, ZnS and ZnO are used successfully in thin film form [6-8]. This mechanical wave is introduced into the specimen either immediately or after some delay encountered in an intermediate propagation medium. A thin layer of a proper bonding material is necessary to inject the waves from the transducer in to the material, so that there is matching of the acoustical impedances of the specimen and the transducer.

Ultrasonic velocity measurements in a solid have two-fold objectives. On one hand one needs highly accurate absolute measurement of velocity in order to determine properties related to lattice vibrations of the solid. Interatomic forces are directly related to the elastic moduli and hence to the velocities of stress waves in different directions. The relations between the elastic moduli and elastic wave velocities for different propagation directions and polarisations for various crystal systems are available in standard text books and are discussed in chapter 1. These relations are given in this thesis as and when required.

On the other hand, one gets very important information about changes in a solid when parameters like temperature, pressure etc. are varied by measuring the corresponding changes in wave velocities. In this case, velocity changes are of interest and absolute accuracy is not usually necessary. A high sensitivity of the measurement to such changes is important because they are usually small. Thus the systems for the measurement of ultrasonic velocity generally fall into these two classes; one in which absolute accuracy is the main objective and the other in which sensitivity is the main objective. Accordingly, we can divide

the methods of velocity measurements into the following two categories.

(a) Continuous Wave (CW) methods

(b) Pulse methods

2.3 Continuous wave methods

A standing wave pattern can be obtained in a specimen by applying an acoustic excitation such that an integral number of half wavelengths are set up between the opposite faces of the sample. For a sample of length L the number of excited resonances of frequency f is $n = 2Lf/v$ whereby the sound velocity v can be determined [9]. Using frequency modulation techniques one can measure changes in velocity and attenuation with high precision. Details of this method are given in a number of references cited [10,11]. A major source of uncertainty in this method is the possibility of erroneous readings due to reflections of waves from discontinuous surfaces rather than the end phases. Corrections for the frequencies of the resonant modes are required in this technique. CW methods are seldom used for low temperature work because of sample heating due to the large input power into the sample.

In the cw composite oscillator technique [11] a transducer-specimen combination can be treated as a two-terminal network. The impedance is measured by balancing a radio frequency bridge [12,13]. With this technique it is possible to measure small changes in velocity of the order of one part in 10^7.

2.4 Pulse methods

The pulse methods have become very popular and are capable of many variations. In this method, in its simplest form, an ultrasonic pulse of short duration is injected into the sample by a transducer. The acoustic pulse transmitted

through the specimen is detected by another transducer bonded at the opposite face of the specimen. The time taken by pulse to travel through the specimen is measured by displaying the received signal on an oscilloscope. By this method velocity of longitudinal as well as transverse waves can be measured. An advantage of the pulse technique is that the acoustic signal can be propagated even through lossy materials like ceramics, polymers etc. Improvements in both precision and accuracy of this method have been achieved by Birch [14]. Instead of two transducers, a single transducer which acts as the transmitter and receiver can also be used. The initial pulse sent into the sample is almost perfectly reflected at the opposite air-sample interface and it returns to the transducer-sample interface where all but a small fraction of energy is again returned to the sample. By the time the first echo has arrived back at the transducer, the transducer has been turned off. The transducer converts a small amount of the energy of the returned pulse into electrical energy. This electrical signal is amplified by an appropriate receiver and the result is displayed on an oscilloscope. The other portion of the acoustic energy gets reflected at the transducer-sample interface and the process described above is repeated. The received signals can be seen on the oscilloscope screen as a series of echoes. Because of multiple reflections, each time the stress wave passes through the sample, a fraction of its energy is absorbed or scattered. The result is an exponentially decaying echo pattern . A typical echo pattern is shown in Fig.2.1. By measuring the time between two successive echoes and the thickness of the sample, ultrasonic velocity can be determined. Attenuation can be measured by observing the decay rate of the successive echoes.

Considering the plane attenuated wave as represented by

$$A(x,t) = A_0 \, e^{-\alpha x} \, e^{i(\omega t - kx)}, \qquad (1)$$

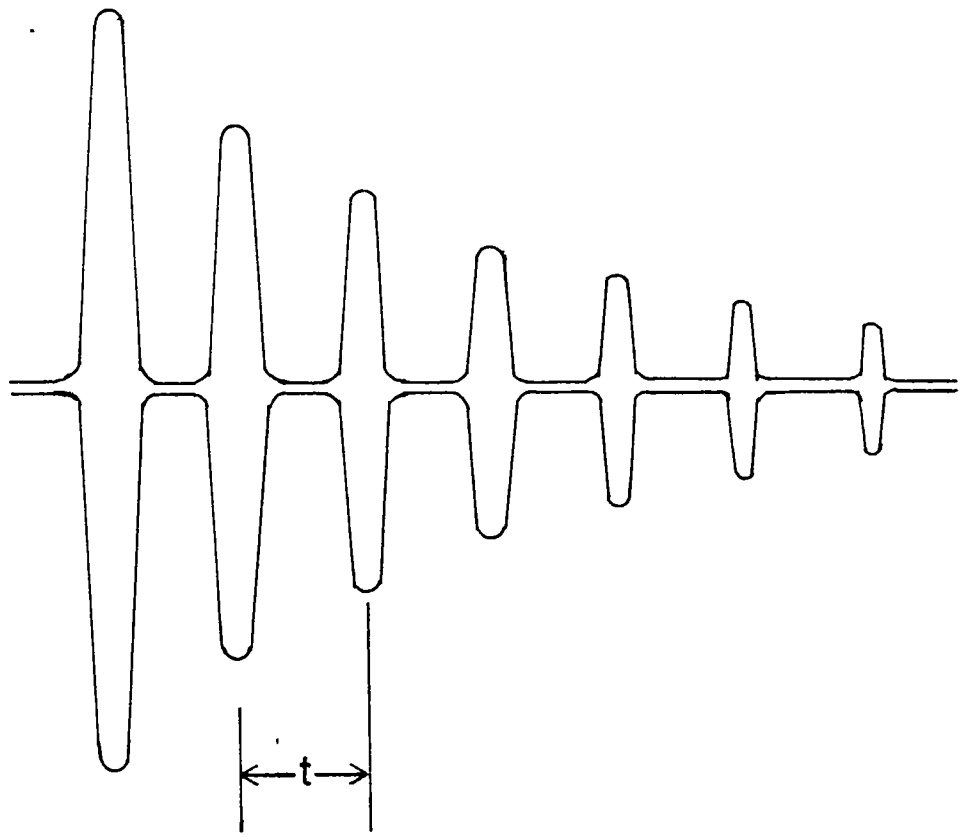

Fig.2.1 A typical exponentially decaying echo pattern. Only the envelope is shown.

the attenuation factor α can be defined as the imaginary part of the complex propagation vector. The phase velocity v_p is given by the real part.

Then the attenuation can be expressed as

$$\alpha = \frac{1}{x_2 - x_1} 20 \log_{10} \frac{A(x_1)}{A(x_2)} \text{dB/unit length} \qquad (2)$$

where $A(x_1)$ and $A(x_2)$ are the amplitudes of two echoes and $x_2 - x_1$ represents the distance travelled by these echoes. Thus the attenuation α can be determined either by comparing the amplitude of two echoes or by making use of a calibrated exponential decay curve which is presented together with the pulse echo pattern on the oscilloscope. The exponential decay curve can be fitted to the echo pattern, and the attenuation is then obtained immediately from the time constant of the decay curve from a calibrated dial.

Details of the pulse techniques have been described by several authors [15-35]. Most commonly, an rf pulse packet consisting of a finite number of sinusoidal waves obtained by gating the output of an oscillator is used. The determination of absolute velocity values by this pulse technique requires the accurate measurement of time interval between echoes and the sample thickness. In measurement of time intervals, it is necessary to eliminate errors due to pulse rise time, pulse length, pulse shape, pulse repetition rate, the characteristics of the receiving system and that due to impedance mismatch introduced by transducer and the bond. The shape of the pulse will remain unaltered only if there is no velocity dispersion. The velocity must be independent of frequency except when the material itself exhibits dispersion [18]. If the medium is dispersive the different component frequencies of the pulse will travel with different velocities and the pulse shape changes as it progresses. The precision of direct velocity measurement is about ±0.2%. By using improved techniques to measure the time between two echoes a more

accurate velocity determination is possible. There are a number of techniques for this purpose and among them the most important and widely used ones are pulse superposition technique, sing-around technique and pulse echo overlap technique. In the following sections the first two are briefly explained and the third one is discussed in more detail as we have used the third technique in our measurements.

2.4.1 Pulse superposition method

Among the pulse techniques the pulse superposition technique [19-21] is highly accurate for measuring ultrasonic velocity in solids. A single transducer is used on the specimen and multiple echoes are observed on the oscilloscope. In the preferred mode of operation, the rf pulse generator pulses the transducer once per round trip of the waves in the sample. The rf pulse is triggered from a definite phase point of the signal from the cw oscillator. Generally, the frequency of this cw oscillator is adjusted so that its period is equal to an integral multiple of the round trip time of the ultrasonic wave in the specimen. The cw oscillator frequency is completely independent of the rf frequency. The cw oscillator frequency is then measured using a frequency counter and this gives the reciprocal of the time of travel of the wave within the sample. From this the velocity of the ultrasonic wave in the sample can be determined. The method is called "superposition" because the ultrasonic pulses are actually superposed within the specimen.

The absolute accuracy of this technique arises from the fact that the method is capable of measuring accurately from any cycle of one echo to the corresponding cycle of the next echo with only a small systematic error due to the phase shift of $\pi/2$ from the face of the transducer to infinity caused by diffraction [22]. However it is not as versatile as the pulse echo overlap method, which will be discussed in

detail in the following sections, due to the fact that this method cannot accommodate buffer rods or broad band pulses. This technique is discussed in detail by many authors [19-21,23].

2.4.2 Sing-Around system

The sing-around technique is an automated method for measuring ultrasonic velocity to moderately high accuracy and for monitoring changes in ultrasonic velocity to high accuracies [24].

In this method measurement must be made by through-transmission *i.e.*, with two transducers. A triggered transmitter sends an electrical pulse to the transmitting transducer, which generates a mechanical wave in the specimen. This wave is received by the receiving transducer and amplified. The leading edge of the received and amplified signal is used to generate a trigger signal that initiates a new pulse from the transmitter. This loop runs continuously. The frequency of occurrence of the trigger signal is measured by a frequency counter. Then the travel time through the loop is the reciprocal of the number of trigger signals counted per second.

The travel time through the loop is greater than the travel time through the specimen due to the delays associated with the electrical circuits, rise time of the amplified pulse etc.. If all these incremental delays are considered and corrected the absolute accuracy of the system would be better than one part in 10^4 or 100 ppm. In the absence of the requisite corrections the precision can be as good as two parts in 10^5 or 20 ppm. It is a good, but not necessarily ideal, method for making absolute measurements, but it is very useful for certain types of relative measurements such as measurement of changes in velocity if the specimen geometry is compatible with other considerations.

2.5 Pulse Echo Overlap method

The pulse echo overlap (PEO) method is a very versatile and highly accurate technique for measuring velocity of ultrasonic waves in materials and structures [23,25-28]. The absolute accuracy of this method arises from the fact that the method is capable of measuring accurately from any cycle of one echo to the corresponding cycle of the next echo. The pulse echo overlap method is able to handle diffraction phase corrections properly [22,29]. So the absolute accuracy of the PEO method may exceed the accuracy of most other methods eventhough the precision of some others may exceed that of the PEO.

The main features of this technique which other methods generally do not possess simultaneously are the following.

1. The PEO method may operate either with the transducer bonded directly to the specimen or with a buffer rod (or liquid column or lead-in-wire) interposed between the specimen and the transducer.
2. The PEO method may be operated with broad band pulses [30] as well as rf bursts. One advantage of broad band pulses is that proper overlap can be set up with the broad band echoes unambiguously. If rf is to be used it can be switched on after the overlap is established.
3. The PEO method can be set up to make through transmission measurements [25] of the travel time on a single pass between two transducers.
4. The PEO method can be adapted to measure group velocity [31] as well as phase velocity [27] by using the envelopes of moderately narrow band of rf bursts.
5. In PEO method the attenuation of the ultrasonic wave can be measured simultaneously.

The disadvantage of this method is that it is

difficult to automate it as its echoes are overlapped by the observer in 'scope time' and not in real time.

2.5.1 The Pulse Echo Overlap System

The PEO setup for measuring ultrasonic velocity is shown in Fig.2.2. The rf pulse is applied to the sample through a transducer which is bonded to the sample. A series of echoes is obtained and seen on the oscilloscope screen as explained in the previous sections. The aim of the experiment is to measure the time between two echoes from which the velocity can be calculated. The principle of measurement is to make the two echoes of interest overlap on the oscilloscope screen by driving the x-axis with a frequency whose period is the travel time between the signals of interest. Then one echo appears on one sweep and the other on the next sweep on the oscilloscope screen. Thus echo overlap is effected optically on the viewing oscilloscope. Instead of driving the x-axis directly using cw, a trigger pulse generated from this can also be used to trigger the x-axis of the oscilloscope which is set in internal sweep in external trigger mode and this technique is more convenient. This cw is supplied by the cw oscillator shown in Fig.2.2. For jitter free overlap the signals of interest must be synchronised with the phase of the cw voltage. This condition is achieved by generating the repetition rate of the input rf pulse from the phase of the cw voltage by a frequency divider. Division by a large integer of the order of 100 or 1000 allows all the echoes from one pulse to be attenuated before the next pulse is applied. The output of the frequency divider is a trigger signal synchronous with the phase of the cw voltage. This trigger signal triggers a pulsed rf oscillator or pulser which is connected to the transducer. The echoes are amplified by an amplifier and a diode limiter circuit keeps the input pulse from overloading the amplifier. The trigger signal also triggers two

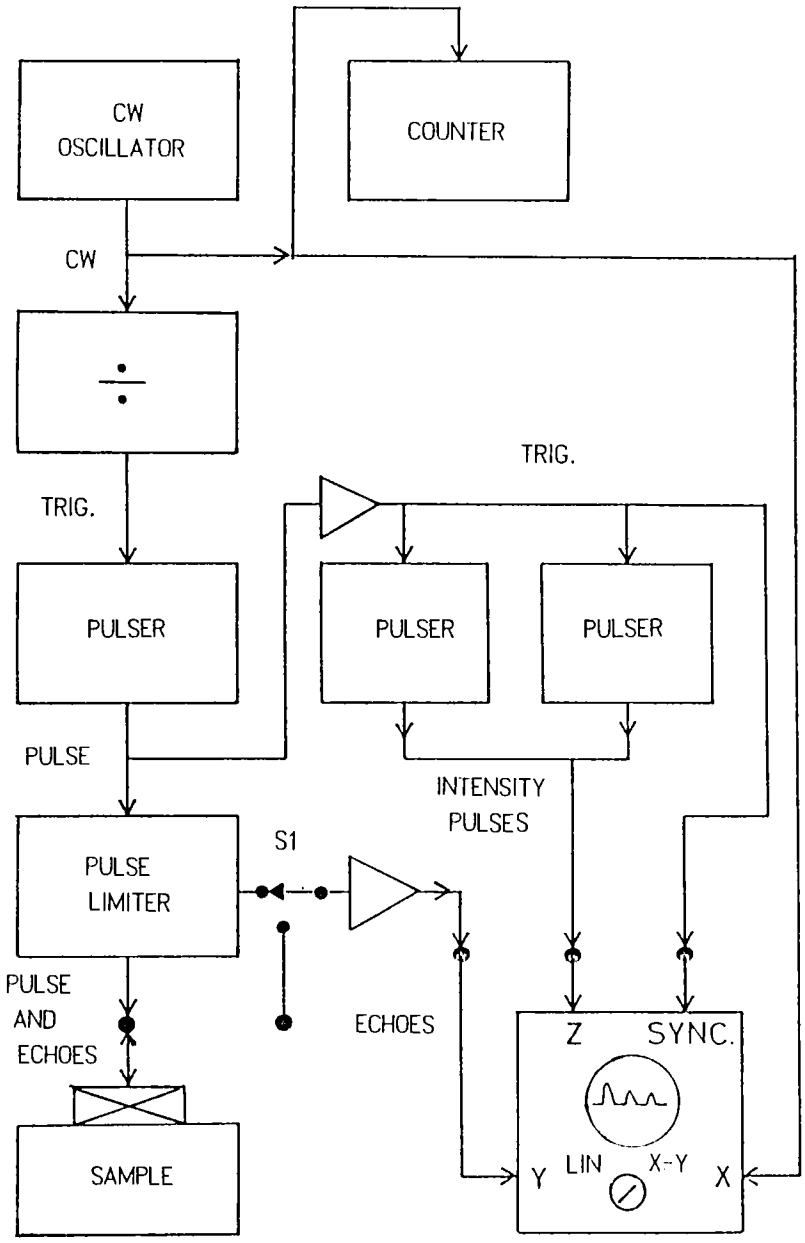

Fig.2.2 Basic block diagram showing Pulse Echo Overlap (PEO) setup for measuring travel time of ultrasonic waves.

intensifying pulses which are applied to the oscilloscope to select any pair of echoes in which we are interested and to blank out all other signals. The overlap is adjusted by adjusting the cw frequency and by measuring this cw frequency, the travel time can be measured.

To make a measurement, one first sets the oscilloscope on the triggered mode of operation. The delays and widths of the intensifying pulses are then adjusted to cover the signals of interest. The frequency of the cw oscillator is set approximately the reciprocal of the travel time between the signals of interest. The oscilloscope is then switched to the driven x-axis mode of operation. The intensity of the oscilloscope is adjusted so that only the two selected echoes are visible. Then the cw frequency is adjusted so that the two signals overlap as shown in Fig.2.3. Instead of rf pulser a broad band pulse can also be used to excite the transducer.

In order to accomplish an overlap, any pair of echoes can be chosen. This PEO method was first enunciated [25] as a means of measuring delay in nondispersive delay lines. The overlap in that case is first set by observing the envelopes of the echoes of Gaussian shape, then adjusted by observing the carrier frequency. The cycle-to-cycle match of the carrier frequency nearest to the overlap of the envelopes is assumed to be correct. This method gives a possibility of one cycle of mismatch relative to the true delay in the specimen. But this gives the true system delay for the purpose of comparing specimens and measuring their changes versus independent variables. By this method precision upto 1 ppm can be achieved in the vicinity of 15 MHz.

In order to decide which cycle is the proper one in each echo for matching, a technique called Mc Skimin Δt criterion [19,20] is used. It was developed for the pulse superposition technique initially and later it was proved by

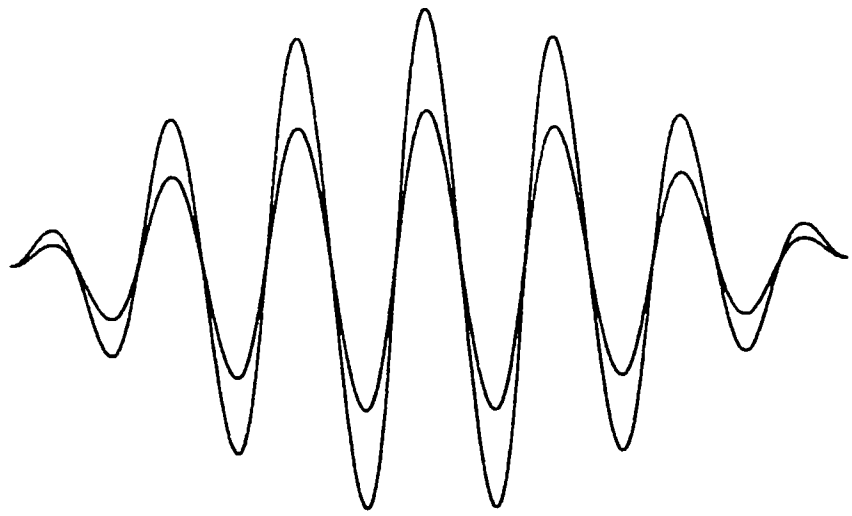

Fig.2.3 Echo pair in the overlapped condition.

Papadakis [26] that the same could be applied to the pulse echo overlap method when run with rf pulses exciting transducers bonded to the specimen directly. The cycle-to-cycle matching in the overlapped condition depends on the Mc Skimin Δt criterion in exactly the same way in both methods.

2.5.2 The Mc Skimin Δt criterion

Consider a burst of ultrasonic waves of principally one frequency echoing back and forth within a specimen. The specimen is bare on one end but has a transducer bonded to the other end. The transducer is half a wavelength thick at its resonant frequency and the bond has a finite thickness. The transducer is unbacked. We can consider the effect of the bond and transducer upon the phase of the reflected wave at the bonded end of the specimen in order to choose the correct cycle-to-cycle matching of one echo with any subsequent echo. Fig.2.4 gives a sketch of the specimen geometry.

The phase angle γ relating the reflected wave phase to the incident wave phase is shown in the figure. The phase angle is a function of the acoustic impedances, the thickness of the layers and the frequency. Z_s, Z_1 and Z_2 are the specific acoustic impedances for the specimen, bond and the transducer respectively. The impedance looking into the termination (bond and transducer) from the specimen is Z_d, given by the transmission line theory as [23]

$$Z_d \equiv jZ_e = jZ_1\left[\frac{(Z_1/Z_2)\tan B_1 l_1 + \tan B_2 l_2}{(Z_1/Z_2) - \tan B_1 l_1 \tan B_2 l_2}\right] \qquad (3)$$

where B_1 and B_2 are the propagation constants in the bond and transducer and l_1 and l_2 are the thicknesses of the bond and transducer respectively. Z_d is used to define the ratio of reflected to incident pressure as

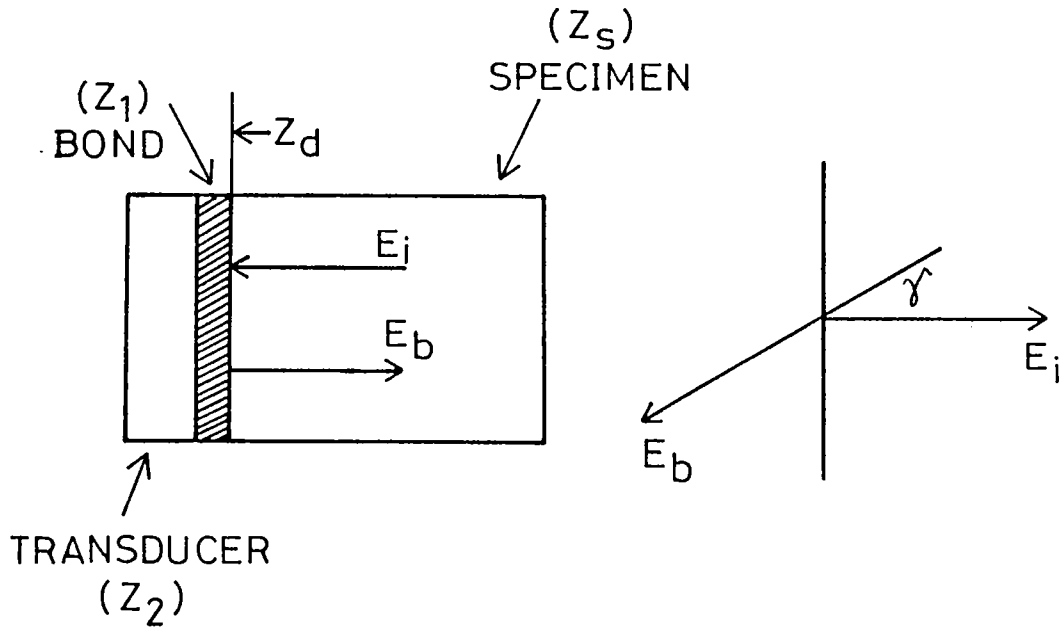

Fig.2.4 Specimen geometry showing transducer, bond and sample.
Z_1- Bond impedance ,Z_2 - Transducer impedance,
Z_s - Sample impedance and γ - The phase angle generated at each reflection of the echoes at the specimen/bond/ transducer interface.

$$\frac{E_b}{E_i} = \frac{Z_d - Z_s}{Z_d + Z_s} \qquad (4)$$

With Z_d imaginary, there is a phase angle γ given by

$$\tan \gamma = -2Z_e Z_s/(Z_s^2 - Z_e^2) \qquad (5)$$

for the vectors shown in Fig.2.4.

In the above formulae there is only one unknown *i.e.*, the bond thickness l_1 and one running variable, the ultrasonic frequency f impressed upon the transducer by the rf pulse generator. By varying f, we can change B_1 and B_2 which are $2\pi f/v_1$ and $2\pi f/v_2$respectively. γ is a measure of the effect of the transducer and bond on the reflected wave.

Mc Skimin [19,20] has shown that the measured travel time t_M is made up of the true round trip travel time t plus some increment given by

$$t_M = pt - (p\gamma/2\pi f) + n/f \qquad (6)$$

Here p is the number of round trips in the measurement. For example, for the first and third echoes, p = 2. The phase angle γ per reflection yields a fraction $\gamma/2\pi$ of the period of the rf so that a time increment $\gamma/2\pi f$ is generated per round trip. n is the number of cycles of mismatch in the overlap measurement. The objective of the mathematical analysis is to develop a method to make n = 0 and minimise and estimate the residual γ.

In eqn.(3), for l_2 equals to half a wavelength (*i.e.*, operation at resonant frequency) $B_2 l_2 = \pi$ rad. and $\tan B_2 l_2 = 0$. If at the same time the bond is very thin $B_1 l_1 << 1$ and $\tan B_1 l_1 \approx B_1 l_1 << 1$. Considering these conditions, γ in eqn.(5) reduces to

$$\gamma \approx -2(Z_1/Z_s) B_1 l_1 \qquad (7)$$

for thin bonds and resonant operations. One result is that γ

is a small negative quantity. At other operating frequencies, the contribution of tan B_2l_2 would be dominant in γ and would contribute to γ in t_M. We can use this dependence of t_M on frequency to eliminate n, the cycle mismatch. For this consider the measurement of t_M at a higher frequency f_H and a lower frequency f_L (for instance, at resonant frequency $f_H = f_r$ and at $f_L = 0.9f_r$). Then t_H is the measured time at f_H and t_L is the measured time at f_L. *i.e.*,

$$t_H = pt - (p\gamma_H / 2\pi f_H) + (n/f_H)$$
$$t_L = pt - (p\gamma_L / 2\pi f_L) + (n/f_L) \qquad (8)$$

where the same overlap condition (same n) has been maintained by shifting the repetition frequency slightly as the rf frequency is changed. Subtraction eliminates 't', the true travel time, as

$$\Delta t_M = t_L - t_H$$
$$= 1/f_L[\, n - (p\gamma_L/2\pi)\,] - 1/f_H[\, n - (p\gamma_H/2\pi)\,] \qquad (9)$$

Eqn. (9) expresses Mc Skimin's Δt criterion for finding n = 0 ie if f_H and f_L are measured or if t_H and t_L are measured, and if γ_L and γ_H are calculated from l_1, l_2, v_1, v_2, Z_1, $Z_2$and Z_s by equations (3) and (5) then there is only one possible value for Δt_M when n = 0 or we can say that if n = 0 is set in the measurement, the measured value of Δt_M will agree with the value calculated theoretically. It is important to note that it is sufficient if approximate values of velocities and densities are known to calculate the impedance $Z = \rho V$.

So in the following way one can calculate the correct value of Δt_M from experiment. From eqn. (9), for n = 0, we get

$$\Delta t_M = p/2\pi\ [(\gamma_H/f_H) - (\gamma_L/f_L)] \qquad (10)$$

In order to get the n = 0 condition experimentally, initially Δt_M is evaluated from eqn.(10) for different values of bond thicknesses B_1l_1. Then ΔT ($= T_L - T_H$) is experimentally

determined for different overlap conditions by taking time measurements for frequencies f_L and f_H. Assuming that the bond thickness is very small (thin bond) it can be seen that normally one value of experimental ΔT will be in the range calculated and this can be identified as the n = 0 case.

After getting the n = 0 case, bond thickness corresponding to that ΔT value can be calculated and from this γ_H can be calculated. After calculating γ_H the accurate travel time t_M can be calculated from eqn. (6).

One expects $\pi/2$ rad. of phase shift from the phase of the transducer to infinity; so the total diffraction contribution t_D to the travel time is always less than $\tau/4$ where τ is the period of the ultrasonic frequency. In eqn. (6) the diffraction delay time t_D must be added to t_M, the measured travel time before the true travel time $t^{(T)}$ is calculated. Recalling $t_M^{(T)}$ as the corrected measurement, we have

$$t_M^{(T)} = t_M + t_D$$

and

$$t_M^{(T)} = pt^{(T)} - (p\gamma/2\pi f) + (n/f) \qquad (11)$$

This is discussed at length by Papadakis [29].

A computer program written in BASIC to make the corrections numerically has been used to make the Mc Skimin criteria in our measurements.

2.5.3 Precision and accuracy of the PEO method

Precision and accuracy are two important terms in ultrasonic measurements. Precision is very important for monitoring small changes when only one parameter extrinsic to the measurement itself is varied. Accuracy is needed when many parameters, including some intrinsic to the measurement, are changed or when the actual value of a physical constant such as an elastic modulus is desired. In this case one should

consider all sources of error in travel time t_M.

In PEO method the precision of the measurement depends mainly on the investigator's visual acuity in overlapping the two echoes of interest. The probable error is about $\tau/100$ or smaller [31] where τ is the period of the rf in the burst although some measurement [28] indicate close to 1° of phase matching. For a 10 MHz wave travelling 100 μs, the error due to alignment is thus 10 ppm or less. Mc Skimin and Andreath [21] have reported precision of 1 part in 10^7 under certain conditions. Papadakis [32] has reported precision of 5 parts in 10^6. The other error in this case is the counting error of ± 1 once the overlap is set. If the overlap is observed for a particular cw frequency (F), for every multiples mF we get the overlap. The advantage in going to large multipliers is in minimising the influence of the ± 1 count error in the frequency counter, counting the cw frequency. With a larger frequency, ± 1 is a smaller fractional error.

When it comes to absolute accuracy, in addition to the above mentioned errors, there are other sources of errors like the phase angle γ due to the bond thickness, diffraction effects and variations in electronics. Considering all these, except the counting error, statistically with p = 1 for the worst case we get the error as [23,31]

$$e \leq 0.0150\tau \qquad (12)$$

So when frequency and round trip p is increased the error will reduce further.

When broad band pulses are used for measurement, all the errors except the counter error increase. It is still probable that e in eqn. (12) will be less than $0.1\tau_c$ where τ_c is the period of the centre frequency of the spectrum of the broad band pulse. For media of very low attenuation the error will be much lower.

2.6 Ultrasonic attenuation measurements

Ultrasonic attenuation α is measured as the logarithm of the ratio of the amplitudes of the ultrasonic wave at two distances along its propagation path. If one has a plane wave and a linear sensor that could not perturb the wave, then [23,36]

$$\alpha = \frac{\ln (A_1/A_2)}{x_2 - x_1} \quad \text{nepers / unit length}$$

$$= \frac{20 \log (A_1/A_2)}{x_2 - x_1} \quad \text{dB / unit length} \qquad (13)$$

where A_1 and A_2 are the amplitudes of echoes sensed at positions x_1 and x_2. However, one never has plane waves and nonperturbing sensors; so techniques as discussed below, have been developed to overcome these difficulties.

In the pulse technique we know that for an rf pulse several echoes will be produced. To generate a useful quasi-planar wave, the transducer must be many wavelengths in diameter. To minimise the perturbing effect of the transducer upon the echoes, the following conditions should be fulfilled: [23]

1. The rf burst should be at the fundamental or an odd harmonic of the resonance frequency of the piezo-electric transducer. This causes echo waves entering the transducer to return to the specimen in phase with the portion reflected at the bond, preventing destructive interference which would appear as excess attenuation.
2. The bond must be very thin to eliminate phase shifts within it, which would also have the above effects.
3. The electromechanical coupling coefficient of the piezoelectric transducer should be low to make sure that little energy would be absorbed in the transducer. This absorption will appear as excess attenuation.

4. The electrical impedance of the transducer should be mismatched with the electrical impedance of the receiving circuitry for the above mentioned reason.

The use of quarts crystal plates (X-cut for longitudinal, Y-cut for shear) of high impedance operated from 50 or 93 ohm systems is a good choice.

Various schemes have been developed to find the amplitudes of echoes. Comparison pulses run through an attenuation box and a delay line have been applied on alternate or dropped oscilloscope sweeps to find amplitude directly in decibels [33]. Another method involves displaying an electrically generated decaying exponential function curve and the echo train on alternate sweeps of an oscilloscope [34]. The decaying exponential is calibrated in decibels per microsecond. The slope of the decaying exponential can be varied so that the attenuation between any pair of echoes can be measured.

An automatic version of this attenuation measuring system has been developed by MATEC. In this two gates with variable delay are set on the two echoes of interest to sample them. The amplitude of the first echo is held constant by an AGC circuitry; and the amplitude of the second echo is sampled at its peak. Detected outputs obtained from a superhetrodyne system is used for this. A calibrated logarithmic amplifier converts the sampled amplitudes to decibels relative to the constant amplitude of the first echo. The decibel level is recorded on a built-in strip chart that has several calibrated scales and a variable baseline, so that small changes in attenuation can be measured at various total loss levels. In addition to the strip chart a readout meter also can be used.

Thus there are several attenuation measuring schemes to perform attenuation measurement depending on the application.

2.7 The present experimental setup

The block diagram of the experimental setup used in this work for measuring ultrasonic velocity using pulse echo overlap technique and attenuation by pulse comparison method is given in Fig.2.5. The main parts of the system are the MATEC Model 7700 pulse modulator and receiver together with Model 760 V rf plug-in, Model 122 B decade divider and dual delay generator, Model 110 high resolution frequency source, Model 2470B attenuation recorder, Model 70 impedance matching network, HIL Model 2722 frequency counter and HIL Model 5022 oscilloscope. In order to carry out temperature dependant studies a cryostat is used which will be discussed separately in the next section. In order to control the temperature of the cryostat a temperature controller (Lakeshore Model DR 82C) is connected to the setup.

The heart of this system is the pulse modulator and receiver with the rf plug-in. The pulse oscillator can be triggered either with an external sync pulse or with an internally produced one. It gives a peak power of 1 KW and gives a total receiver gain of 110 dB. It can provide rf frequency in the range 10-90 MHz. A video output from a super hetrodyne receiver and amplified rf echoes are provided in this unit. The cw signal from the high resolution frequency source is applied to the decade divider and dual delay generator, which is the key interfacing unit between the cw source and the pulsed oscillator in the PEO method. The cw source should be extremely stable in this case. The output of this cw source is highly stable and can be varied from 0.5 Hz to above 50 MHz. This cw source is operated at a frequency whose period is equal to the round trip time in the sample under investigation. The trigger signal for the pulsed oscillator is obtained from the divided sync output of the decade divider and dual delay generator. The output of the cw source is applied to this decade divider and dual delay

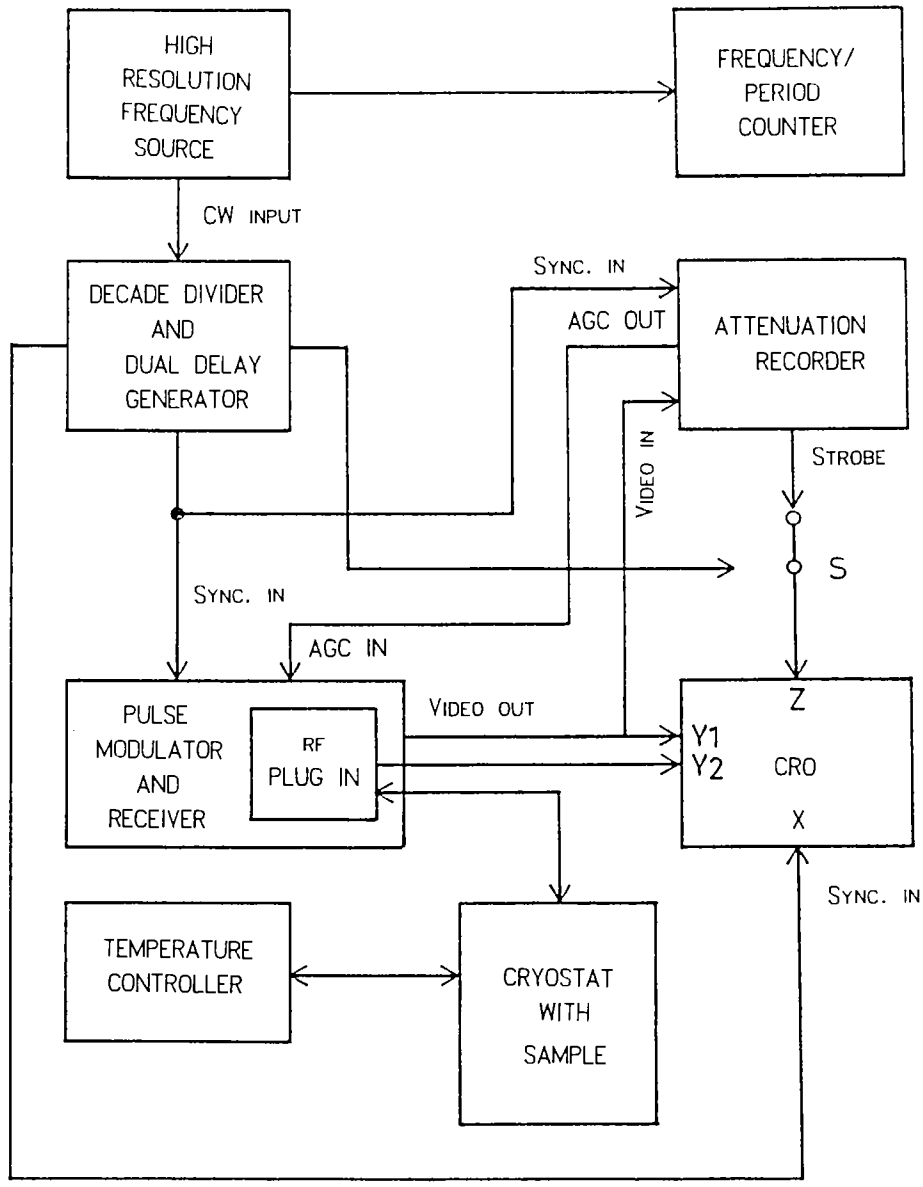

Fig.2.5 Block diagram of the experimental setup for measuring ultrasonic velocity by Pulse Echo Overlap technique and attenuation by Pulse Comparison technique simultaneously.

generator and the divided sync output is obtained by dividing this cw signal by 10, 100 or 1000 which can be selected. This division is used for a jitter free operation of the echoes and to allow all echoes to be attenuated before the next rf pulse is applied. Another output of this is the sweep sync out for the external trigger of the oscilloscope. This can be set in two modes; either equal to the divided frequency of the divided sync output or equal to the applied cw frequency itself. The first one is for getting a stable echo pattern on the oscilloscope and the latter for overlapping purpose. It also provides two strobe outputs whose width and distance can be controlled. This strobe signal is applied to the Z-axis of the oscilloscope for intensifying the desired echo pair. The frequency counter is directly connected to the high resolution frequency source to measure the frequency of the cw wave. For attenuation measurements the Model 2470B attenuation recorder is incorporated in the setup. This also has a strobe output for selecting the desired echo pair for attenuation measurement. It provides the necessary AGC output to connect to the pulse modulator and receiver for keeping the amplitude of the first echo to be constant during the measurement. The video output signal is applied to this. The calibrated logarithmic amplifier converts the amplitudes of the two echoes to the corresponding decibel values. The attenuation value can be either recorded in a strip chart by an x-t recorder provided or can be seen on a pannel meter. The sensitivity of the attenuation recorder can be varied. There is provision for adjusting attenuation offset which provides electronic cancellation of high attenuation values when small changes in attenuation are to be measured or recorded. Using this arrangement the maximum sensitivity range of 0.01 dB/division can be used while the attenuation is very high like 20 dB or so.

The transducer is bonded to the sample using proper

bonding medium. This is connected to the pulse output of the system through an impedance matching network in order to match the impedances of the cable and the transducer for optimum power transfer. Keeping the sweep sync. out at the divided position we can observe the echo pattern on the oscilloscope screen. Then using the strobe signals from the decade divider and dual delay generator, which is connected to the Z-axis of the oscilloscope, we can select any echo pair by blanking out the other ones. Now the approximate time difference between the two echoes are noted from the oscilloscope screen and the frequency of the high resolution frequency source is adjusted so that its period is equal to the time difference. Then the sweep sync. out is changed to the direct position. Now we can see that the echoes are approximately overlapped. By adjusting the cw source we can overlap the two selected rf echoes exactly. The overlapping can be done with the detected echo pattern (video out) also. Now the frequency can be measured from the frequency counter from which the travel time can be determined. By taking the reading for six or seven overlaped conditions and repeating again for a lower frequency ($0.9f_R$) Mc Skimin Δt criterian can be applied for getting corrected velocity.

For measuring attenuation, the video output is connected to the attenuation recorder also. Now using the strobe signal from this attenuation recorder as the intensifying signal for the oscilloscope we can select any desired echo pair. Switch S in Fig.2.5 is used to select the desired strobe. This enables to open a gate so that the amplitudes of these two echoes can be sampled and the attenuation can be read out or recorded on the chart recorder.

In order to make temperature dependant studies, a temperature controller (Lakeshore Model DR 82C) is connected to the cryostat. This is a three mode control (Proportional - Integral - Derivative (PID)) and there is provision to use two

temperature sensors - one as control sensor and the other as sample sensor. Either platinum RTD or silicon diode sensors can be used with the system.

Paraffin Oil, Motor oil SAE 40, Nonaq stop cock grease, Silicone grease etc. are found to be very good bond materials for longitudinal measurements at room temperature as well as at relatively high temperatures. Silicone grease and Nonaq stop cock grease are good for low temperature measurements. For transverse waves silicone grease is found suitable below 100°C. The acoustical impedance of Paraffin oil and Motor oil SAE 40 are accurately determined by measuring ultrasonic velocity at 2MHz in them and density and found to be 1.167×10^6 Kg/m^2 Sec. and 1.345×10^6Kg/m^2 Sec.

2.8 Design and fabrication of the cryostat

In any low temperature experimental setup the heart of the system is a cryostat. Since a well designed cryostat is necessary for the proper cooling of the sample, a bath type cryostat has been designed and fabricated, for making low temperature measurements down to liquid nitrogen temperature. In ultrasonic experiments, typical size of the sample is $\approx$ 1 cm^3 and most of the work is on single crystals. So it is most essential that the cooling rate of the sample is very small to avoid cracking of the sample. Moreover, if the cooling rate is very high, there will be thermal gradients within the sample which can cause many undesired effects. Thus a slow and uniform cooling/heating is necessary. In addition, around critical regions the temperature variation should be extremely slow. Taking all these factors into account we have designed and fabricated a stainless steel bath type cryostat.

Fig.2.6 gives a cross sectional view of the cryostat. The main parts are two stainless steel vessels. The choice of thin stainless steel sheets minimises conduction losses. The first chamber is a double walled vessel A of

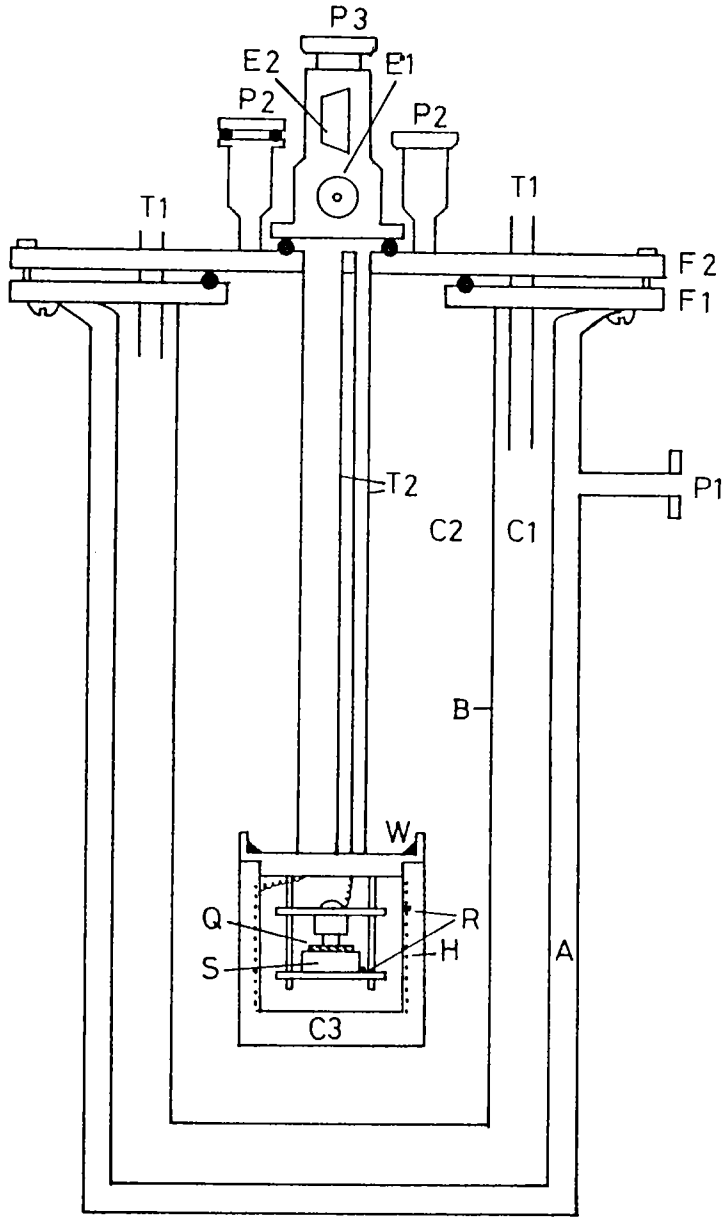

Fig.2.6 Cross section of the cryostat (not to scale)

A - Double walled outer vessel, B - Single walled inner vessel, C1 - Chamber 1, C2 - Chamber 2, C3 - Sample chamber, E1,E2 - Electrical I/O, F1,F2 - Flanges, H - Heater coil, P1,P2,P3 - Evacuation ports, Q - Transducer, R - Temperature sensors, S - Sample, T1- LN_2 guide tube, T2 - Connection tube, W - Wood's metal joint.

approximately 1 m in length and 20 cm in diameter. There is a separation of about 2 cm between this double wall. This space can be evacuated through a port P1 provided on the chamber by connecting it to a rotary vacuum pump. This evacuation further reduces heat loss. This chamber is fixed to an upper annular flange (F1). The second vessel (B) is a single walled stainless steel one and this is also fixed to the flange F1. Both vessels are well polished to avoid radiation losses. So there is a space between these two vessels (chamber C1); and there are two tubes (T1) placed diametrically opposite on the flange F1, which guides to chamber C1, through which liquid nitrogen can be poured. There is an upper flange (F2) which rests over a rubber 'O' ring placed on the annular flange. Two stainless steel tubes (T2) are fixed at its one end to the centre of this upper flange. The other end of this tube is connected to the sample chamber (C3). At the upper side of the flange there are two ports (P3) which can be used either to pour liquid nitrogen into the inner chamber C3 or to evacuate this. At the top of this stainless steel tube, on the flange, there is another port (P3) on which all electrical connectors are fixed. This is also fixed on the upper flange with rubber 'O' ring. The evacuation of the sample chamber is also done through this port. The stainless steel tube takes all the electrical connections from the sample chamber to the appropriate connectors and at the same time it acts as the path to evacuate the sample chamber.

Inside the sample chamber there are small discs which acts as the platforms to place the sample (S) as well as the spring mechanisms for fixing the transducer (Q) and for making electrical contact. These are resting on three long screws and by adjusting the nuts supporting the platform, it can be aligned. Covering this there is a heater (H) wound on a copper chamber. The sample chamber can be vacuum sealed, after making necessary arrangements, using Wood's metal. There are

two temperature sensors (R) in the sample chamber; one is placed very near the heater coil which acts as the control sensor and the other very close to the sample, known as the sample sensor. The control sensor is used to control the temperature while the sample sensor is used to monitor the temperature of the sample very accurately. The rf cable is taken through the small stainless steel tube (T2) and terminates at the BNC (E1) on the top. The terminals of the sensors are taken out through a 9 pin D-type connector (E2) and the heater power from the temperature controller is applied through a 3 pin connector. All these connectors are on the port P3. Thus P3 is used simultaneously for evacuating the sample chamber and taking necessary electrical connections.

2.8.1 Preaparation of Wood's metal

Since ordinary 'O' rings cannot be used at low temperatures in the cryostat we have used Wood's metal to seal the sample chamber for evacuating it after the sample is mounted. Wood's metal is an alloy of Cd, Sn, Pb and Bi in the ratio 1:1:2:4 by weight. For preparing this we have melted appropriate amount of Sn and Bi first. Then Cd is added and the mixture is melted. Finally Pb is added and melted. The resultant alloy has a melting point of about 60°C. This is found ideal for vacuum sealing at low temperature regions.

2.9 System in operation

After placing the sample in the sample chamber properly with transducer bonded on it the sample chamber is sealed with Wood's metal. Generally port P1 and P3 are connected to the rotary vacuum pump, and the sample chamber and the space between the double walls are evacuated. Evacuation of the sample chamber prevents moisture from condensing on the sample while cooling. All the electrical connections are made and the velocity is measured. For cooling

liquid nitrogen is poured first in chamber C1 through one of the tubes. For increasing the efficiency the other tube is connected to the second chamber C2 using a rubber tube so that the cool nitrogen vapour is regeneratively used to cool the second chamber and the sample chamber. By this procedure we can attain a temperature of about 180K. Then liquid nitrogen is poured in the second chamber (C2) through P2 and the sample is cooled to ≈ 80K. In this setup a cooling rate of ≈ 1K/min or less can be attained. Thus by slowly varying the temperature, we can adjust the overlap of echoes on the oscilloscope screen and the velocity changes can be observed. This cryostat is very useful in the temperature range 80-310K.

For measurements in the high temperature region, *i.e.*, above room temperature, there is an oven and we can place the sample inside this instead of the cryostat. Using this a temperature range from room temperature to about 500K is possible. In order to control the sample temperature accurately there is another arrangement. A small glass vessel on which a heater is wound has been fabricated. The sample can be placed inside this and for proper heating of the sample a liquid like paraffin oil or silicone oil can be filled in this. The sample is thus immersed in this liquid and the temperature sensor is placed very near the sample. This is placed inside the closed oven and using the temperature controller the sample temperature can be very accurately controlled within ± 0.1K or better. So the system enables us to vary the sample temperature in the range 80-500K.

A photograph of the experimental setup is shown in Fig.2.7.

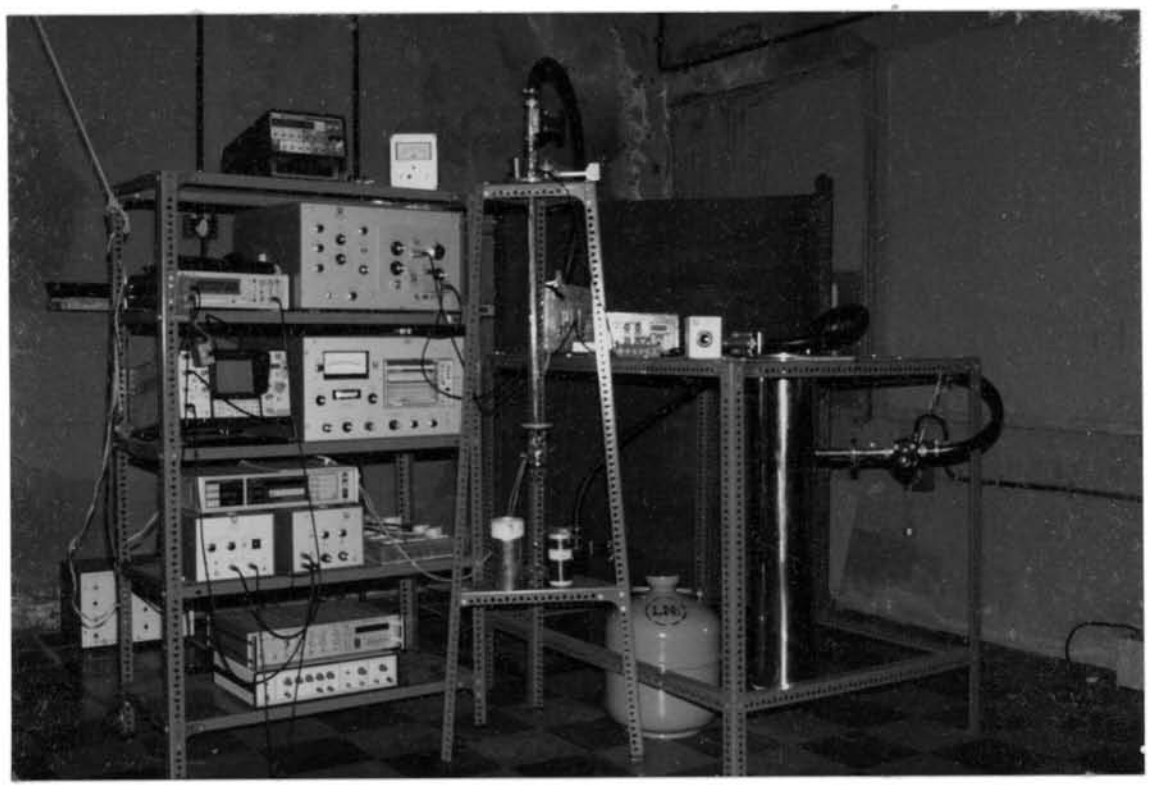

Fig.2.7 Photograph of the equipment

References

1. G.Sorge and U.Straube, *Acta. Physica Slovaca* **36,** 49 (1986).

2. G.Pakulski, *Ferroelectrics* **48,** 259 (1983).

3. H.Beige and G.Schmidt, *Ferroelectrics* **41**, 39 (1982).

4. L.Brillouin, *Ann. Phys. (Paris)* **17,** 88 (1922).

5. A.S.Pain in *Light scattering in solids* (Ed. M.Cardona),Springer, Berlin (1975).

6. D.A.Berlincourt, D.R.Curran and H.Jaffe, *in Physical Acoustics* Vol I, Pt.A, (Ed. W.P.Mason), Academic Press, New York (1964).

7. D.L.White in *Physical Acoustics* Vol I, Pt.B, (Ed. W.P.Mason), Academic Press, New York (1964).

8. J.de Klerk in *Physical Acoustics,* Vol.**IV**, Pt.A (Ed. W.P.Mason) Academic, New York (1966).

9. B.Lüthi and W.Rehwald in *Structural Phase transitions I* (Eds. K.A.Müller and H.Thomas) Springer Verlag, Berlin (1981).

10. D.I.Bolef in *Physical Acoustics* Vol IV, Pt A, (Eds.W.P.Mason and R.N.Thurston), Academic Press, New York (1966).

11. D.I.Bolef and J.G.Miller in *Physical Acoustics* Vol VIII, (Eds.W.P.Mason and R.N.Thurston), Academic Press, New York (1971).

12. A.G.Beattie, H.B.Silsbee and E.A.Uchling, *Bull. Amer. Phys. Soc.* **7**, 478 (1962).

13. G.A.Alers in *Physical Acoustics* Vol.IVA, (Ed. W.P.Mason) Academic Press, New York, (1976).

14. F.Birch, *J. Geophys. Res.* **65**, 1083 (1960).

15. H.B.Huntington, *Phys. Rev.* **72**, 321 (1947).

16. W.P.Mason and H.J.Mc Skimin, *J. Acoust. Soc. Am.* **19**, 464 (1947).

17. J.K.Galt, *Phys. Rev.* **43**, 1460 (1948).

18. A.V.Granato, J.deClerk and R.Truell, *Phys. Rev.* **108**, 895 (1957).

19 H.J.Mc Skimin, *J. Acoust. Soc. Am.* **33**, 12 (1961).

20. H.J.Mc Skimin and P.Andreatch, *J. Acoust. Soc. Am.* **34**, 609 (1962).

21. H.J.Mc Skimin and P.Andreatch, *J. Acoust. Soc. Am.* **41**, 1052 (1967).

22. E.P.Papadakis, *J. Acoust. Soc. Am.* **40**, 863 (1966).

23. E.P.Papadakis in *Physical Acoustics* Vol.XII (Eds. W.P.Mason and R.N.Thurston) Academic Press, New York (1976).

24. N.P.Cedrone and D.R.Curran, *J. Acoust. Soc. Am.* **26**, 963 (1954).

25. J.E.May Jr., *IRE Natl. Conv. Rec.* **6**, Pt.2, 134 (1958).

26. E.P.Papadakis, *J. Appl. Phys.* **35**, 1474 (1964).

27. E.P.Papadakis, *J. Acoust. Soc. Am.* **42**, 1045 (1967).

28. D.H.Chung, D.J.Silversmith and B.B.Chick, *Rev. Sci. Instrum.* **40**, 718 (1969).

29. E.P.Papadakis in *Physical Acoustics* Vol.XI (Eds. W.P.Mason and R.N.Thurston) Academic Press, New York (1975).

30. E.P.Papadakis, *J. Acoust. Soc. Am.* **45**, 1547 (1969).

31. E.P.Papadakis, *J. Acoust. Soc. Am.* **52**, 843 (1972).

32. E.P.Papadakis, *IEEE Trans.* **SU-16**, 210 (1969).

33. R.L.Roderick and R.Truell, *J. Appl. Phys.* **23**, 267 (1952).

34. B.B.Chick, G.Anderson and R.Truell, *J. Acoust. Soc. Am.* **32**, 186 (1960).

35. R.Truell, E.Elbaum and B.B.Chick in *Ultrasonic Methods in Solid State Physics*, Academic Press, New York (1969).

Chapter 3

ULTRASONIC INVESTIGATIONS ON THE HIGH Tc SUPERCONDUCTOR Bi-Sr-Ca-Cu-O

3.1. Introduction

The very important phenomenon of superconductivity was discovered in 1911 by Kammerlingh Onnes [1], but until recently it was strictly a very low temperature phenomenon. The discovery of the new oxide superconductors with transition temperatures upto 126K has generated tremendous excitement for the following two reasons. First they open a new temperature realm for superconducting devices and components which should have widespread commercial applications, and these potential benefits have attracted phenomenal attention from the public. Second, the conventional electron-phonon interaction appears not to be the origin of superconductivity in these materials, leaving the fundamental physics open to further investigations. Thus vigorous research activities have been focussed on the properties of these oxygen deficient perovskite structured ceramics which exhibit superconductivity at remarkably high temperatures. Thus these exotic materials have been the subject of intense research by a large number of scientists from a wide range of fields of basic and applied research. Within a short period, the highest known transition temperature has been raised from 23.3K of the transition metal alloy Nb_3Ge [2,3] to nearly 126K in Tl-Ca-Ba-Cu-O. The ground work for this extraordinary increase in Tc was done by Bednorz and Müller in 1986 [4] who discovered that multiphase mixtures of BaO, LaO and CuO with the nominal composition $Ba_xLa_{5-x}Cu_5O_5$ [3-7] is superconducting around 30K. The superconducting phase was subsequently identified as $La_{2-x}Ba_xCuO_4$ with the highest transition temperature occurring at $x \approx 0.15$ [5]. It was later found that doping with Sr in place of Ba produced higher Tc's

of the order of 36K [6]. Shortly thereafter another major breakthrough was achieved when Wu *et al.* [7] found superconductivity above the boiling point of liquid nitrogen in multiphase samples with the nominal compositions $Y_{1.2}Ba_{0.3}Cu_2O_{4-x}$ and $Y_{0.6}Ba_{0.4}CuO_{3-x}$. Several groups identified the single phase compound responsible for superconductivity as $YBa_2Cu_3O_{7-x}$ [8-10] with Tc in the 90K range. Within a short period, a number of rare earth based copper oxide ceramics have been synthesised with Tc in the 30K and 90K ranges. Superconductivity at temperatures above 100K has been obtained in Bismuth and Thallium based oxide systems Bi-Ca-Sr-Cu-O (Tc ≈ 110K) [11,12] and Tl-Ca-Ba-Cu-O (Tc ≈ 125K) [13] in 1988. These systems do not contain any rare earth which were earlier considered essential for the occurrence of high Tc. A great deal of work has gone into characterising these materials and into the search for newer high Tc compounds.

One of the central features of the conventional superconducting state is that there exists an energy gap in the excitation spectrum for electrons, which was first identified in specific heat measurements. Below the superconducting transition, the electronic term in the specific heat is found to be of the form $\exp(-\Delta/k_BTc)$ which is characteristic of a system with a gap in the excitation spectrum with energy 2Δ. The gap is directly related to the superconducting order parameter, and hence we might expect that $\Delta \rightarrow 0$ as $T \rightarrow Tc$. Another very important discovery in the case of conventional superconductors is that the superconducting transition temperature depends on the isotopic mass of the material. The effect demonstrates that lattice vibrations play an important role in the formation of the superconducting state. For the new oxide superconductors there are some important points to note with regard to Cooper pairing and the BCS theory. The near absence or marginality of

isotope effect in these materials, especially in YBCO (123) compound [14-16] is puzzling both to experimentalists and theorists alike. The question is whether these are phonon mediated BCS superconductors or not. A number of theoretical models ranging from conventional phonon mediated coupling [17,18] to a variety of exotic mechanisms involving plasmons [19,20], charge transfer excitations [21], polarons and bipolarons [22] and a new electronic ground state [23] have been put forward. Despite all the efforts a clear picture of the mechanism of the phenomenon is yet to evolve.

All high Tc superconducting cuprate systems exhibit certain important common features in their properties [24-26]. All of them possess perovskite type structures. At temperatures near Tc these are orthorhombic with a structural transition to a tetragonal phase at high temperatures. They all have low dimensional characteristics, the two dimensional $Cu\text{-}O_2$ sheets being common to them. In 1-2-3 materials a pair of a-b CuO_2 planes sandwiches an a-b CuO plane. In the orthorhombic phase the oxygens in this plane order to form CuO chains along the b direction. The Cu-O bonds are highly covalent and the distances are generally in the $1.90 \pm 0.50 A^{\circ}$ range. The coordination of Cu is essentially square planar. Since these materials superconduct in directions parallel to the copper planes, many theorists believe that this unusual planar arrangement contributes significantly to their remarkable electronic properties. Selected physical parameters of important HTSC materials are tabulated in Table 3.1 [31].

3.2 Ultrasonic studies in high Tc superconductors

The measurement of sound velocity can provide results that are difficult to obtain by other methods. Sound wave propagation can also be used to confirm the results of other measurements. Studies of elastic properties in conventional superconductors, has in the past, been of great

Table 3.1

Different high Tc materials and their physical properties.

Chemical Composition	Label	Tc (K)	axbxc (A°)	density (Kg/m^3)
$La_{1-x}Sr_xCuO_{4-y}$	LSCO	37	3.78x3.78x1.32	6990
$YBa_2Cu_3O_{7-x}$	YBCO	95	3.82x3.88x1.17	6370
$YBa_2Cu_4O_8$	YBC4O	80	3.84x3.87x27.2	6110
$Bi_2Sr_2CuO_6$	Bi2201	9	5.36x5.37x24.6	7045
$Bi_2Sr_2CaCu_2O_8$	Bi2212	85	5.41x5.42x30.9	6450
$Bi_{1-x}Pb_xSr_2Ca_2Cu_3O_{10}$	Bi2223	110	5.40x5.40x37.2	6270
$Tl_2Ba_2CaCu_2O_8$	Tl2212	99	3.86x3.86x29.3	7470
$Tl_2Ba_2Ca_2Cu_3O_{10}$	Tl2223	125	3.85x3.85x33.9	6960
$Nd_{1-x}Ce_xCuO_{4-y}$	NCCO	24	3.95x3.95x12.1	7370

importance in probing their bulk properties. Ultrasonic attenuation measurements lead to determination of the energy gap parameter in them. According to Bardeen, Cooper and Shrieffer (BCS theory), for the case $ql >> 1$, where q is the wave number of the acoustic wave and l is the electron mean free path [27],

$$\alpha_s/\alpha_n = 2f(\Delta) \qquad (1)$$

where f is the Fermi function, Δ is the energy gap and α_s and α_n are the ultrasonic attenuation in superconducting and normal states of the material respectively. One of the sources of measurable attenuation in a metal at low temperatures is electron-phonon interaction. When electron mean free path is smaller than the sound wavelength the attenuation is proportional to l. In the superconducting state, the sound waves interact only with excited quasi particles whose population in a BCS superconductor decays exponentially with temperature. The attenuation should fall as temperature T is lowered below Tc and should be proportional to $\exp(-\Delta/kT)$ if $T<<Tc$. Later it has been proved that this is true for all values of ql. Thus the ultrasonic attenuation due to electron-phonon coupling in the superconducting state is expressed as [28]

$$\alpha_s(T) = \alpha_n \frac{2}{\exp[\Delta(T)/k_B T] + 1} \qquad (2)$$

where k_B is the Boltzmann's constant.

Since ultrasonics is a very good tool to probe the bulk properties of materials, a great deal of work has been done in using ultrasonic technique to investigate the physical properties of high Tc superconductors and a number of papers have appeared in literature. Since the discovery of HTSC in the copper oxide system, there have been a number of reports on the Y-based and La-based materials, some of which show anomalous elastic properties at the superconducting transition. Generally the measurements can be made for two purposes. (i) To measure absolute values of velocities and

elastic moduli. (ii) To study the general temperature dependence of velocity and attenuation. Ultrasonic studies on high Tc materials are limited primarily to ceramic specimens because of the difficulties in growing large enough single crystals. Available single crystals are usually in the form of thin platelets that do not allow the determination of the whole set of the elastic constants, and because of small dimensions, do not allow precise measurements of elastic constants. Ultrasonic waves get attenuated greatly while being propagated through porous ceramic samples. In YBCO samples it has been estimated from Pippard's theory [30] that $\alpha_n \sim 7 \times 10^{-7}$ dB/cm for longitudinal waves of 10MHz [29,43]. This value is much lower than the resolution of the measuring equipment. The part of the attenuation that can be taken as absolute, ie independant of external conditions, consists mainly of scattering from grain boundaries and geometric scattering. The former source is responsible for most of the attenuation and is, in the MHz range, of the order of a few dB/cm [31]. Dominec *et al.* [32] have shown in Bi2212 that this is in agreement with a general model of scattering from grain boundaries.

The major work in single crystalline LSCO material has been done by Migliori *et al.* [33]. The bulk modulus as determined from high pressure experiments [34] ranges from 135 to 211 GPa in LSCO. This is much higher than the results reported from ultrasonic experiments [31]. Similar observations have been made in YBCO. The values of Bulk modulus in YBCO ranges from 100 to 189 GPa and from 155 to 176 GPa for various ReBCO samples [34] where Re stands for rare-earth. It has been seen that the values from high pressure experiments are much higher than those from ultrasonic experiments and the moduli increases with higher oxygen content [31]. The increase of oxygen content correlates with the increase of Tc, of the energy gap, of the frequency of a certain Raman mode and of the Debye temperature. The

absolute velocities in Bi based samples have been reported only in Bi2212 [31]. Fanggao *et al.* [35] found a higher shear velocity and a lower longitudinal velocity in a quenched sample of Bi2212 that had a higher oxygen content than a slowly cooled sample. All experiments show that moduli are lowest in Bi2201 and highest in Bi2223 samples.

3.3 Temperature dependence of ultrasonic velocity and attenuation

When solid matter cools, it usually becomes stiffer. Consequently elastic constants and sound velocities increase. Then the normal change of sound velocity can be written as [36]

$$\frac{\Delta V}{V} = \frac{\gamma^2 T^4}{\rho V^2} \frac{12\pi^4}{5\,\Theta^3} k_B n$$

at low temperatures ($T < 10K$)

$$\frac{\Delta V}{V} = \frac{-TC_P(T)\gamma^2}{\rho V^2}$$

at higher temperatures (3)

where C_P is the specific heat, k_B the Boltzman's constant, n number of atoms per unit volume, Θ Debye temperature and γ the effective Grüneisen parameter related to the mode of propagation. The velocities in all HTSC materials except LCO and LSCO increase from room temperature to 4K by 4-10%. Deviations from this general behaviour are caused by phase transitions and similar phenomena in the material. In the case of HTSC the anomalies may be categorised into two; the anomalies around the superconducting transition Tc and those above Tc. The important effect in YBCO is the thermal hysteresis of the velocity, *i.e.*, that the velocity is higher higher upon cooling than upon subsequent heating. This is seen from 230 to 235K in some samples [31]. Its magnitude is upto 8%. It is more pronounced in coarsegrained samples than in fine grained ones. It depends on the oxygen content and is

largest for $\delta \approx 0.3$. Its origin is still unclear. It has been attributed to a phase transition, twinning, twin boundary movements, reordering of oxygen and relaxation of tension on grain boundaries. Similar hysteritic effects also appear in thermal conductivity [37]. There are a number of published data dealing with the anomaly in ultrasonic velocity and attenuation at Tc as well as above Tc [38-56]. The peak in velocity between 170 and 240K in YBCO has been investigated and attributed to the oxygen ordering along the one dimensional Cu-O chain [47,55]. In one case of BSCCO samples also, anomaly in velocity and attenuation have been reported [46] and they have been attributed to a second order phase transition. Attenuation also shows similar behaviour.

There are several reports showing a discontinuity in the velocity curve at Tc in YBCO and LSCO. Bishop *et al.* [40] have reported a pronounced hardening of the sound velocity of $\sim$ 1000 ppm that starts at the superconducting transition which cannot be explained by the standard thermodynamics of the BCS model which describes conventional superconductors. Abd-Shukor [38] reports an anomaly in the transverse velocity in YBCO which he attributes to volume preserving transitions such as superconducting transition. Xu *et al.* [41] and Bhattacharya *et al.* [42] report anomalous ultrasonic attenuation in YBCO at Tc as well as at high temperatures. The anomaly at Tc cannot be correlated to the BCS type mechanism. The anomalies at high temperatures suggest the existence of a structural transition in that temperature region. They have observed a peak at about 10K below Tc in YBCO for longitudinal waves of frequency 10 MHz. Sun *et al.* [56] have attributed this peak to a relaxation process, because the peak position could be moved to Tc by increasing the frequency of ultrasound and the height of the peak becomes larger at the same time. This relaxation peak seems to have no relationship with superconductivity and may be caused by phonon-phonon coupling in grain boundaries.

3.4 Ultrasonic measurements on Bi-Sr-Ca-Cu-O superconductors

The Bismuth family of oxide superconductors have the general formula $Bi_2Sr_2Ca_{n-1}Cu_nO_{4+2n}$ with n = 1, 2 and 3. Only the compound with n = 3 is found to have a Tc over 100K. The other two members of the family, *i.e.*, those with n = 1 and n = 2 differ greatly from the one with n = 3 in their Tc values and lattice parameters. The three Bi systems and their Tc values are shown below.

$Bi_2Sr_2Ca_{n-1}Cu_nO_{4+2n}$			
n = 1	$Bi_2Sr_2Cu_1O_6$	20K	2201 phase
n = 2	$Bi_2Sr_2CaCu_2O_8$	80K	2212 phase
n = 3	$Bi_2Sr_2Ca_2Cu_3O_{10}$	110K	2223 phase

All these phases are found to be present when a Bi superconductor is prepared. Both the low temperature and high temperature phases are orthorhombic in structure. Many attempts have been made, including adding and doping different elements, to stabilise the high Tc 2223 phase. Takano *et al.* [57] succeeded in increasing the amount of the 2223 phase by the substitution of Pb for Bi. The increase of Tc by the substitution of Sb and Pb has been reported by Liu *et al.* [58]. The melting point of the Pb doped material decreases as the Pb concentration increases, and the synthesis temperature decreases. Thus the addition of Pb stabilises the 110K superconducting phase and it is best when Pb concentration x is in the range 0.2 to 0.3 for samples with general formula $Bi_{2.1-x}Pb_xSr_2Ca_2Cu_3O_y$ [59-62]. Addition of Pb beyond 0.4 leads to the formation of Ca_2PbO_4 which tends to deteriorate the formation of the superconducting phase [59].

Eventhough the studies on high Tc superconductors are limited primarily to ceramic specimens because of the difficulty in obtaining large enough single crystals, acoustic

properties of high Tc materials have been investigated extensively. Lesser amount of work has been reported on the Bi system compared to YBCO.

The studies of ultrasonic velocity and attenuation in Bi system do not show a uniform behaviour. The temperature where velocity and attenuation anomalies occur seem to vary from sample to sample. However, in this case also the anomalies can be divided into two as that around Tc and that above Tc. In most cases no significant anomaly around Tc is reported. Dominec *et al.* [31] observes no peculiarities either around Tc or at any other region due to the low resolution of the equipment. Some papers show ultrasonic anomaly around Tc in Bi2223 system. Reports on the anomaly around Tc have been published in other Bi systems also [46,65,68]. Dong *et al.* [43] have studied Bi samples with preferred orientations obtained by hot pressing after sintering in air and found that a tendency of softness and instability in the lattice begins to occur in the range between 10 and 50K above Tc. They have reported that anomalies in attenuation are present at transition temperature of all superconducting phases, which cannot be interpreted as due to coupling between acoustic phonons and electrons. The possibilities of strong coupling between acoustic phonons and optical phonons and between optical phonons and electrons are speculated. The anomalies in attenuation around Tc may be due to the enhancement of coupling between acoustic phonons and optical phonons, driven by superconducting transitions in which the optical phonon-electron interaction could occur. Thus the anomalies around Tc may be evidence that the coupling between optical phonons and electrons is responsible for high Tc superconductivity. Anomaly in ultrasonic velocity for Pb doped Bi2223 sample has been reported by other workers also [53] showing a phase transition like phenomenon. Hysteresis in velocity at temperature below 250K has been reported on these systems by several workers [53,63-65].

Coming to the anomalies above Tc, many workers report at least two peaks above Tc in attenuation and velocity. The first one is the pretransition anomaly usually occuring between 10 and 50K above Tc (ie in the region 120-170K) and is an important feature of Bi based samples. This is found to be present in all superconducting phases; even in phases with lowest Tc. The second one is a peak occuring between 200 and 260K. A slope change in sound velocity around 200K and 260K have been reported by several workers [43,50-53]. Sharp anomalies in velocity, attenuation and specific heat have been reported in this range by Yusheng *et al.* [66,67]. He *et al.* [44] reported a remarkable sudden rise in both velocity and attenuation near 209K. Specific heat measurements on the same samples showed clear anomaly at about 210K and temperature dependant X-ray studies revealed a sudden increase in lattice constant c near 210K implying some changes in fine structure. Hu *et al.* [46] also have reported ultrasonic velocity and attenuation anomaly at 240K. This also is associated with a specific heat jump at the same temperature. So a second order phase transition, which occurs between 200 and 250K, may be the cause for this anomaly and this temperature is highly sample dependant.

In this respect for resolving the controversies we wanted to investigate these in more detail. We have carried out ultrasonic velocity measurements in a Pb doped Bi superconductor, with Pb = 0.3 since this doping level gives the best single phase superconducting sample.

3.5 Experimental

3.5.1 Sample preparation

Conventional solid state reaction of the component oxides in stoichiometric proportions does not yield single phase samples of Bi-based high Tc superconductors. The reason for this appears to be the relatively low melting point of Bi_2O_3 as compared to the other component oxides which leads to

a loss of Bi and to intergrowth of different phases. However, through partial substitution of Pb for Bi, intergrowth of different phases can be suppressed. The volume fraction of the high Tc phase in a sample can be enhanced to 90% by Pb doping.

Sintered polycrystalline samples of Pb doped BSCCO have been prepared by the well established solid state reaction method. Powder samples of Bi_2O_3, $SrCO_3$, $CaCO_3$, CuO and PbO are mixed well in the required atomic proportions and calcined at 800°C for about 20 hours. The calcined material has been crushed, powdered and then made into pellets of ≈ 10mm diameter at a pressure of about 4 metric tonns. The pellets are then sintered at 820°C for nearly 100 hours. All treatments are done in air and air quenching is done after sintering. In Pb doped samples the Pb atoms go into Bi sites. The best sample is obtained when the Pb concentration x is in the range 0.2 to 0.3 for samples with general formula $Bi_{2.1-x}Pb_xSr_2Ca_2Cu_3O_y$. The sample used in the present study is with x = 0.3 or the sample has the formula $Bi_{1.8}Pb_{0.3}Sr_2Ca_2Cu_3O$. Ultrasonic measurements require good samples with minimum porosity and voids so that comparatively good echoes can be obtained.

Superconducting property of these samples have been verified by making electrical resistivity measurements. It is found that the samples undergo superconducting transition at around 110K.

3.5.2 Ultrasonic measurements

The sample of approximately 5mm thickness and 10mm diameter is chosen and the faces are carefully polished so that they are plane and parallel to each other. A 10 MHz longitudinal transducer has been mounted over the surface of the sample with silicone grease as the bond. The sample is placed inside the cryostat which is described in the previous chapter. More than three good echoes have been obtained and

the travel time between the successive echoes have been measured as explained in the previous chapter. The velocity is calculated after measuring the thickness of the sample. In this particular case no Mc Skimin correction has been applied to the velocity data because it is a ceramic material for which the relative change in velocity with temperature, rather than the absolute velocity is important. The measurements have been carried out from room temperature (300K) to about 80K. In order to assure a uniform temperature distribution within the sample a cooling rate of less than 0.5K/min has been used in the measurement.

3.6 Results and discussions

Ultrasonic velocity data taken as a function of temperature in the range 300-80K is plotted in Fig.3.1. In this figure there is a striking clear phase transition like anomaly which starts at about 120K and extends beyond Tc to about 107K. The superconducting transition is occurring in this transition region. This large anomaly cannot be interpreted in terms of BCS theory. Similar effects have been observed by other workers also [43,46,53]. So it is evident that this can be a structural phase transition due to mode softening which starts just above the superconducting transition and the superconducting transition is occurring at the background of this transition. Dong *et al.* [43] also found that tendencies of softness and instability in crystal lattice begins to occur in the range between 10 and 50K above Tc. They have also suggested that the superconducting transitions are present on the background of rapid decrease in attenuation with the decrease of temperature, which seems to indicate the existence of strong superconducting fluctuation above Tc. In addition to this we have obtained a clear change in slope in the velocity curve at around 210K and 250K. Similar results have been obtained by other workers also [43, 50-53]. Anomalies in specific heat in the same temperature ranges also

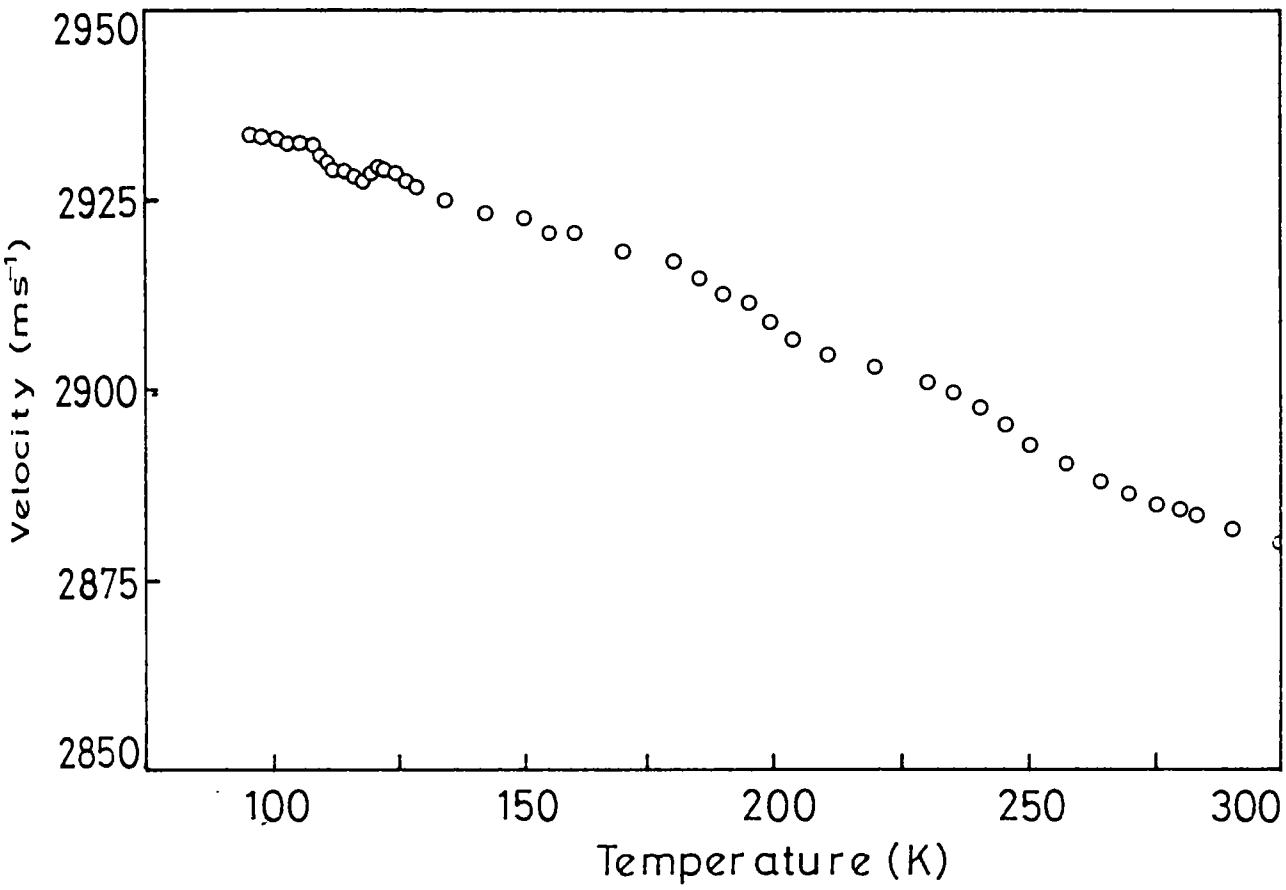

Fig.3.1 Variation of longitudinal ultrasonic velocity in $Bi_{1.8}Pb_{0.3}Sr_2Ca_2Cu_3O_y$

have been reported [44,46]. Temperature dependant X-ray studies also show an increase in the lattice constant c near 210K [44]. This may be due to some second order type transition occurring at this temperature region.

3.7 Conclusions

The ultrasonic velocity as function of temperature shows anomalous behaviour around Tc and above Tc. A phase transition is occurring around Tc which starts above Tc at about 120K. The superconducting transition is occurring in the background of this transition. So this softening may be associated with the superconducting transition. There is also slope changes in the velocity curve around 210K and 260K which is an evidence for the existence of some phase transitions above Tc.

References

1. H.Kammerlingh Onnes, *Leiden. Comn.* **120b, 122b,124c**, (1911).

2. M.R.Beasley and T.H.Geballe, *Phys. Today* **36,** 60 (1984).

3. J.Müller, *Rep. Prog. Phys.* **43**, 663, (1980).

4. J.G.Bednorz and K.A.Müller, *Z. Phys.* **B64**, 189 (1986).

5. J.D.Jorgensen, H.B.Schuttler, D.G.Hinks, D.W.Capone II, K.Zhang, M.B.Brodskym and D.J.Scalapino, *Phys. Rev. Lett.* **58,** 1024 (1987).

6. R.J.Cava, R.B.van Dover, B.Batlogg and E.A.Rietman, *Phys. Rev. Lett.* **58**, 408 (1987).

7. M.K.Wu, J.R.Ashburn, C.J.Torng, P.H.Hor, R.L.Meng, L.Gao, Z.J.Huang, Y.Q.Wang and C.W.Chu, *Phys. Rev. Lett.* **58,** 908 (1987).

8. D.H.Hinks, L.Doderholm, D.W.Capone II, J.D.Jorgenson, Ivan K. Schuller, C.U.Serge, K.Zhang and J.D.Grace, *Appl. Phys. Lett.* **50**, 1688 (1987).

9. P.M.Graut, R.B.Beyers, E.M.Engler, G.Lim, S.S.P.Perkin, M.L.Ramirez, V.Y.Lee, A.Nazzal, J.E.Vasquez and R.J.Savoy, *Phys. Rev.* **B35**, 7242 (1987).

10. K.Semba, T.Tsuruni, M.Hikita, T.Itawa, J.Noda and S.Kirithatra, *Jpn. J. Appl. Phys.* **26**, L429 (1987).

11. H.Maeda, Y.Tanaka, F.Fukutomi and T.Asano, *Jpn. J. Appl. Phys.* **27**, L209 (1988).

12. J.M.Tarascon, Y.LePage, P.Barboux, B.C.Bagley, L.H.Greene,

W.R.McKinnon, G.W.Hull, M.Giroud and D.M.Hwang, *Phys. Rev.* **B37**, 9382 (1988).

13. Z.Z.Sheng and A.M.Herman, *Nature* **332**, 138 (1988).

14 D.W.Murphy, S.Sunshine, R.B.Van Dover, R.J.Cava, B.Batlogg, S.M.Zahurak and L.F.Shneemeyer, *Phys. Rev. Lett.* **58**, 1888 (1987).

15. B.Batlogg, R.J.Cava, A.Jayaraman, R.B.Van Dover, D.W.Murhy, L.W.Rupp, H.S.Chen, A.White, K.T.Scott. A.M.Mujsce and E.A.Rietman, *Phys. Rev. Lett.* **58**, 2333 (1987).

16. L.C.Bourne, A.Zettl, T.W.Barbee III and M.L.Cohen, *Phys. Rev.* **B36**, 3990 (1987).

17. W.E.Pickett, H.Krakaner, D.A.Papaconstantopoulus and L.L.Boyer, *Phys. Rev.* **B35**, 7252 (1987).

18. W.Weber, *Phys. Rev. Lett.* **58**, 1371 (1987).

19. H.Ihara, M.Hirabayaschi, N.Terada, Y.Kimura, K.Senzaki, M.Akimoto, K.Bushida, F.Kawashima and R.Uzaka, *Jpn. J. Appl. phys.* **26**, L460 (1987).

20. J.Ruvalds, *Phys. Rev.* **B35**, 8869 (1987).

21. C.M.Varma, R.Schmitt and E.Abrahams, *Solid State Commun.* **62,** 681 (1987).

22. B.K.Chakraverthy, *J. Phys.(Paris)*, **40**, L99 (1979).

23. P.W.Anderson, *Science* **235**, 1196 (1987).

24. C.N.R.Rao, *J. Solid State Chem.* **74**, 147 (1988).

25. C.N.R.Rao (Ed.), *The Chemistry of Oxide Superconductors*, Blackwell, Oxford (1988).

26. C.N.R.Rao (Ed.), *Progress in High Temperature Superconductivity*, Vol.II, World Scientific, Singapore (1988).

27. G.Rickayzen in *Superconductivity* Vol.I, (Eds. R.D.Parks) Marcel Dekker, New York (1969).

28. J.R.Schrieffer in *Theory of Superconductivity* , Benjamin New York (1964).

29. S.Mase, Y.Horie and nd Y.Terashi (Unpublished)

30. A.B.Pippard, *Phil. Mag.* **46**, 1104 (1955).

31. J.Dominec, *Supercond. Sci. Tech.* **6**, 153 (1993).

32. J.Dominec, C.Laermans, A.Vanelstraete and V.Plechácek, *J.Less-common Met* **164&165**, 568 (1990).

33. A.Migliori, W.M.Visscher, S.Wong, S.E.Brown, I.Tanaka, H.Kojina and P.B.Allen, *Phys. Rev. Lett.* **64**, 2458 (1990).

34. W.H.Fietz, H.A.Ludwig, B.P.Wagner, K.Grube, R.Benischke, and K.Wühl, *Proc. NATO ARW on Frontiers of High Pressure Research*, Pingree Park, CO, USA, (1991).

35. Chang Fanggao, M.Cankurtaran, G.A.Saunders, D.P.Almond, P.J.Ford and A.Al-Kheffagi, *Supercond. Sci. Tech.* **3**, 546 (1990).

36. J.Y.Prieur, H.Ji, J. Joffrin, M.Chapellier, G.Chardin, H.Kitazawa and K.Katsumata, *Physica* **B165 & 166**, 1285 (1990).

37. A.Jezowski, *Solid State Commun.* **71**, 419 (1989).

38. R.Abd-Shukor, *Jpn. J. Appl. Phys.* **31**, L1034 (1992).

39. H.Kamioka, N.Okuda and S.Nitta, *Jpn. J. Appl. Phys.* **30**, 1204 (1991).

40. D.J.Bishop, A.P.Ramirez, P.L.Gammel, B.Batlogg, E.A.Rietmann, R.J.Cava and A.J.Millis, *Phys. Rev.* **B36**, 2408 (1987).

41. M.F.Xu, H-P. Baum, A.Schenstrom, B.K.Sharma, M.Levy, K.J.Sun, L.E.Toth, S.A.Wolf and D.U.Gubser, *Phys. Rev.* **B37**, 3675 (1988).

42. S.Bhattacharya, M.J.Higgins, D.C.Johnston, A.J.Jacobson, J.P.Stokes, J.T.Lewandowski and D.P.Goshorn, *Phys. Rev.* **B37**, 5901 (1988).

43. J.Dong, Tingzhang Deng, F.Li and Y.Yao, *Phys. Rev.* **B42**, 301 (1990).

44. Y.S.He, J.Xiang, F.G.Chang, J.C.Zhang, A.S.He, H.Wangand V.A.Gu, *Physica* **C162-164**, 450 (1989).

45. J.Dominec, C.Laermans and V.Plechácek, *Physica* **C165 & 166**, 1287 (1990).

46. J.Hu, S.Zhang Q.Zhang, W.Cai, D.Tingzhang, Z.Liangkun, Y.He and J.Xiong, *Physica* **C162-164**, 444 (1989).

47. H.Yusheng, Z.Baiwen, L.Sihan, X.Jiong, L.Yongming and C.Haoming, *J. Phys. F: Met. Phys.* **17**, L243 (1987).

48. K.J.Sun, W.P.Winfree, M.F.Xu, M.Levy, B.K.Sarma, A.K.Singh, M.S.Osofsky and V.M.Le Tourneau, *Phys. Rev.*

B42, 2569 (1990).

49. D.J.Bishop, P.L.Gammel, A.P.Ramirez, R.J.Cava, B.Batlogg, and E.A.Rietmann, *Phys. Rev.* **B35**, 8788 (1987).

50. S.Koyama, U.Endo and T.Kawai, *Jpn. J. Appl. Phys.* **27**, L1861 (1988).

51. H.K.Liu, S.X.Dou, N.Savvides, J.P.Zhour, N.X.Tan, A.J.Bourdillon, M.Kiviz and C.C.Sorell, *Physica* **C157**, 93 (1989).

52. S.Kobayashi, S.Yasuyoshi and S.Wada, *Jpn. J. Appl. Phys.* **28**, L772 (1989).

53. K.Gopal and S.Ramana Murthy, *J. Acoust. Soc. Ind.* **XVIII**, 65 (1990).

54. S.Bhattacharya, M.J.Higgins, D.C.Johnston, A.J.Jacobson, J.P.Stokes, D.P.Goshorn and J.T.Lewandowski, *Phys. Rev. Lett.* **60**, 1181 (1988).

55. T.Laegreid and K.Fossheim, *Europhys. Lett.* **6**, 81 (1988).

56. K.J.Sun, W.P.Winfree, M.F.Xu, B.K.Sarma, M.Levy, R.Caton and R.Selim, *Phys. Rev.* **B38**, 11988 (1988).

57. M.Takano, J.Takada, K.Oda, H.Kitaguchi, Y.Miura, Y.Ikeda, Y.Tomii and H.Mazaki, *Jpn. J. Appl. Phys.* **27**, L1041 (1988).

58. H.B.Liu, Z.Q.Mao, L.Zhou, W.J.Zhang, J.Lu, B.Y.Li, Z.J.Chen, L.Z.Cao, Y.Z.Ruan, D.K.Peng and Y.H.Zhang, *Mod. Phys. Lett.* **B3**, 581 (1989).

59. A.Oota, A.Kirihigashi, Y.Sasaki and K.Ohba, *Jpn. J. Appl.*

Phys. **27**, L2289 (1988).

60. C.K.Rhee, C.J.Kim, A.G.Lee, I.H.Kuk, J.M.Lee, I.S.Chang, C.S.Kim, P.S.Han, S.I.Pyan and D.Y.Won, *Jpn. J. Appl. Phys.* **28**, L1137 (1989).

61. S.Koyama, U.Endo and T.Kawai, *Jpn. J. Appl. Phys.* **27**, L1867 (1988).

62. N.Kobayashi, H.Kawabe, K.Kusaba, M.Kikuchi, Y.Syono and Y.Muto, *Physica* **C162-164**, 27 (1989).

63. T.Fukami, A.A.A.Youssef, Y.Horie and S.Mase, *Physica* **C161**, 34 (1989).

64. V.Plechácek and J.Dominec, *Solid State Commun.* **74**, 633 (1990).

65. Y.Wang, L.Sun, J.Wu and M.Gu, *Solid State Commun.* **75**, 495 (1990).

66. H.Yusheng, X.Jiong, W.Xin, He Aishang, Z.Jincang and C.Fanggao, *Phys. Rev.* **B40**, 7384 (1989).

67. H.Yusheng, X.Jiong, Z.Jincang, He Aisheng, C.Fanggo and Li Fuxue, *Mod. Phys. Lett.* **B4**, 651 (1990).

68. Y.N.Wang, J.Wu, J.S.Zhu, H.M.Shen, Y.F.Yan and Z.X.Zhao, *Physica* **C162-164**, 454 (1989).

Chapter 4

ULTRASONIC STUDIES IN Ag DOPED Gd-Ba-Cu-O SUPERCONDUCTORS

4.1 Introduction

There has been a great deal of interest in understanding the physical properties of high Tc oxide superconductors ever since superconductivity in the 30K range in the multiphase oxide system La-Ba-Cu-O was reported by Bednorz and Müller in 1986 [1]. Among the high Tc cuprates the $REBa_2Cu_3O_{7-\delta}$ (1-2-3) type systems are the most studied ones where RE stands for rare earth. The first material among them is $YBa_2Cu_3O_{7-\delta}$ and after this many studies have been made on this material with chemical substitutions at various sites. One of the most interesting results was that Yttrium atom could be replaced almost entirely by any of the rare earths, with the exception of Ce, Pr and Tb without altering the superconducting properties [2,3]. The superconducting properties are not affected by the substitution of Gd for Y despite the fact that the Gd ion carries a large magnetic moment [4].

In 1-2-3 systems both tetragonal and orthorhombic structures occur. For $\delta = 0$ the structure is orthorhombic and contains CuO_2 sheets with Cu at the corners of squares and the O atoms at the edge centres. The Cu atoms in these sheets are the plane Cu atoms. Pairs of these sheets are seperated by intervening RE layers with the RE atoms located above and below the centres of the CuO_2 squares. Above and below this unit there are, first, BaO layers with the O atoms in line with the Cu atoms in the CuO_2 squares and the Ba atoms in line with the RE; and, second, CuO layers with the Cu atoms in line with those in the CuO_2 layers, but only half of the O sites corresponding to those in the CuO_2 layers are filled. The O atoms are ordered along chains in the b-direction, and this

ordering is associated with the orthorhombic structure. The Cu atoms in these layers are the "chain" Cu atoms. δ can take values between 1 and 0 and as δ increases from zero, O atoms move from the chain sites and ordering of the O atoms in those planes are disrupted. For $\delta \geq 0.4$ the long range order disappears and the structure becomes tetragonal. *In situ* neutron powder diffraction experiments [5-7] have revealed that oxygen vacancy ordering on the CuO basal plane of the 1-2-3 system plays a key role in the tetragonal to orthorhombic phase transition observed in these materials. Thus due to the presence of two chemically inequivalent Cu sites and variable oxygen stoichiometry, these 1-2-3 type systems exhibit many anomalous properties.

Ultrasonics is one of the standard methods of probing superconductivity. Studies of acoustic anomalies in the conventional superconductors have, in the past, been of great importance in probing their elastic properties and measuring the superconducting energy gap. A thorough knowledge of these elastic properties of high Tc materials is necessary to gather information about the different phononic interactions taking place in these samples at Tc and other temperature regions. Since the discovery of high Tc superconductivity in 1-2-3 systems, many researchers have investigated the acoustic properties of these materials [8-24]. Generally the anomalies associated with these superconductors can be divided into two classes. One is the anomaly around Tc and the other is the anomalies occuring above Tc, especially in the 200-250K temeprature range. Bhattacharya *et al.* [8,23] have studied the acoustic properties in YBCO and La-Sr-Cu-O systems near the transition point. In an isotropic solid the bulk modulus B and shear modulus G are related to the Lamés constant as

$$\rho V_l^2 = B + 4/3\ G$$
$$\rho V_s^2 = G \qquad (1)$$

For polycrystalline materials G represents an average value. The longitudinal velocity does not yield the bulk modulus alone. By measuring both V_l and V_s , G and B can be separated. The thermodynamics of a second order phase transition yields [25-27] the following relations for the bulk and shear moduli and the strain at the transition temperature

$$\frac{\Delta B}{B} = \frac{-\Delta C_p}{Tc} B \left[\frac{\partial Tc}{\partial P}\right]^2$$

$$\frac{\Delta G}{G} = \frac{T\Delta S}{Tc} G \left[\frac{\partial^2 Tc}{\partial \sigma_s^2}\right] \qquad (2)$$

$$\Delta\varepsilon_\alpha = \frac{T\Delta S}{Tc} B \left[\frac{\partial Tc}{\partial \sigma_\alpha}\right]$$

where ΔC_p refers to the discontinuity in the specific heat and ΔS is the entropy change at Tc; σ_s is the shear stress, ε_α is the generalized strain and σ_α is the conjugate stress. For a mean field transition a discontinuity occurs at Tc in the bulk modulus itself (or any modulus involving a volume preserving distortion) and in the temperature derivatives of G and $\varepsilon\alpha$ *i.e.*, G and $\varepsilon\alpha$ are expected to show kinks at Tc since ΔS is continuous at Tc [28]. Bhattacharya *et al.* [23] have obtained a hardening in elastic modulus at Tc. They report the existence of another anomaly above Tc at T_s = 95K in La-Sr-Cu-O system and at ≈ 120K in Y-Ba-Cu-O system suggesting that the state between T_s and Tc is the "normal" state preceding superconductivity. The anomalous elastic behaviour at and below Tc is dominated by the shear modulus and not by the bulk modulus, implying an unusually strong coupling of the order parameter to shear distortions. Hardening of elastic modulus below Tc has been reported by other workers also [9-12]. The behaviour is identical for shear as well as longitudinal waves except for the fact that anomaly is larger in the case of shear waves. Sun *et al.* [12] report a small dip in velocity at Tc on the velocity versus temperature curve and

a faster velocity change in the superconducting state compared to the normal state. Horn *et al.* [29] have reported the temperature variation of lattice constants of 123 systems as there is an orthorhombic distortion occuring at temperatures between 60 and 140K and showed a maximum difference between b and a appearing around the superconducting transition. This does not change the volume of the unit cell and area of a unit basal plane. The softening at Tc may be due to this structural instability. The transition occuring above Tc *ie.*, at T_s is also important since it suggests that the state between T_s and Tc is the true normal state from which the bulk superconducting condensation occurs and it is suggested that the rotation of the Cu-O complex in the a-b plane can be responsible for this [23]. It is also suggested that the pronounced hardening of the shear modulus below Tc may be due to the depletion of an excitation that cocondenses with the carriers and that also couples strongly to transverse acoustic phonons. Increase in attenuation has also been reported by several authors at the transition point [8,12,23,24]. For this, phonon-phonon interactions provide a satisfactory explanation [8,23]. The sound damping is given by the Mason-Bateman formula (for the $\omega\tau < 1$ regime) [30]

$$\alpha \approx \frac{D(\gamma)\ C_p\ T}{\rho V^3}\ \omega^2\tau \qquad (3)$$

where $D(\gamma)$ is a measure of anharmonicity γ and τ is the thermal relaxation time. If τ is limited by the scattering of phonons by the carriers in the normal state, then the condensation of carriers below Tc enhances τ and thereby increases α. At lower temperatures the effect of τ saturates and the decrease in α is dominated by $C_p(T)$. Temperature dependence of thermal conductivity is a straight test of this since $K \sim \alpha/T$. Xu *et al.* [24] suggest that fluctuations contributed by the one dimensional nature of the CuO network also can account for this anomalous attenuation.

Since the 200K temperature range is an important

region in the case of high Tc superconductors, there are several reports which show anomalous changes in sound velocity and attenuation in the 123 system above 200K [8,14,24]. There is a considerable interest in the properties of high Tc materials in this range since several reports show anomalies in C_P at 220K in several samples and correlate them with the specific heat jump at Tc [31-33]. According to Laegreid [32] the C_P anomaly at 220K is largest in the samples with the largest jump in C_P at 90K. In YBCO Calemzuk [34] has observed a large peak at 220K in C_P measurement. It is correlated to a large and hysteretic change of the Young's modulus and a small resistance anomaly. Laegreid *et al.* [35] have reported that such an anomaly is observed only upon heating and attributed it to annealing of a metastable state. Ultrasonic velocity and attenuation measurements show that a structural instability does occur in YBCO below room temperature. On the connection between the 90K and 220K C_P anomalies, Laegreid *et al.* [32] suggest that ordering in the oxygen system may be responsible for the 220K anomaly. Xu *et al.* [24] have observed an attenuation peak at 252K and suggest that the maxima are produced by a relaxation mechanism. He Yusheng *et al.* [14] report about anomalies in velocity and attenuation peaks around 250K and 160K as there is some kind of lattice instability or structural phase transition. Thus in YBCO system the lattice instability near 160K and 250K have been investigated and attributed to the oxygen ordering readjustments along the one dimensional Cu-O chain [14,15,32].

In spite of all these results, the mechanisms are still unclear and yet to be explored. In order to obtain a clear understanding about this metastability and to gain an insight into some of the possible reasons for the existing controversies in experimental results, we have undertaken ultrasonic velocity and attenuation measurements in Ag doped $GdBa_2Cu_3O_{7-\delta}$ (Gd123) system. As Ag is a noble metal with a stable charge state, doping it in 123 systems has been

reported before [36-40]. At low and moderate concentrations, Ag is believed to substitute Cu at the chain site and influence oxygen-vacancy ordering in these chains. Since anomalous ultrasonic velocity change above Tc has been reported to be arising due to oxygen order-disorder phase transitions, Ag doping is expected to influence such anomalies and throw light on the mechanism of superconductivity in these materials.

4.2 Experimental

Samples studied here have a general formula $GdBa_2(Cu_{1-x}Ag_x)_3O_{7-\delta}$ with x = 0, 0.01, 0,02, 0.03 and 0.05. These are prepared by the standard solid state reaction method. Stoichiometric mixtures of Gd_2O_3, $BaCO_3$, CuO and Ag_2O powders are thoroughly mixed and calcined in the form of loosely packed pellets for about 80 hours with three intermediate grindings. Samples are then powdered and pelletised under a pressure of nearly 100 Kg cm^{-2} and sintered at 900°C for 24 hours and then furnace cooled to room temperature.

DC resistivity from 77K to room temperature (300K) has been measured using a four probe setup. Oxygen contents of the samples are determined by iodometric titration.

Ultrasonic measurements at 10 MHz have been carried out in the temperature range 85-300K. Pelletised samples of diameter ≈ 10mm and thickness ≈ 4.5mm have been used for the measurements. The faces of the samples have been well polished so that they are plane and parallel to each other. 10 MHz X-cut quartz transducer has been mounted on the sample with silicone grease as the bond. The velocity as well as attenuation have been measured as a function of temperature using the experimental setup described in chapter 2. Reasonably good echoes are obtained in four of the samples. The quality of the echoes obtained from sample with x = 0.05

is found to be poor for the PEO method employed here. So the ultrasonic measurements have been restricted to first four samples with x = 0, 0.01, 0.02 and 0.03. The cooling rate was kept ≤ 1K/min.

4.3 Results and discussions

The variation of the ratio of the change in longitudinal velocity to the room temperature velocity ($\Delta V/V_{300}$) with temperature for all the four samples is shown in Fig.4.1. All the curves show a small softening near Tc and below Tc there is a marked change in slope *ie.*, the velocity increase becomes faster compared to the normal state. Another striking feature of the graph is that there is a broad peak around 207K in the case of pure sample *i.e.*, sample with x = 0. This peak is found to shift to the high temperature side with Ag doping. In the case of sample with x = 0.01 it is at about 245K.For the sample with x = 0.02 the peak is not so pronounced as in the case of other samples but the temperature at which the peak occurs is clear. The variation of this temperature at which the broad peak occurs (T_{vp}) with Ag doping concentrations is shown in Fig.4.2. At low concentrations of Ag (x ≈ 0.01) the peak shifts to higher temperatures. Further increase in Ag concentration does not shift the peak significantly as shown in the Fig.4.2.

The variation of velocity near Tc indicates a dip and a hardening of elastic modulus at temperatures below Tc. This suggests that a structural instability is occuring at the transition point and a hardening of modulus below Tc which may be due to the depletion of an excitation that cocondenses with the carriers, which couples strongly to the transverse acoustic phonons. The anomalies are not so pronounced due to the fact that it is the longitudinal wave and not the transverse wave used here. The order parameter has a stronger coupling with shear distortions than with compressive distortions, since the superconducting transition is

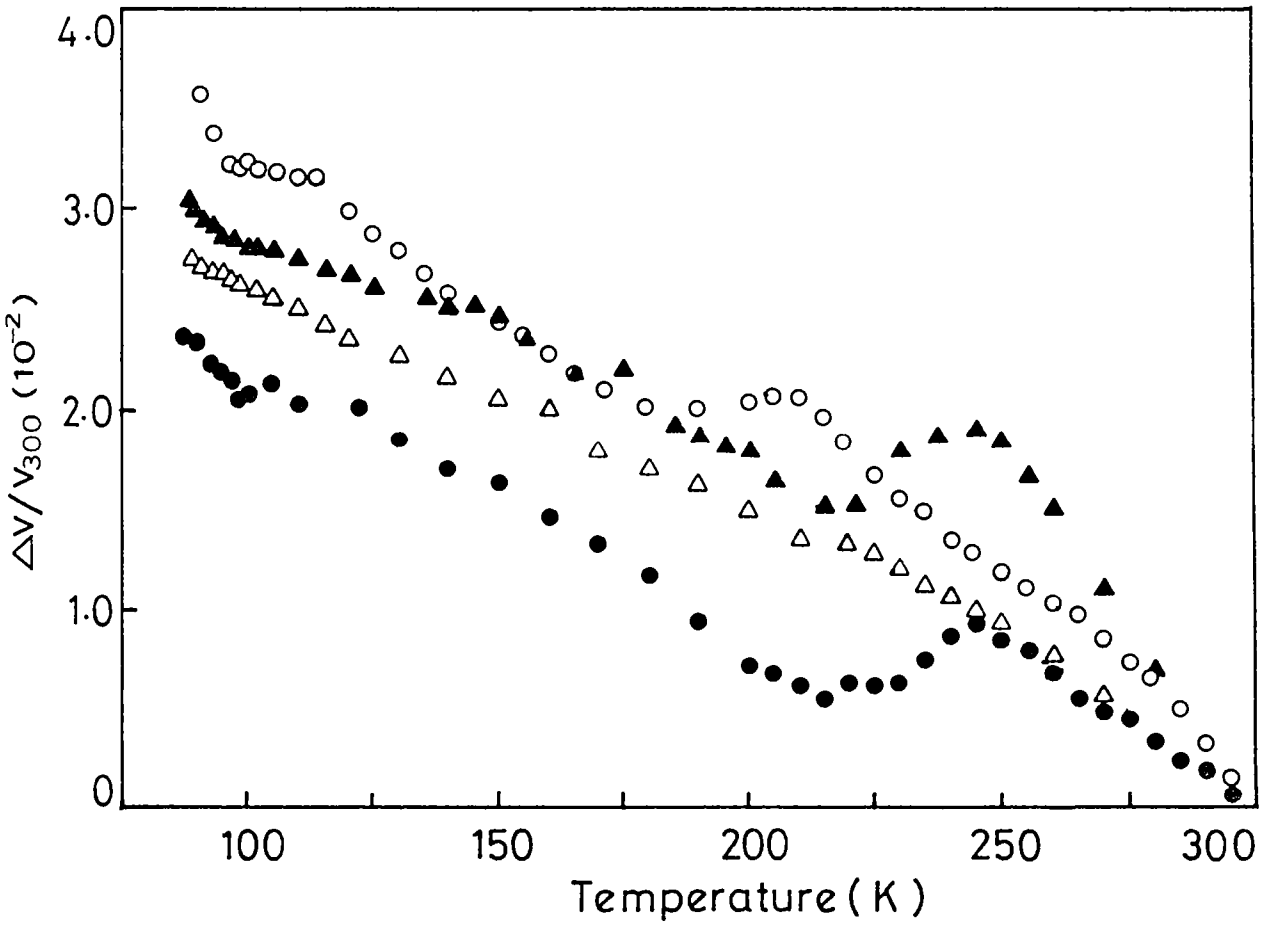

Fig.4.1 Temperature dependence of the relative change in longitudinal velocity ($\Delta V/V_{300}$) for $GdBa_2(Cu_{1-x}Ag_x)_3O_{7-\delta}$ with different x values.
(o) for x = 0, (●) for x = 0.01,
(Δ) for x = 0.02 and (▲) for x = 0.03

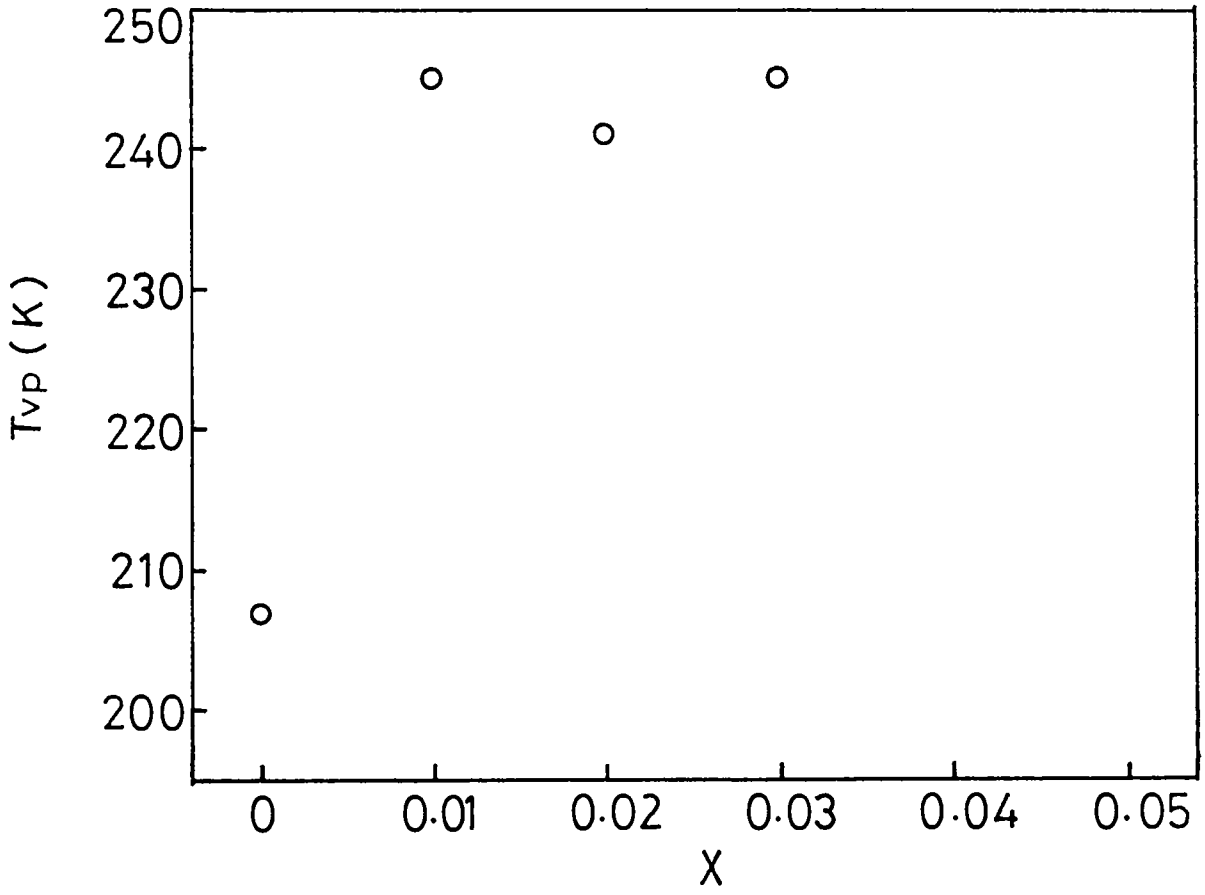

Fig.4.2 Variation of T_{vp} as a function of Ag doping concentration in $GdBa_2(Cu_{1-x}Ag_x)_3O_{7-\delta}$.

associated with a volume preserving shear lattice distortion. Similarly the anomaly above Tc at Ts which is reported by Bhattacharya *et al.* [23] is also not visible in all the measurements which also can be attributed to the same reason.

In order to understand the mechanisms that cause a variation in T_{vp} as shown in Fig.4.2, we have carried out resistivity measurements in all these samples as a function of temperature. The variation of Tc as a function of Ag concentration is shown in Fig.4.3. Tc decreases with increasing Ag concentrations upto 2 at. wt.% (*i.e.*, x = 0.02).On further increase in the Ag concentrations, Tc increases. At still higher Ag concentration, however, Tc once again starts falling. Fig. 4.3 also reveals that the variation of room temperature resistivity (ρ_{300}) with Ag concentration is well correlated to the corresponding Tc variation.

To understand the dependence of Tc on Ag concentration in these samples, we investigated the dependence of oxygen stoichiometry on Ag concentration. As shown in Fig.4.4 the oxygen content decreases with increase in Ag concentration. Thus in the low Ag concentration regime the decrease in Tc and the increase in the room temperature resistivity can be understood if Ag substitutes Cu(1) in the lattice decreasing the oxygen stoichiometry and affects oxygen ordering. For Ag concentration beyond 2 at.wt. % the increase in Tc and the fall in resistivity indicate that at higher concentrations, Ag mostly goes into the grain boundaries. Presence of Ag as pure metal in the grain boundaries is responsible for this fall in room temperature resistivity.

At still higher concentrations of Ag, *i.e.*, with x = 0.05 the samples show semiconducting behaviour and do not show superconductivity down to 77K. To understand this behaviour we note that in this concentration range, while most of the Ag go into the grain boundaries, higher Cu deficiency results in the formation of other insulating phases like Gd_2BaCuO_5, BaO,

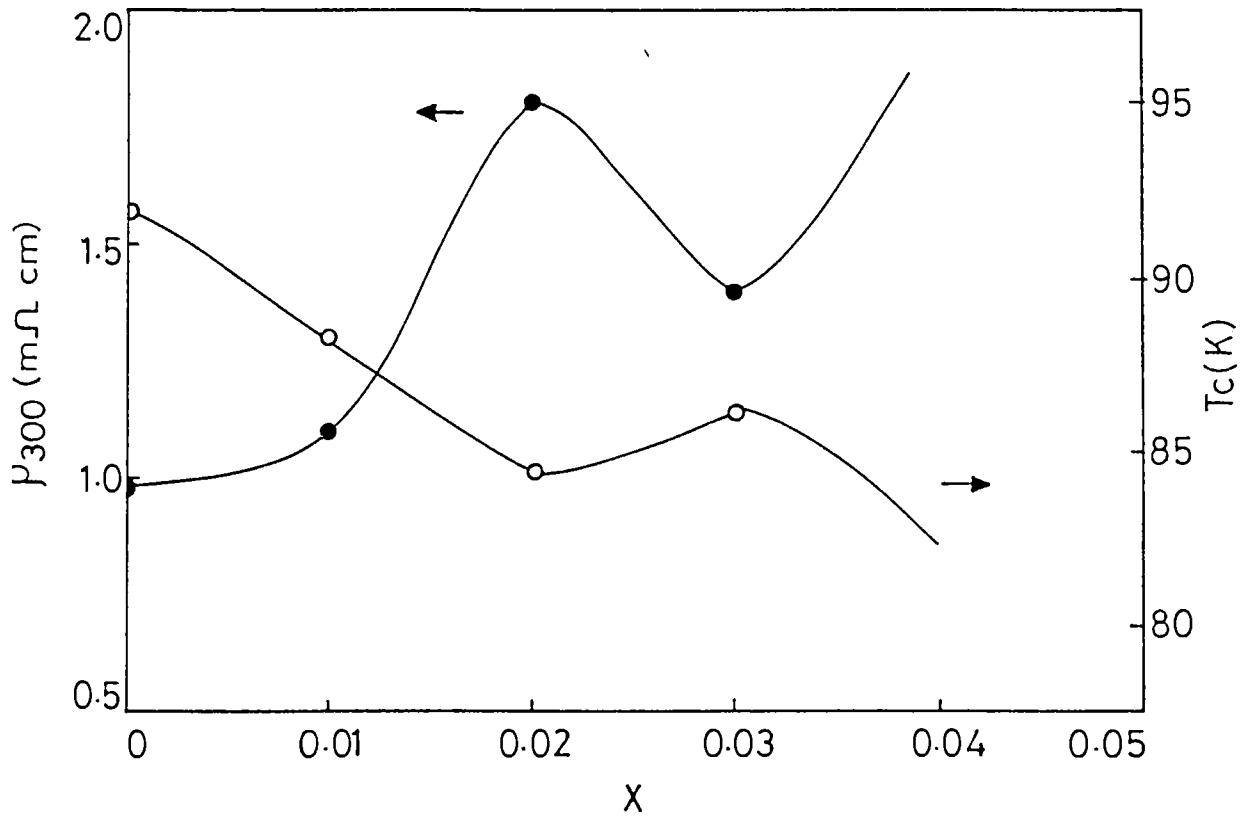

Fig.4.3 Variation of transition temperature Tc (O) and room temperature resistivity ρ_{300} (●) as a function of Ag doping concentration x in $GdBa_2(Cu_{1-x}Ag_x)_3O_{7-\delta}$.

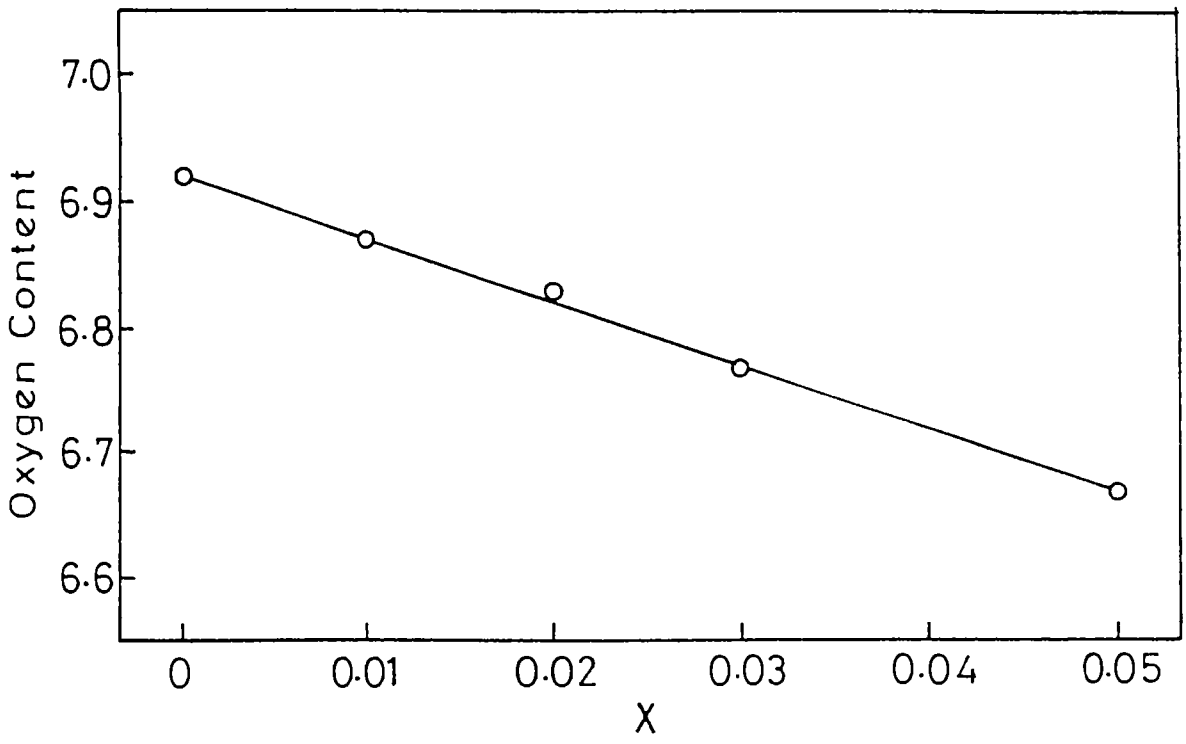

Fig.4.4 Dependence of oxygen stoichiometry on Ag concentration in $GdBa_2(Cu_{1-x}Ag_x)_3O_{7-\delta}$

Gd_2O_3, $BaCuO_2$ etc. making the sample a mixed phase one. Those insulating phases also occupy the grain boundaries increasing the normal state resistivity by an order and suppressing the Tc value. The difficulty in making ultrasonic measurements in this sample is due to the occurance of such a mixed phase in the sample.

The peak in the velocity curve at 207K in the case of pure sample may be due to the reordering of O ions in the one dimensional Cu-O chain. This is because the 123 system generally remains in a metastable state. With increasing Ag concentration the increase in Tvp is due to the fact that the oxygens are locked to Ag and so a higher temperature is necessary for the reordering to occur. On further increasing the Ag content, some of the Ag goes into the grain boundaries as pure metal. The sample seems to go into a relatively stable state and consequently there is no significant shift in Tvp at higher Ag concentrations, compared to the initial sharp increase. Addition of Ag in excess of 2 at.wt. % results in silver cluster formation but this is again in the same condition and hence Tvp does not shift significantly. The variation in Tc and ρ_{300} with Ag doping concentrations substantiate these arguments. Thus it is reasonable to conclude that Ag doping do influence the metastability of the 123 system at low Ag doping levels. Increase in Tvp with Ag concentration in the low concentration regime indicates that the oxygen reordering occurs at a higher temperature than in the case of undoped Gd 123.

ρ_{300} and Tc data (Fig. 4.3) indicate that Ag goes into the lattice of Gd 123 at low concentrations. Ag is known to have a stable 1^+ charge state unlike Cu which can have charge states 1^+, 2^+or 3^+depending on oxygen coordination. The oxygen atoms around Ag are tightly bound providing it a fixed oxygen coordination. The oxygen reordering in such case requires higher activation energy and can occur at high

temperatures. Therefore Tvp is expected to increase with Ag doping at low concentrations as observed. At higher Ag doping levels, the excess Ag goes into the grain boundaries or form clusters but these do not influence the oxygen reordering in the Cu-O chain and hence the sample is in a relatively higher stable state and hence Tvp does not shift significantly at higher Ag doping levels.

Ultrasonic attenuation also shows a similar type of behaviour. The temperature dependence of attenuation shows a dip at the temperature at which a peak in the velocity occurs. The variation of attenuation (α) vs. temperature is shown in Fig.4.5. Upon cooling, below this dip attenuation again shows a peak at temperature at which the velocity curve shows a minimum. Near Tc attenuation again increases from its usual trend of decrease. This increase in attenuation may be due to the increase in thermal relaxation time and the hardening of the lattice due to the superconducting transition as explained before. Sample with $x = 0.03$ has an attenuation curve with a number of irregular peaks and it is not shown in the figure. This can be attributed to the presence of additional phases in the grain boundary, such as pure Ag.

4.4 Conclusions

The temperature dependence of ultrasonic velocity in Gd 123 shows anomalies around Tc as well as on the higher temperature side around 207K. The anomaly around Tc can be due to the superconducting transition. The 207K anomaly is attributed to the reordering occuring in the one dimensional Cu-O chain in the superconductor. Since the Ag doped in the Gd 123 is found to go to the lattice site it is found that the peak observed in the velocity curve at 207K in the case of undoped Gd 123 shifts to high temperature side with Ag doping. The Cu-O reorientation occuring in the sample can be due to the metastability of the system and upon Ag doping a higher temperature is required for this reorientation transition to

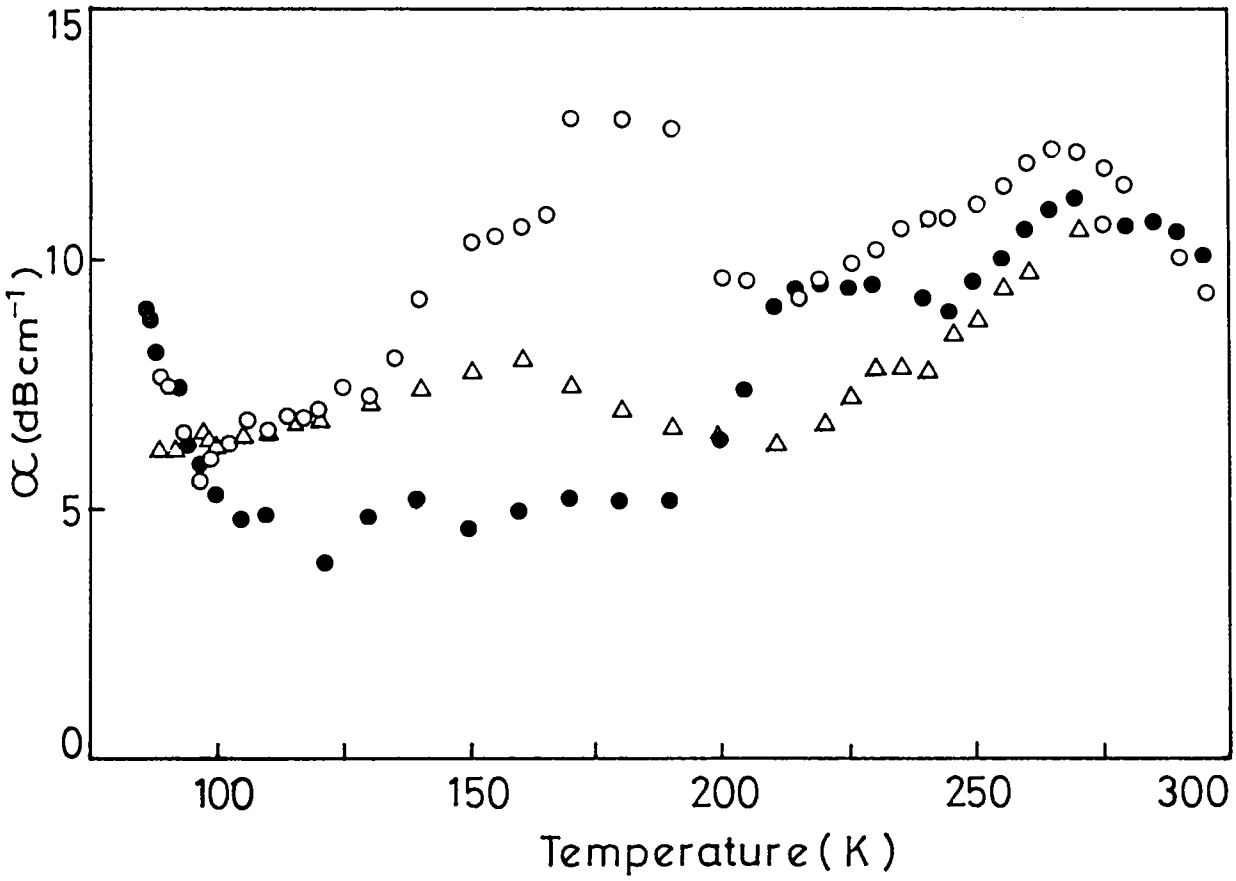

Fig.4.5 Variation of ultrasonic attenuation with temperature for $GdBa_2(Cu_{1-x}Ag_x)_3O_{7-\delta}$ with different x value.
(O) for x = 0 , (●) for x = 0.01 and
(△) for x = 0.02

occur. In the lower Ag concentration regime this shift remains almost the same and after a particular level of Ag doping the sample quality becomes poor and the sample does not show any superconducting property due to the presence of different constituent phases in the sample. Thus with low concentrations of Ag the temperature at which Cu-O ordering occurs can be shifted to high temperature significantly.

References

1. J.G.Bednorz and K.A.Müller, *Z.Phys.***B64**, 189 (1986).

2. D.W.Murphy, S.Sunshine, R.B.Van Dover, R.J.Cava, B.Batlogg, S.M.Zahurak and L.F.Schneemeyer, *Phys. Rev. Lett.* **58,** 1888 (1987).

3. P.H.Hor, R.L.Meng, Y.Q.Wang, L.Gao, Z.J.Haung, J.Bechtold, K.Forster and C.W.Chu, *Phys. Rev. Lett.* **58**, 1891 (1987).

4. H.A.Mook, D.McK. Paul, B.C.Sales, L.A.Boatner and L.Cussen, *Phys. Rev.* **B38**, 12008 (1988).

5. J.E.Greedan, A.H.O'Reilly and C.V.Stager, *Phys. Rev.* **B35**, 8770 (1987).

6. J.D.Jorgensen, B.W.Veal, W.K.Kwok, G.W.Crabtree, A.Umezawa, L.J.Nowicki and A.P.Paulikas, *Phys. Rev.* **B36**, 5731 (1987).

7. J.D.Jorgensen, M.A.Beno, D.G.Hinks, L.Soderholm, K.J.Volin, R.L.Hitterman, J.D.Grace, I.K.Schuller, C.U.Segre, K.Zhang and M.S.Kleefisch, *Phys. Rev.* **B36**, 3608 (1987).

8. S.Bhattacharya, M.J.Higgins, D.C.Johnston, A.J.Jacobson, J.P.Stokes, J.T.Lewandowski and D.P.Goshorn, *Phys. Rev.* **B37**, 5901 (1988).

9. D.J.Bishop, A.P.Ramirez, P.L.Gammel, B.Batlogg, E.A.Rietman, R.J.Cava and A.J.Millis, *Phys. Rev.* **B36**, 2408 (1987).

10. R.Abd-Shukor, *Jpn. J. Appl. Phys.* **31**, L1034 (1992).

11. H.Kamioka, J.Okuda and S.Nitta, *Jpn. J. Appl. Phys.* **30**, 1204 (1991).

12. K.J.Sun, W.P.Winfree, M.F.Xu, B.K.Sarma, M.Levy, R.Caton and R.Selim, *Phys. Rev.* **B38**, 11988 (1988).

13. Y.Horie, Y.Terashi, H.Fukuda, T.Fukami and S.Mase, *Solid State Commun.* **64**, 501 (1987).

14. H.Yusheng, Z.Baiwen, L.Sihan, X.Jiong, L.Yongming and C.Haoming, *J. Phys F. Met Phys.* **17**, L243 (1987).

15. T.Laegreid and K.Fossheim, *Europhys. Lett.* **6**, 81 (1988).

16. S.Hoen, L.C.Bourne, C.M.Kim and A.Zettl, *Phys. Rev.* **B38**, 11949 (1988).

17. H.Mathias, W.Moulton, H.K.Ng, S.J.Pan, K.K.Pan, L.H.Peirce, L.R.Testardi and R.J.Kennedy, *Phys. Rev.* **B36**, 2411 (1987).

18. A.Migliori, Ting Chen, B.Alari and G.Grüner, *Solid State Commun.* **63**, 827 (1987).

19. K.J.Sun, W.P.Winfree, M.F.Xu, M.Levy, B.K.Sarma, A.K.Singh, M.S.Osofsky and V.M.Le Tourneau, *Phys. Rev.* **B42**, 2569 (1990).

20. X.M.Xie, T.G.Chen and Z.L.Wu, *Phys. Rev.* **B40**, 4549 (1989)

21. A.Hikata, M.J.McKenna and C.Elbaum, *Phys. Rev.* **B40**, 5247 (1989).

22. V.N.Nikiforov, V.V.Moshchalkov, M.G.Mikheev, V.V.Rzhevskie and L.I.Leonyuk, *Physica* **C185-189**, 1161 (1991).

23. S.Bhattacharya, M.J.Higgins, D.C.Johnston, A.J.Jacobson, J.P.Stokes, D.P.Goshorn and J.T.Lewandowski, *Phys. Rev. Lett.* **60**, 1181 (1988).

24. M.F.Xu, H.P.Baum, A.Schenstrom, B.K.Sarma, M.Levy, K.J.Sun, L.E.Toth, S.A.Wolf and D.U.Gubser, *Phys. Rev.* **B37**, 3675 (1988).

25. L.R.Testardi, *Phys. Rev.* **B3**, 95 (1971).

26. L.R.Testardi, *Phys. Rev.* **B12**, 3849 (1975).

27. L.R.Testardi in *Physical Acoustics* Vol.X (Eds. W.P.Mason and R.N.Thurston) Academic Press, New York (1973).

28. G.A.Alers in *Physical Acoustics* Vol.4A (Ed. W.P.Mason) Academic Press, New York (1966).

29. P.M.Horn, D.T.Keane, G.A.Held, J.L.Jordansweet, D.L.Kaiser and F.Holtzberg, *Phys. Rev. Lett.* **59**, 2772 (1987).

30. W.P.Mason and T.B.Bateman, *Phys. Rev. Lett.* **10**, 151 (1963).

31. M.Slaski, T.Laegreid, O.M.Nes and K.Fossheim, *Mod. Phys. Lett.* **B3,** 585 (1989).

32. T.Laegreid, K.Fossheim, E.Sandvold and S.Julsrud, *Nature*, **330**, 637 (1987).

33. T.Laegreid, K.Fossheim, O.Traetteberg, E.Sandvold and S.Julsrud, *Physica* **C153-155**, 1026 (1988).

34. R.Calemczuck, E.Bonjour, J.Y.Harry, L.Forro, C.Ayacha, M.J.M.Jurgens, J.R-Mignod, B.Barbara, P.Burlet, M.Couach, A.F.Khoder and B.Salce, *Physica* **C153-155**, 960 (1988).

35. T.Laegreid, K.Fossheim,and F.Vassenden, *Physica* **C153-155**, 1096 (1988).

36. Y.H.Kao, Y.D.Yao and L.W.Song, *Int. J. Mod. Phys.* **B3**, 573 (1989).

37. Y.D.Yao, Y.H.Kao, J.J.Simmins, R.L.Snyder, Z.Tao and K.W.Jones, *Mod. Phys. Lett.* **B3**, 499 (1989).

38. C.V.Tomy, A.M.Umarji, D.T.Adroja, S.K.Malik, R.Prasad, N.C.Soni, A.Mohan and C.K.Guptha, *Solid State Commun.* **64**, 889 (1987).

39. A.K.Gangopadhyay and T.O.Mason, *Physica* **C178**, 64 (1991).

40. Y.H.Kao, Y.D.Yao, L.Y.Jang, F.Xu, A.Krol, L.W.Song, C.J.Sher, A.Parovsky, J.C.Phillips, J.J.Simmins and R.L.Snyder, *J. Appl. Phys.* **67**, 353 (1990).

Chapter 5

ELASTIC AND THERMAL PROPERTIES OF YTTRIUM BARIUM ZIRCONATE

5.1 Introduction

The discovery of superconductivity above 90K in $YBa_2Cu_3O_{7-\delta}$ (YBCO) and other ceramic materials has led to a considerable amount of research work on oxide superconductors. From a technological point of view, one of the main applications of these superconductors is in the form of thin and thick films for fabricating electronic devices. The chemical reactivity of YBCO imposes severe restrictions on the availability of substrates for depositing thin films [1-4]. MgO and $SrTiO_3$ are found to be the least reactive among the commonly available substrates [5,6]. It has been reported [7] that addition of ZrO_2 to YBCO results in the formation of a second phase YBa_2ZrO_6 (YBZO) which is very stable and does not show any detrimental effects on the superconducting property of YBCO films deposited on it. In order to characterise this material to be used as a substrate material, measurement of elastic and thermal properties have been carried out on it.

When choosing a material as the substrate for the deposition of thin films many desirable factors such as nonreactivity of the substrate material with the deposited thin film, low dielectric constant for microwave applications and high thermal conductivity are to be taken into account. Moreover, it should have a normal temperature dependence for its physical properties. The ability of a substrate to withstand rapid temperature changes without undergoing any damage is generally referred to as its thermal shock resistance. This complex quantity is related to the thermal conductivity, specific heat and elastic moduli of the material since these parameters govern the resultant strain [8]. We have measured the specific heat, thermal conductivity and

longitudinal elastic modulus of Yttrium Barium Zirconate (YBZO) as a function of temperature to determine the stability of this material as the temperature is lowered to 90K. The dielectric constant and loss factor have also been measured as a function of frequency in the range 30Hz to 13MHz at room temperature.

5.2 Sample preparation

YBa_2ZrO_6 samples have been prepared by the conventional ceramic processing method. High purity Y_2O_3, $BaCO_3$ and ZrO_2 are wet mixed in the molar ratio and calcined at 1300°C for 8 hours. The calcined material is then ground and pressed in the form of pellets and sintered at 1400°C for 12 hours with intermediate grinding and the samples are furnace cooled. Addition of a small amount of CuO (0.5 wt.%) is found to be necessary to stabilise the YBZO phase and to retain the mechanical properties [7]. Absence of CuO leads to crumbling of the pellets into powder with impurity phases as shown in the X-ray powder diffraction pattern shown in curve A of Fig.5.1. Curve B in Fig.5.1 shows the X-ray powder diffraction pattern for YBZO with 0.5 wt.% CuO in the precursor powder and heat treated at 1400°C for 4 hours. The XRD pattern does not show the peaks of CuO probably due to its very small quantity or it might have run out of the pellets in liquid form at the sintering temperature. YBZO has cubic structure and the X-ray powder pattern can be indexed in accordance with similar materials like YBa_2NbO_6 [9].

The chemical reactivity of YBZO with YBCO has been studied using X-ray analysis. Equimolar ratios of these two materials have been mixed and pressed into pellets. The pellets are then heat treated at 950°C for 15 hours and then cooled slowly to room temperature in a flow of oxygen. The X-ray diffraction pattern of the resultant material showed a composite mixture of YBCO and YBZO phases indicating that

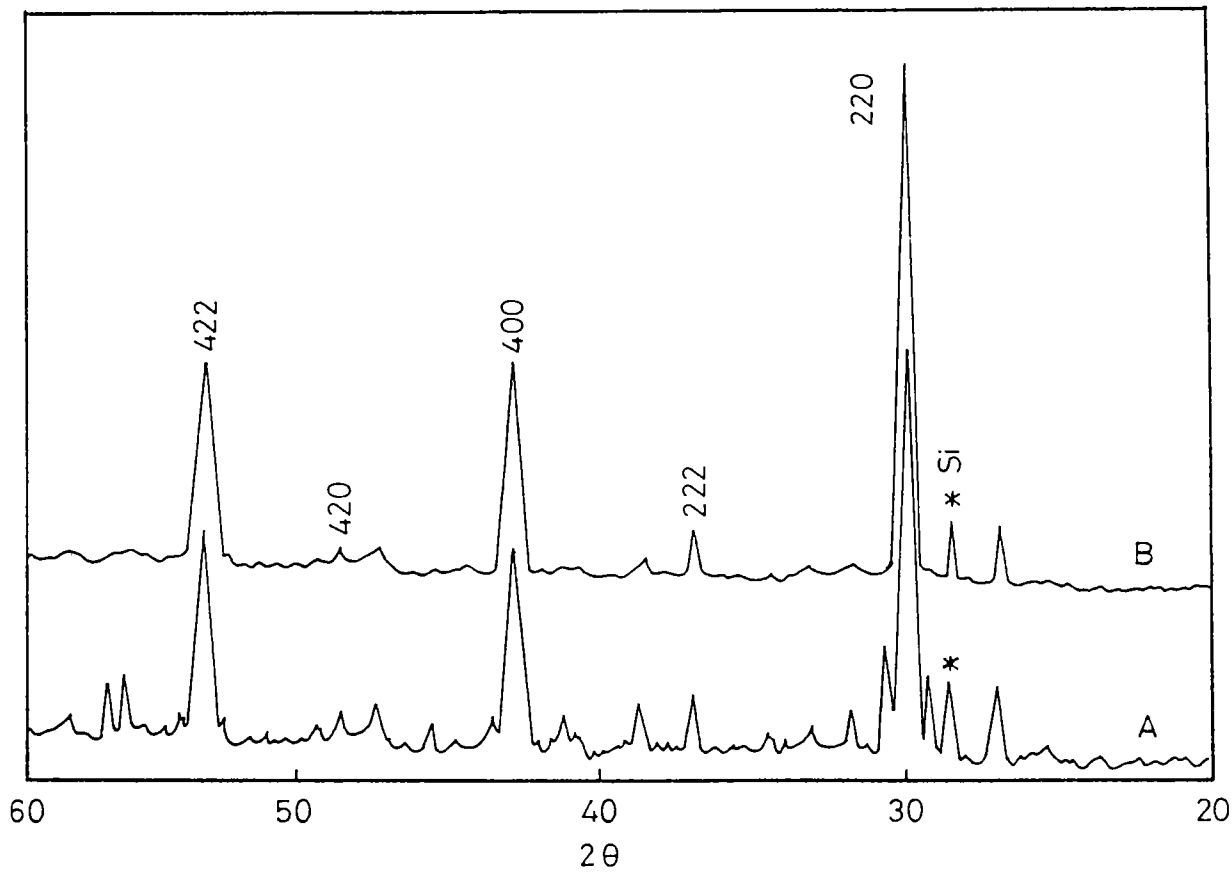

Fig.5.1 X-ray powder diffraction pattern for (A) YBa_2ZrO_6 without any CuO addition heated at 1550°C. (B) YBa_2ZrO_6 with 0.5 wt.% CuO heated at 1400°C. Silicone has been added as an internal standard.

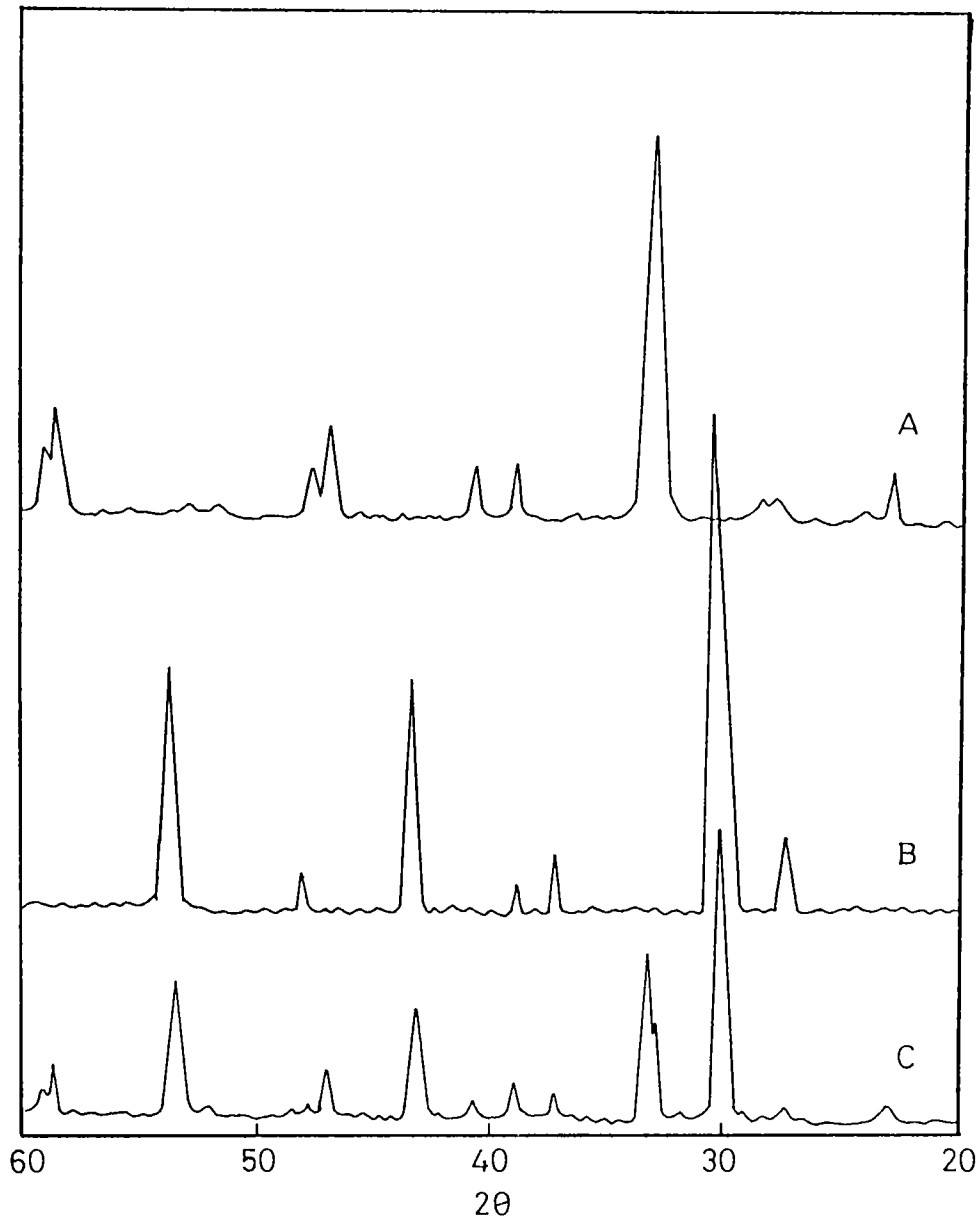

Fig.5.2 X-ray powder diffraction pattern for (A) pure $YBa_2Cu_3O_{7-\delta}$, (B) pure YBa_2ZrO_6, (C) equimolar mixture of $YBa_2Cu_3O_{7-\delta}$ and YBa_2ZrO_6 heated at 950°C.

there is no chemical reaction between them. The X-ray pattern for YBCO, YBZO and the mixture are given in Fig.5.2. If there had been chemical reaction, then the X-ray pattern would have shown additional peaks due to the new phases formed due to the reaction.

5.3 Dielectric properties of YBZO

The dielectric properties of YBZO samples have been measured in the frequency range 30Hz to 13MHz using an impedance analyser (Hewlet Packard Model HP4192A). The variations of the dielectric constant and dissipation factor with frequency are shown in Fig.5.3. It is found that the dielectric constant and loss factor are slightly higher than those of Al_2O_3 but much less than those of $SrTiO_3$, a common substrate for YBCO thin films.

5.4 Elastic properties of YBZO

In order to study the temperature variation of the elastic properties of YBZO we have measured the longitudinal ultrasonic velocity at 10MHz as a function of temperature. The sample for measurements has been in the form of a disc of thickness ≈ 2.5mm. The opposite faces of the sample have been polished so that they are plane and parallel to each other. The measurements have been carried out using Pulse Echo Overlap technique [10] as explained in chapter 2 in the temperature range 300-90K. The density of the sample has been determined to be ≈ 5260 Kg/m^3. The variation of longitudinal elastic constant C_{11} is thus obtained and plotted as a function of temperature and is shown in Fig.5.4. As the temperature decreases the elastic constant increases which is the normal behaviour of solids. A small change in slope is observed around 225K. Below this temperature also the elastic constant decreases but at a slightly reduced rate. No significant hysteresis in the variation of the elastic modulus

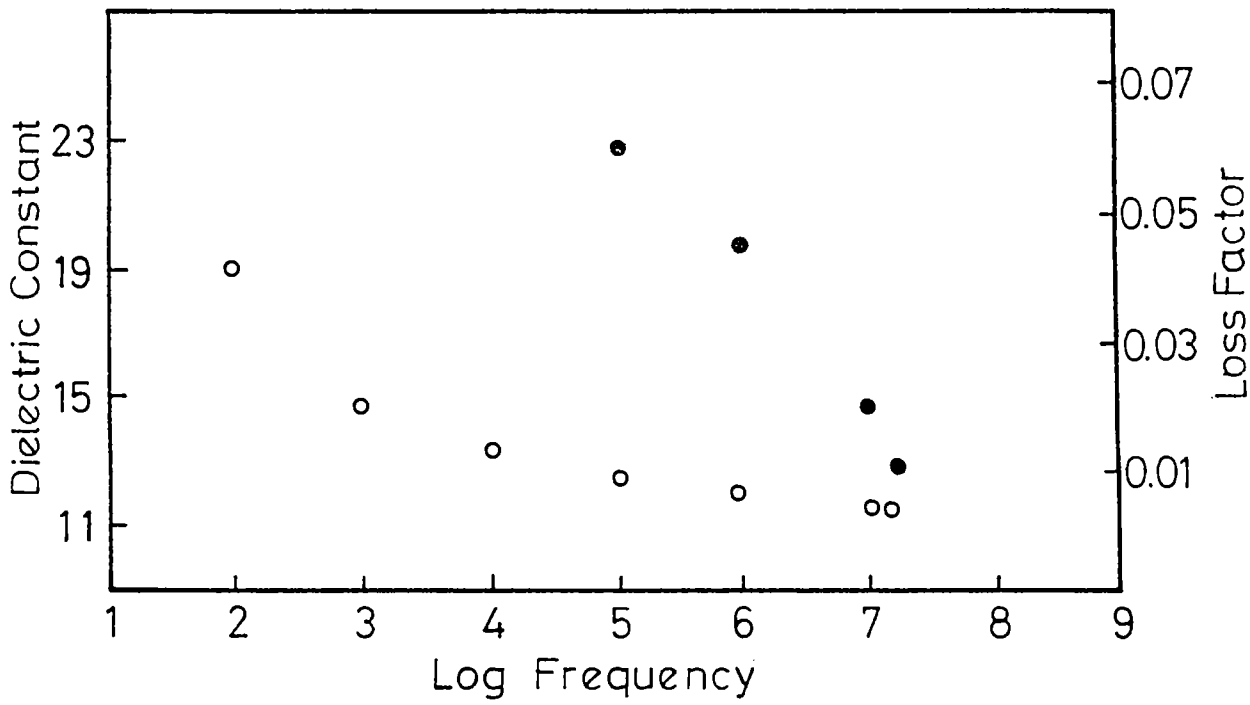

Fig.5.3 Variation of dielectric constant (O) and loss factor (●) with frequency at room temperature.

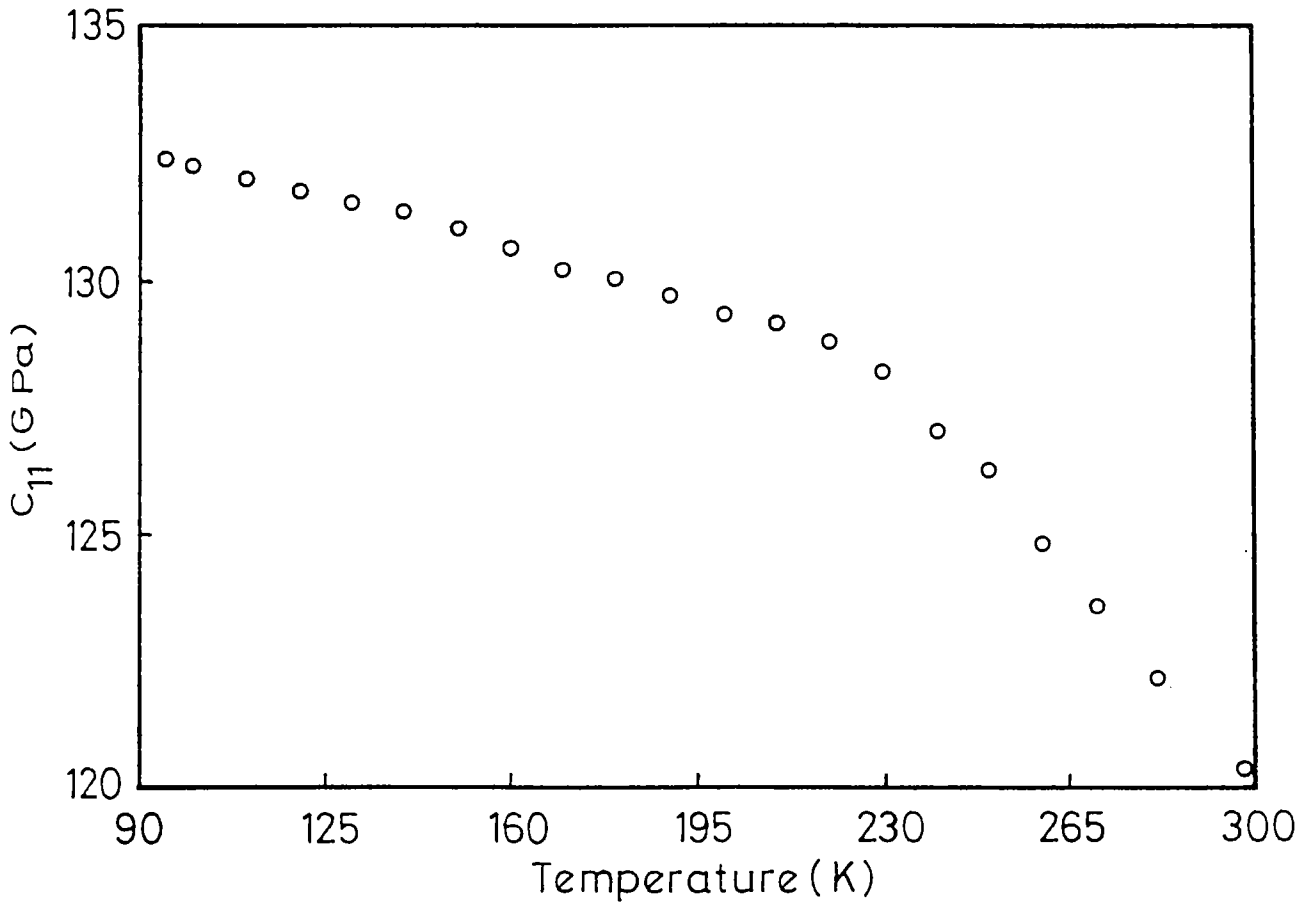

Fig.5.4 Variation of longitudinal elastic modulus C_{11} with temperature of YBa_2ZrO_6 sample.

has been found between cooling and heating cycles.

5.5 Thermal properties - Specific heat and Thermal conductivity

We have measured the specific heat and thermal conductivity as a function of temperature in a wide range of temperature. Specific heat has been measured from 90 to 475K and thermal conductivity from 90 to 300K.

The specific heat of the sample is measured using a differential scanning calorimeter (Perkin Elmer DSC-7) by the ratio method [11] with sapphire as the specific heat standard. First the base line is obtained by making the run without any sample in either sample holders. Then a known quantity (20.1mg) of sapphire is taken in an aluminium pan and sealed. The thermogram is obtained by placing this sapphire pan in the sample holder and an empty pan as reference in the reference holder. The curve is plotted along with the base line. Similarly the DSC curve is obtained for powdered YBZO sample (47.10mg), along with the base line. From these two plots the specific heat is calculated using the relation

$$C_{PS} = \frac{H_S \, M_R}{H_R \, M_S} C_{PR} \qquad (1)$$

where C_P, H and M are the specific heat, heat flow with respect to the base line and mass respectively.Here the subscripts s and R refer to the sample and reference respectively. The run is carried out between 90K and 475K. Thus the specific heat of the sample at different temperatures in this range have been determined as described above. The specific heat of sapphire at different temperatures is known from published data [12]. The calculation is carried out using a program written in BASIC which can calculate the specific heat from the heat flow given as input. The measured variation of specific heat for YBZO in the temperature range 100-475K is shown in Fig.5.5.

Thermal conductivity measurement has been carried

out by combining the thermal diffusivity (α) data obtained from photoacoustic (PA) technique [13] and the specific heat values. The thermal diffusivity α is measured as a function of temperature using the PA technique. A PA spectrometer in which the cell has provisions to change the backing material of the sample and temperature is used for this. A powerful Xe lamp, a mechanical chopper and a lock-in amplifier are the other modules of the setup [14]. The sample for this measurement has been prepared by hand lapping and polishing the bulk material and is thinned down to approximately 80μm. The PA amplitude as well as the phase have been measured as a function of chopping frequency f. The thickness of the sample is so chosen that it is thermally thin for $f < f_c$, the characteristic frequency, and thermally thick for $f > f_c$. The log of PA amplitude is plotted against log of chopping frequency. The slope of this log-log plot changes sharply at f_c at which the sample undergoes a change from a thermally thin regime to a thermally thick regime and the thermal diffusivity α is determined by [13]

$$\alpha = f_c l^2 \qquad (2)$$

where l is the thickness of the sample. The measurements have been carried out at different fixed temperatures between 90 and 300K. Then the thermal conductivity is determined by combining the specific heat data discussed in the earlier part of this section and the thermal diffusivity data, making use of the relation

$$K = \alpha \rho C_p \qquad (3)$$

The variation of thermal conductivity as a function of temperature in the range 90-300K is shown in Fig.5.6.

5.6 Results and discussion

The X-ray studies given in Fig.5.2 shows that YBZO is nonreactive with YBCO, which makes it suitable for use as a substrate material for preparing 1-2-3 superconducting thin

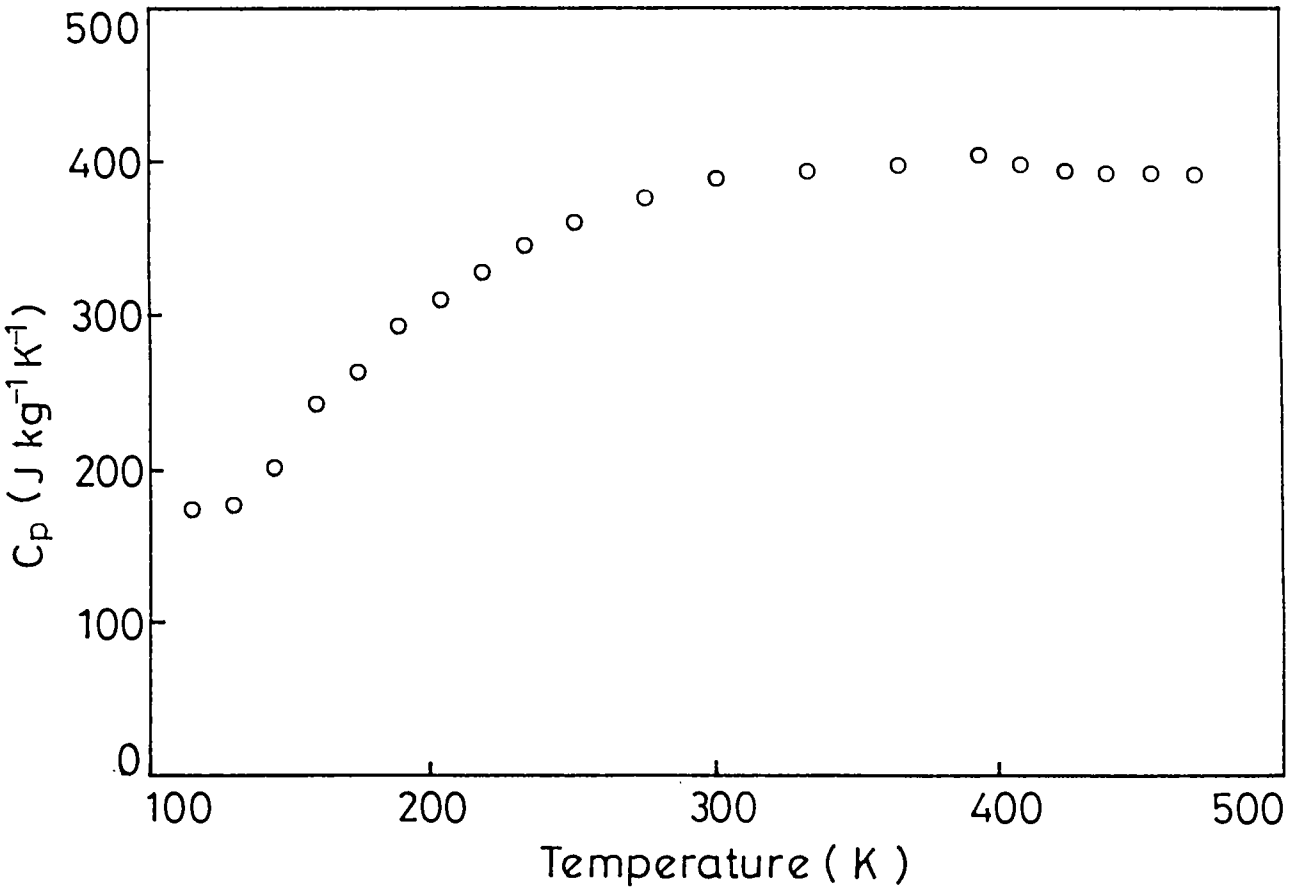

Fig.5.5 Variation of specific heat C_p with temperature of YBa_2ZrO_6 sample.

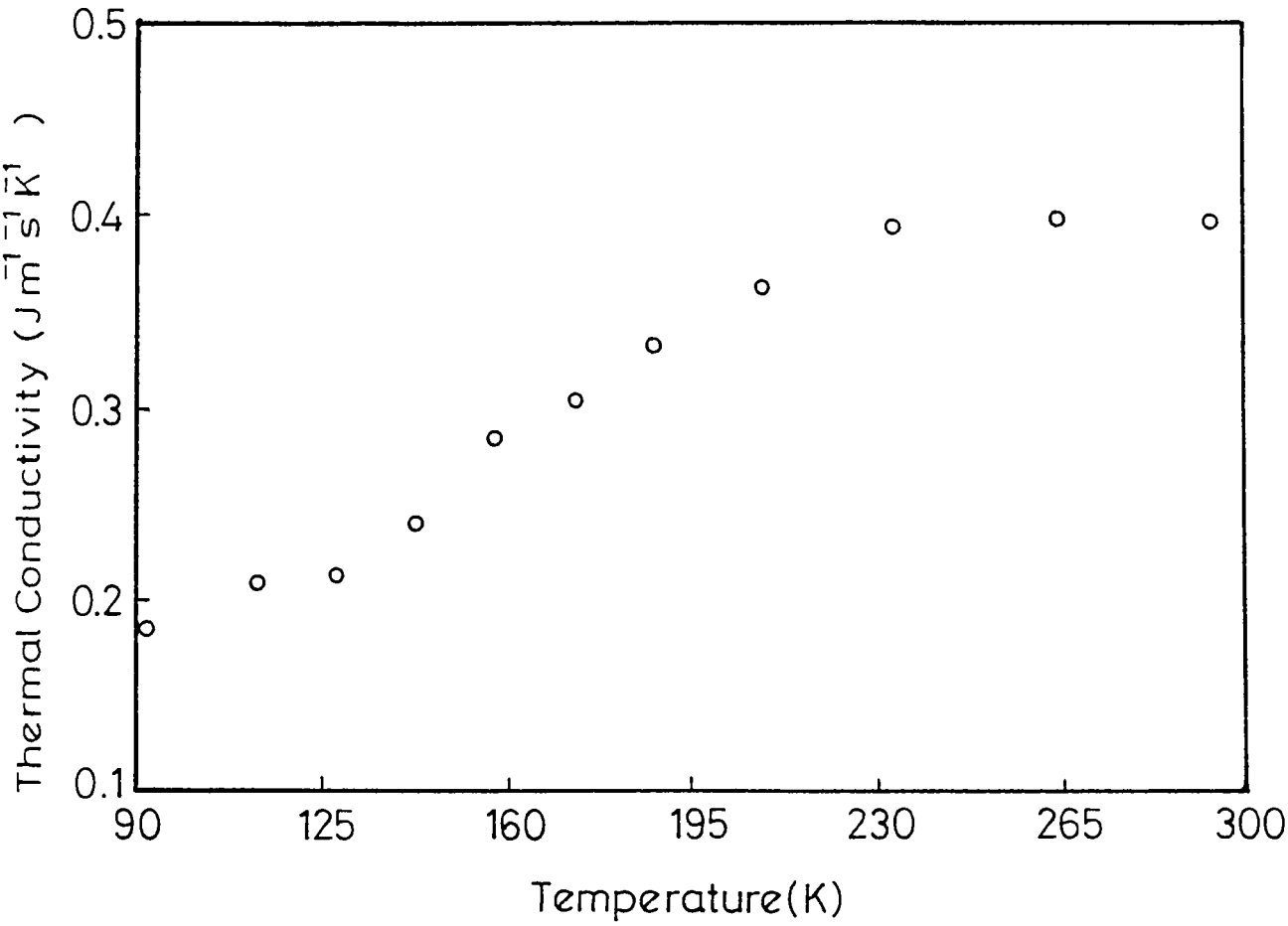

Fig.5.6 Variation of thermal conductivity K with temperature of YBa_2ZrO_6 sample.

films. The dielectric constant and the loss factor for YBZO as a function of frequency at room temperature are shown in Fig.5.3. The dielectric constant and loss factor are slightly higher than those of Al_2O_3 but much less than those of $SrTiO_3$, a commonly used substrate material for 1-2-3 thin films.

The temperature dependence of the longitudinal elastic modulus (C_{11}) is shown in Fig.5.4. There is a small slope change in the curve at ≈ 230K. Except this the variation is quite smooth as exhibited by a normal material. The specific heat curve shown in Fig.5.5 again shows a normal behavior in which the specific heat increases till ≈ 230K and then remains almost constant. The slope change in the elastic constant variation at around 230K may be correlated to this behaviour in specific heat variation. The thermal conductivity shown in Fig.5.6 shows an increase at low temperatures and attains a maximum value at around 230K. The thermal conductivity in this region is found to follow the corresponding specific heat variation.

The elastic constants of a solid are directly related to the forces between atoms and the structure energy. Satisfactory correlations between the lattice energy and elastic moduli have been proposed and work quite well for materials with the same structure and bond type. As the temperature is increased, thermal expansion increases the separation between atoms and slightly decreases the force necessary for further separation. Correspondingly there is a small decrease in the elastic moduli as the temperature is increased. This has been verified in almost all normal materials. The behaviour of YBZO is also a normal one (Fig.5.4).

The results of heat capacity measurements on ceramic materials is that heat capacity increases from a low value at low temperature to a nearly constant value at high temperatures. For YBZO it is clear from Fig.5.5 that the heat capacity increases from a low value at low temperatures to a

constant value at high temperatures. The constant value corresponds to the vibrational contribution to the heat capacity. The behaviour of YBZO in its heat capacity variation is quite similar to those exhibited by other ceramics. Abrupt changes in heat capacity takes place if the material undergoes any transformation. Since YBZO does not undergo any phase transition, there is no unusual variation in heat capacity.

The conduction of heat in dielectric solids is a result of phonon-phonon interactions. In a general form thermal conductivity can be represented by the relation

$$K = 1/3 \int C(\omega) v\, \ell(\omega)\, d\omega \qquad (4)$$

where $C(\omega)$ is the contribution to the specific heat per frequency interval for lattice waves of frequency ω and $\ell(\omega)$ is the attenuation length for lattice waves or phonon mean free path. In addition to the umklapp processes, various lattice imperfections give rise to anharmonicities and result in phonon scattering, which further decreases the mean free path and affects conductivity. At sufficiently high temperatures, the imperfection scattering is independent of temperature and vibrational frequency for all types of imperfection. At low temperatures the mean free path corresponding to phonon-phonon interactions become large, such that a variety of different scattering mechanisms resulting from lattice imperfections give rise to a number of specific results. If more than one process is operative, the effective value of $1/\ell$ is found by adding $1/\ell$ for each process which corresponds to adding the thermal resistances for each process. Experimental results are in general agreement with theoretical predictions. The mechanism and temperature dependence of thermal conductivity in dielectric solids are quite well understood.

For most of the ceramic materials, at temperatures near room temperature and above, phonon-phonon interaction and scattering resulting from lattice imperfections are the processes of major importance. In dielectric crystals as well

as in single-phase crystalline ceramics the following mechanism is responsible for the observed temperature variation of the thermal conductivity. At very low temperatures the phonon mean free path becomes of the same magnitude as the sample size, boundary effects dominate and conductivity decreases to zero at 0K. At some low temperature the thermal conductivity reaches a maximum, and phonon-phonon interactions lead to $K \approx \exp(-\theta/\alpha T)$ where θ is the Debye temperature. This exponential temperature dependence changes to $K \approx 1/T$ as the temperature is raised above the Debye temperature. If the temperature is raised to a sufficiently high level, the mean free path decreases to a value near the lattice spacing, and the conductivity is expected to be independent of temperature.

5.7 Conclusions

YBa_2ZrO_6 has been synthesised as a single phase material for the first time. Addition of a small amount of CuO is found to be necessary for obtaining single phase YBZO and to retain the mechanical properties. The YBZO does not react with YBCO up to 950°C. The variation of elastic constant, thermal conductivity and specific heat shows that it has stable thermal and elastic properties. Thus these results suggest that YBa_2ZrO_6 is a suitable material for the preparation of thin films of the high Tc superconductor YBCO.

References

1. J.P.Franck, J.Jung and M.A.K.Mohamed, *Phys. Rev.* **B36**, 2308 (1987).

2. S.W.Filipczuk, *Physica (Utrecht)* **C173**, 1 (1991).

3. H.Schmidt, K.Hradil, G.Gieres, W.Hosler and O.Eibles, *Physica (Utrecht)* **C180**, 34 (1991).

4. A.M.Campero, L.G.Turner and E.L.Hall, *Appl. Phys. Lett.* **52**, 2068 (1988).

5. W.M.Tierman, R.B.Hallock, J.C.W.Chien and B.M.Gong, *Phys. Rev.* **B44**, 4661 (1981).

6. K.Agatzuma, T.Ohara, H.Hateishi, K.Kaiho, K.Ohkubo and H.Karasawa, *Physica (Utrecht)* **C153/155**, 814 (1988).

7. K.V.Paulose, J.Koshy and A.D.Damodaran, *Solid State Commun.* (in press).

8. R.Brown in *Hand Book of Thin Film Technology* (Eds. L.I.Maisel and R.Glang) Mc.Graw Hill Publishing Company, NewYork (1983).

9. JCPDS File No. 24-1042, 23-839.

10. E.P.Papadakis *in Physical Acoustics* Vol XII (Eds. W.P.Mason and R.N.Thurston) Academic Press, Ney York (1976).

11. M.J.O'Neill, *J. Anal. Chem.* **38**, 1331 (1966).

12. G.T.Furukawa, T.B.Douglas, R.E.McCoskey and D.C.Ginnings, *J. Research of the National Bereau of Standards* **57**, 67 (1956).

13. P.Charpentier, F.Lepoutre and L.Bertrand, *J.Appl. Phys.* **53**, 608 (1982).

14. K.N.Madhusoodanan, J.Philip, G.Parthasarathy, S.Asokan and E.S.R.Gopal, *Phil. Mag.* **B58**, 123 (1988).

Chapter 6

ULTRASONIC STUDY OF PHASE TRANSITIONS IN PHOSPHATE DOPED TGS CRYSTALS

6.1 Introduction

Triglycine sulphate (TGS) is a very well known ferroelectric crystal which is very interesting from fundamental physics as well as technological points of view. The ferroelectric behaviour at room temperature in single crystals of TGS and isomorphous TGSe (Triglycine Selenate) had been discovered by Mathias *et al.* way back in 1956 [1]. TGS [$(NH_2CH_2COOH)_3H_2SO_4$] is a uniaxial ferroelectric crystal with Curie temperature about 322.6K. The crystal is monoclinic both above and below the transition temperature [2,3]. The transition is a second order order- disorder type one. Below Tc the space group of the crystal is $P2_1$ and above Tc it changes to $P2_1/m$ which is centrosymmetric and thus nonpiezoelectric. In the ferroelectric phase the spontaneous polarization is directed along the Y-axis. TGS is used as a model system for the study of second order phase transitions through the critical region. It is an extensively studied material. The technological importance of TGS is due to its pyroelectric properties. It is a widely used material in pyroelectric devices such as IR imaging sensors.

Due to the interest from both fundamental science and technological points of view, a lot of work have been done on the physical properties of this material. The piezoelectric, electrostrictive and low frequency elastic properties of TGS have been thoroughly investigated by Ikeda *et al.* [4]. The static ferroelectric properties near the phase transition temperature have been studied in detail by several workers [5,6]. Detailed theoretical studies on acoustic as well as specific heat data have been carried out by several workers in the transition region with a goal in mind of

verifying experimentally the logarithmic corrections in certain critical quantities as predicted by theory [7,8]. Near the transition, below Tc, the acoustic properties of TGS vary greatly because of the linear interaction between the deformation and the polarization of the ultrasonic wave. As far as $T \approx Tc - 0.01K$, these changes are in accordance with the Landau - Khalatnikov relaxation theory [9], which states that TGS crystals have at the phase transition point a discontinuous change in the velocity and maximum absorption of a longitudinal ultrasonic wave propagating at right angles to the Y-axis, which is the polar axis [8,10]. In the case of a unipolar crystal, the maximum anomaly in velocity as well as attenuation is obtained for a wave propagating through the medium with its propagation vector perpendicular to the polar axis. In this case the order parameter is the spontaneous polarization P_2 and the elastic coefficients affected by the transition are C_{33}, C_{11}, C_{22}, C_{12}, C_{13}, C_{23}, C_{55}, C_{15}, C_{25} and C_{35} [7].

Coming to the technological applications of TGS, it is a widely used material as pyroelectric detectors. It possesses very attractive pyroelectric properties and has the basic pyroelectric material figure of merit $P/K \approx 1.1 \times 10^{-5}$ C/m^2K where P is the pyroelectric coefficient and K is the dielectric constant of the crystal. A drawback of TGS crystal is its spontaneous depolarization with time. A suggestion to get over this problem has been to dope TGS with foreign ions. But inorganic ions, such as transition metal ions, cause a decrease in the pyroelectric coefficient P which considerably lowers the detection sensitivity of the crystal [11]. Molecules of organic compounds such as L-α alanine have a relatively large dipole moment and cause a rigidification of TGS structure [12]. The basic material figure of merit P/K is found to increase when TGS crystals are doped with either one of the two radical groups PO_4^{-3} or AsO_4^{-3} [13,14]. Several

dielectric and related studies have been done on TGS crystals doped with various dopants to understand the effect of doping on the properties of this material [13-17]. Due to the above reasons, since it is very interesting to know the effect of doping on the critical behaviour of this material, several ultrasonic studies have also been reported on TGS crystals with different dopants such as transition metal ions, nitroaniline etc. [18-24]. All of them have reported a broadening of the velocity curve at the transition point giving a deviation from the standard Landau-Khalatnikov behaviour. One argument for this is the increase of internal electric field in the crystal upon doping. It has been reported that the internal field in the case of pure TGS is about 0.05kV/cm and it can be increased to about 5kV/cm upon doping with Pd^{2+} ions, whereas doping with Fe^{3+} leads to deterioration of the internal field [21]. Strukov *et al.* [23] have put forward a theoretical treatment for the variation of velocity near the critical region on the application of an external field. They have explained the experimental observations phenomenologically with an effective electric bias applied in their formulation and shown that the sharp jump in velocity and specific heat near the phase transition is smoothened out and the curves become broader. Since the influence of the internal field can be considered as equivalent to an external electric field, the smoothening of ultrasonic velocity can occur due to this increased internal fields [21]. Several papers have appeared which discuss the influence of defects, external irradiation and impurities on the nature of critical anomalies of the thermodynamic parameters of ferroelectric crystals [25-27]. According to Levanyuk [25] the defects present in the crystal can be considered as something like frozen fluctuations of the order parameter and so the anomalies due to defects can be expected to be similar to known fluctuation anomalies. For pure matter the anomaly of sound absorption in the low temperature phase

is connected both to the relaxation of the order parameter and with its thermal fluctuations, while in the high temperature phase, is connected only with the thermal fluctuations of the order parameter. The presence of defects which can be regarded as nucleation centres of an assymetrical phase, gives rise to formation of regions of relaxation absorption at T > Tc and the size of this region increases as T → Tc. This leads to an additional absorption of sound. Studies on X-ray and γ-ray irradiated TGS [28] and effect of dislocations [29] also have been carried out by several workers from this point of view. The dielectric measurement results are found to support the theory of increased internal field due to doping [15-17]. In spite of all these efforts several questions still remain unanswered regarding the mechanism of the changes in the critical region in doped materials. Moreover, no systematic studies have been carried out on the acoustic anomalies in phosphate doped TGS crystals near the critical region.

We have carried out ultrasonic investigations on TGS with different levels of phosphate substitution in the site of sulphate groups (TGSP). The main advantage of phosphate doping is that for certain ranges of phosphate doping the pyroelectric coefficient can be made almost double that of pure TGS [13,14]. The ferroelectric and pyroelectric properties of these samples are discussed in detail by Fang *et al.* [13]. An increase in Tc from 49°C to 51°C has been reported by them.

6.2 Experimental

6.2.1 Sample preparation

Single crystals of pure and doped TGS for the present studies have been grown by the slow evaporation of the appropriate aqueous solution at constant temperature. All the crystals have been grown in the ferroelectric phase. Triglycine sulphate crystals are usually grown by the chemical reaction

$$3NH_2CH_2COOH + H_2SO_4 \longrightarrow (NH_2CH_2COOH)_3H_2SO_4$$

i.e., glycine and sulphuric acid mixed in the stoichiometric ratio react and yield triglycine sulphate.

In the case of phosphoric acid substitution the reaction is

$$3NH_2CH_2COOH + (1-x)H_2SO_4 + xH_3PO_4 \longrightarrow (NH_2CH_2COOH)_3(1-x)H_2SO_4xH_3PO_4$$

In the present investigations we have used samples with x = 0, 0.25 and 0.50. Thus the samples are designated as given in the following table (Table 6.1)

Table 6.1

x	H_3PO_4/H_2SO_4	Sample
0	0	TGS
0.25	1/3	TGS(0.75)P(0.25)
0.50	1	TGS(0.50)P(0.50)

The solution is kept in a constant temperature water bath which is kept constant at about 39^0C. The seed crystals are suspended in the solution and the solution is stirred continuously in alternate directions during growth to keep the concentration the same everywhere in the solution. The maximum value of x is limited to 0.50 because for higher values of x no single crystals are formed. Upto x = 0.50 good optical quality crystals can be obtained. It can be noticed that due to doping the [010] face is developed very well so that cutting normal to the ferroelectric axis can be accomplished very conveniently. Single crystals thus obtained are used for the present measurements.

The lattice parameters of TGS are as follows a = 9.15A°, b = 12.69A°, c = 5.73A° and β = 105° 40′ and the faces are identified from crystal morphology [2] by measuring the interfacial angles using a contact goniometer. Another axial system proposed by Hoshino *et al.* [3] are also widely used

which gives lattice parameters as a′ = 9.41A°, b′ = 12.64A°, c′ = 5.73A° and β = 110° 23′ which can be expressed as the transformation from the former as a′ = a + c, b′ = b, c′ = -c [3]. Throughout our measurements, we have followed the axial system proposed by Wood *et al.* [2]. The density of the samples are measured using Archimedes principle and found that the densities are 1.688 x 10^3 Kg/m^3, 1.684 x 10^3 Kg/m^3 and 1.679 x 10^3 Kg/m^3 respectively for TGS, TGS(0.75)P(0.25) and TGS(0.50)P(0.50).

6.2.2 Ultrasonic measurements - Velocity and attenuation

TGS is a monoclinic crystal and so there are 13 independent elastic coefficients as explained in chapter 1. In the matrix form it can be written as follows

$$\begin{bmatrix} C_{11} & C_{12} & C_{13} & - & C_{15} & - \\ C_{12} & C_{22} & C_{23} & - & C_{25} & - \\ C_{13} & C_{23} & C_{33} & - & C_{35} & - \\ - & - & - & C_{44} & - & C_{46} \\ C_{15} & C_{25} & C_{35} & - & C_{55} & - \\ - & - & - & C_{46} & - & C_{66} \end{bmatrix}$$

The whole elastic constants have been measured by several workers both in the ferroelectric [29-32] and paraelectric phases by Brillouin scattering as well as pulsed ultrasonics techniques. The extraction of these 13 elastic constants from the ultrasonic velocity data is rather complex. General methods using Christoffel's equations is explained in chapter 1. For monoclinic crystals, it has been worked out by several workers [32, 34-37]. In order to isolate all the 13 elastic constants, eighteen ultrasonic velocities in six equivalent directions are necessary. They are given in detail in Table 6.2. From this table it is clear that among the eighteen directions the pure modes are only three viz., V_2, V_5

Table 6.2

Ultrasonic velocity and elastic constants for monoclinic crystals

Velocity	Direction of propagation	Polarization	Relationship between Elastic constant (ρV_n^2) and Wave velocity (V_n)
V_1	[100]	[100]	$\frac{1}{2}\left\{C_{11}+C_{55}+\sqrt{(C_{11}-C_{55})^2+4C_{15}^2}\right\}$
V_2	[100]	[010]	C_{66}
V_3	[100]	[001]	$\frac{1}{2}\left\{C_{11}+C_{55}-\sqrt{(C_{11}-C_{55})^2+4C_{15}^2}\right\}$
V_4	[010]	[100]	$\frac{1}{2}\left\{C_{44}+C_{66}-\sqrt{(C_{44}-C_{66})^2+4C_{46}^2}\right\}$
V_5	[010]	[010]	C_{22}
V_6	[010]	[001]	$\frac{1}{2}\left\{C_{44}+C_{66}+\sqrt{(C_{44}-C_{66})^2+4C_{46}^2}\right\}$
V_7	[001]	[100]	$\frac{1}{2}\left\{C_{33}+C_{55}-\sqrt{(C_{33}-C_{55})^2+4C_{35}^2}\right\}$
V_8	[001]	[010]	C_{44}
V_9	[001]	[001]	$\frac{1}{2}\left\{C_{33}+C_{55}+\sqrt{(C_{33}-C_{55})^2+4C_{35}^2}\right\}$
V_{10}	[101]	$[\bar{1}01]$	$\frac{1}{4}\left\{C_{11}+C_{33}+2(C_{15}+C_{35}+C_{55}) - \left[4(2C_{35}+C_{33}-C_{11}-2C_{15})^2+(C_{15}+C_{35}+C_{13}+C_{55})^2\right]^{1/2}\right\}$

continued..

Velocity	Direction of propagation	Polarization	Relationship between Elastic constant (ρV_n^2) and Wave velocity (V_n)
V_{11}	[101]	[010]	$\frac{1}{2}(C_{66}+C_{44}+2C_{46})$
V_{12}	[101]	[101]	$\frac{1}{4}\left\{C_{11}+C_{33}+2(C_{15}+C_{35}+C_{55}) + \left[4(2C_{35}+C_{33}-C_{11}-2C_{15})^2 + (C_{15}+C_{35}+C_{13}+C_{55})^2\right]^{1/2}\right\}$
V_{13}	[110]	[110]	V_{13} to V_{18} obtained as a root of third order algebraic equations including known stiffness constants. The resulting equations are extensive.
V_{14}	[110]	[001]	
V_{15}	[110]	[$1\bar{1}0$]	
V_{16}	[011]	[011]	
V_{17}	[011]	[$0\bar{1}1$]	
V_{18}	[011]	[100]	

and V_8.

Measuring all these elastic constants is lengthy and time consuming and since our interest is in the study of the effect of doping on the phase transition we have selected two directions. One is along the polar axis b *i.e.*, [010] and another perpendicular to this *i.e.*, [001] since maximum anomaly in the case of TGS occur for the modes propagating perpendicular to the polar axis. In each direction we have measured one longitudinal and two transverse modes. Thus from Table 6.2 the measured velocities are V_4 - V_9 and for convenience we can name these velocities as V_{ba}, V_{bb}, V_{bc}, V_{ca}, V_{cb} and V_{cc} respectively. Crystals of thickness 7-10mm have been cut using a crystal cutter (South Bay Technology Model 650) employing a diamond wheel saw. The directions are determined from morphology by measuring the angle of the natural faces using a contact goniometer. The misorientations in these measurements are less than 20′ in each case. After cutting, the crystal faces are carefully polished using diamond paste so that they are plane and parallel to each other. X cut and Y cut quartz transducers of fundamental frequency 15MHz have been used in these experiments. The transducers are mounted on the sample using a suitable bonding material. For longitudinal waves paraffin oil or Motor oil SAE40 are found to be very good bonds. For transverse waves silicone grease serves as a good bond. Absolute velocities at room temperature (303K) have been measured for the selected directions and modes. The Mc Skimin Δt criterion is applied for measuring the velocities accurately as explained in chapter 2. Thus eighteen velocity measurements have been carried out and the combination elastic constants have been calculated on the three sets of samples.

The temperature dependent studies have been carried out by placing the sample inside the high temperature oven. A platinum resistance thermometer is placed in contact with the sample and the temperature is measured with a resolution of

0.01K. The sample temperature in each case has been controlled within ± 0.1K. All the samples for the measurements are preheated above Tc so as to release any strain inside the crystal developed during growth. The temperature of the sample is varied between 300K and 335K through the transition temperature, and velocity and attenuation are determined as a function of temperature. In this measurement a very low heating rate of 0.1K/min or less is used in order to avoid any thermal gradient in the sample volume. The measurements are carried out in the three samples and for six modes for each sample as mentioned above.

6.3 Results and discussions

The room temperature (303K) values of the velocity and the corresponding elastic constants ρV^2 are tabulated in Table 6.3. Fig.6.1 shows the variation of longitudinal velocity along the c-axis [001] *i.e.*, V_{cc} for the three samples. Fig. 6.2 shows the variation of transverse velocity along the c-axis with wave polarisation in the [100] direction. These are designated by V_{ca}. Fig.6.3 shows the variation of V_{cb}. Similarly Figs.6.4 - 6.6 shows the variation of longitudinal and transverse velocities along the [010] direction. Fig.6.7 gives the variation of ultrasonic attenuation for the longitudinal wave propagating along the c-axis.

Table 6.3 shows that there is no significant change in the absolute value of velocity and elastic constant for TGS upon doping. Atomic absorption analysis on these samples show that the H_3PO_4 getting incorporated into the crystal is much lower than the mole fraction in the solution [13]. This may be the reason for showing an insignificant change in the velocity of ultrasonic waves upon doping. This indicates that there is no significant change in the elastic constant values upon phosphate doping.

The temperature dependence of velocity shows a clear

Table 6.3

Ultrasonic velocities and elastic constants of TGS and TGSP at 303K. (Velocity in m/s and elastic constant in GPa)

Propagation direction	Polarization		TGS	TGS(.75)P(.25)	TGS(.5)P(.5)	
[010]	[010]	V_{bb}	4462	4459	4460	m/s
		ρV_{bb}^2	33.61	33.48	33.40	GPa
[010]	[100]	V_{ba}	1933	1911	1917	m/s
		ρV_{ba}^2	6.31	6.15	6.17	GPa
[010]	[001]	V_{bc}	2483	2474	2469	m/s
		ρV_{bc}^2	10.41	10.31	10.24	GPa
[001]	[001]	V_{cc}	4169	4153	4130	m/s
		ρV_{cc}^2	29.34	29.04	28.64	GPa
[001]	[100]	V_{ca}	2549	2537	2578	m/s
		ρV_{ca}^2	10.97	10.84	11.16	GPa
[001]	[010]	V_{cb}	2434	2425	2428	m/s
		ρV_{cb}^2	10.00	9.903	9.898	GPa

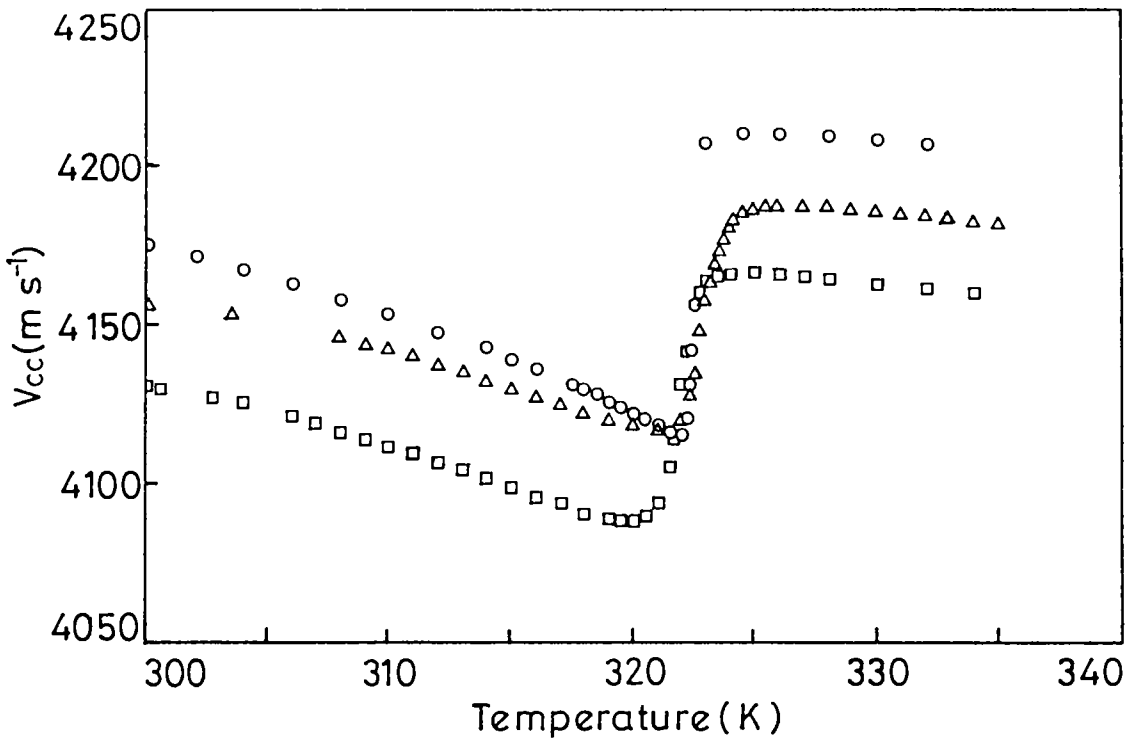

Fig.6.1 Variation of longitudinal velocity (V_{cc}) along the c-axis - [001] - with temperature.
(○) - pure TGS
(△) - TGS(0.75)P(0.25)
(□) - TGS(0.50)P(0.50)

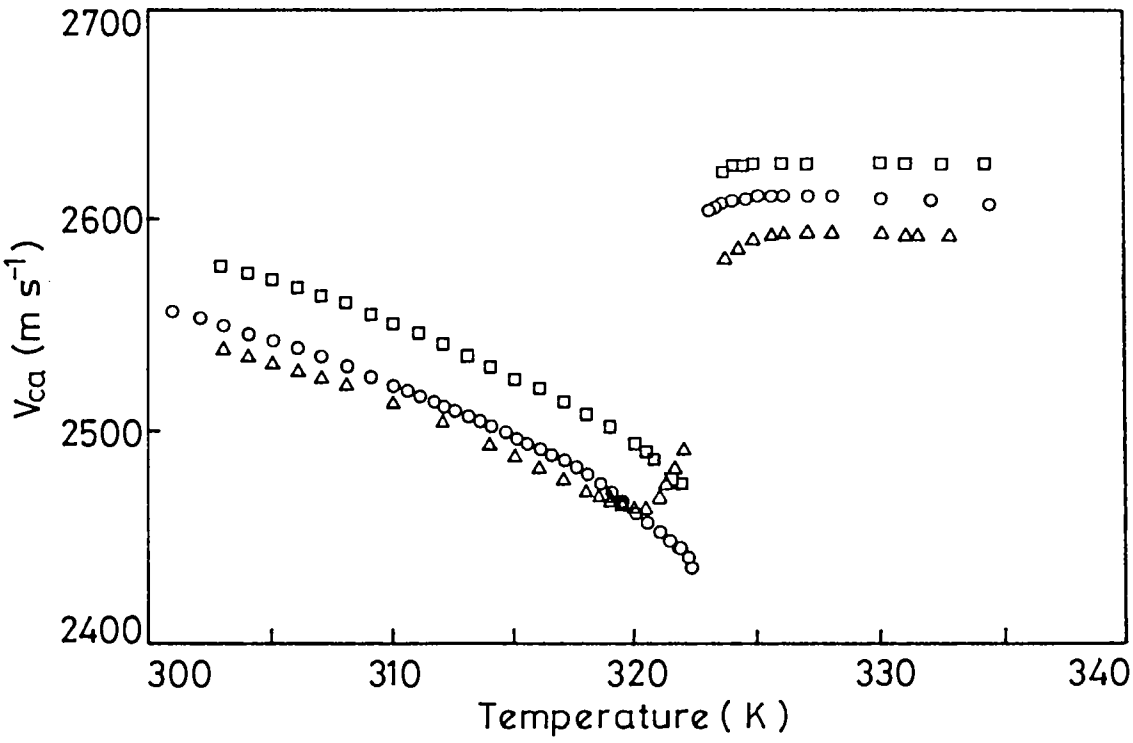

Fig.6.2 Variation of transverse velocity (Vca) along the c-axis with wave polarization in the [100] direction with temperature.

(O) - pure TGS
(△) - TGS(0.75)P(0.25)
(□) - TGS(0.50)P(0.50)

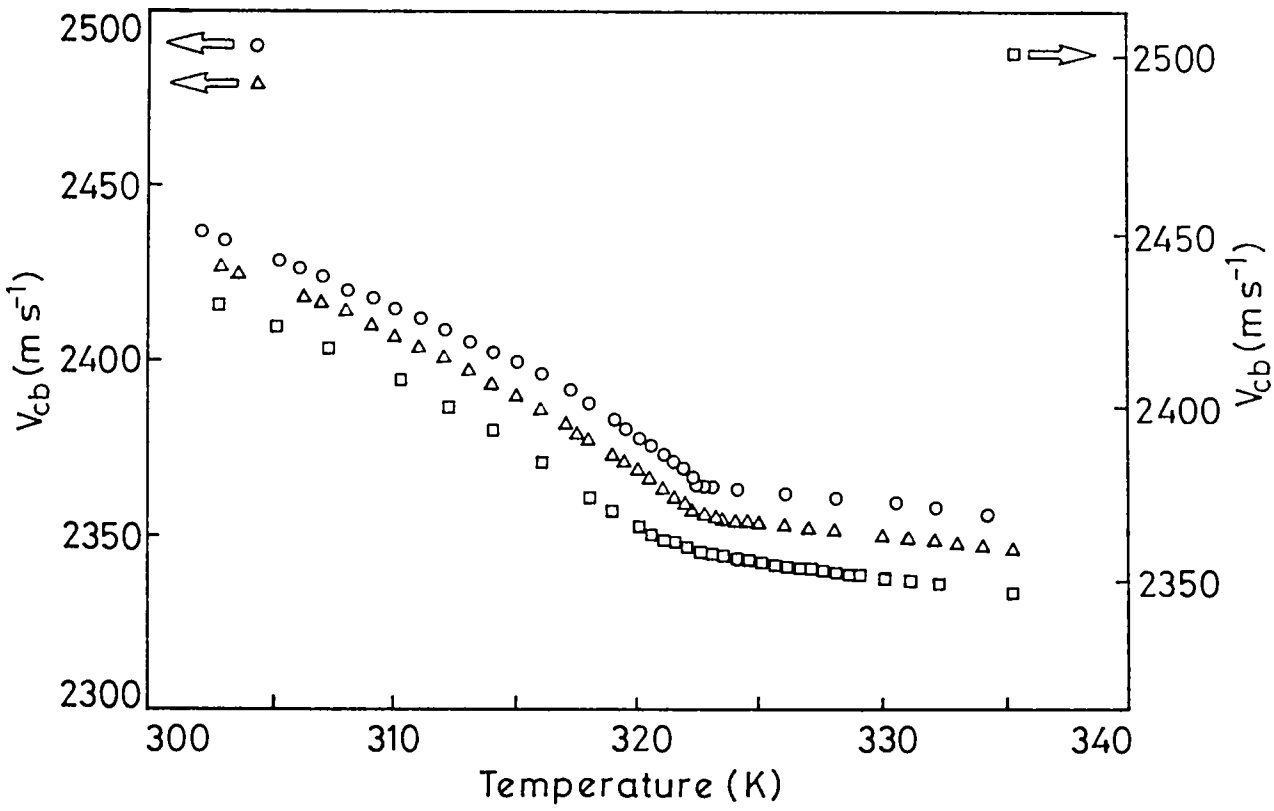

Fig.6.3 Variation of transverse velocity (V_{cb}) along the c-axis with wave polarisation in the [010] direction with temperature.

(O) - pure TGS

(Δ) - TGS(0.75)P(0.25)

(□) - TGS(0.50)P(0.50)

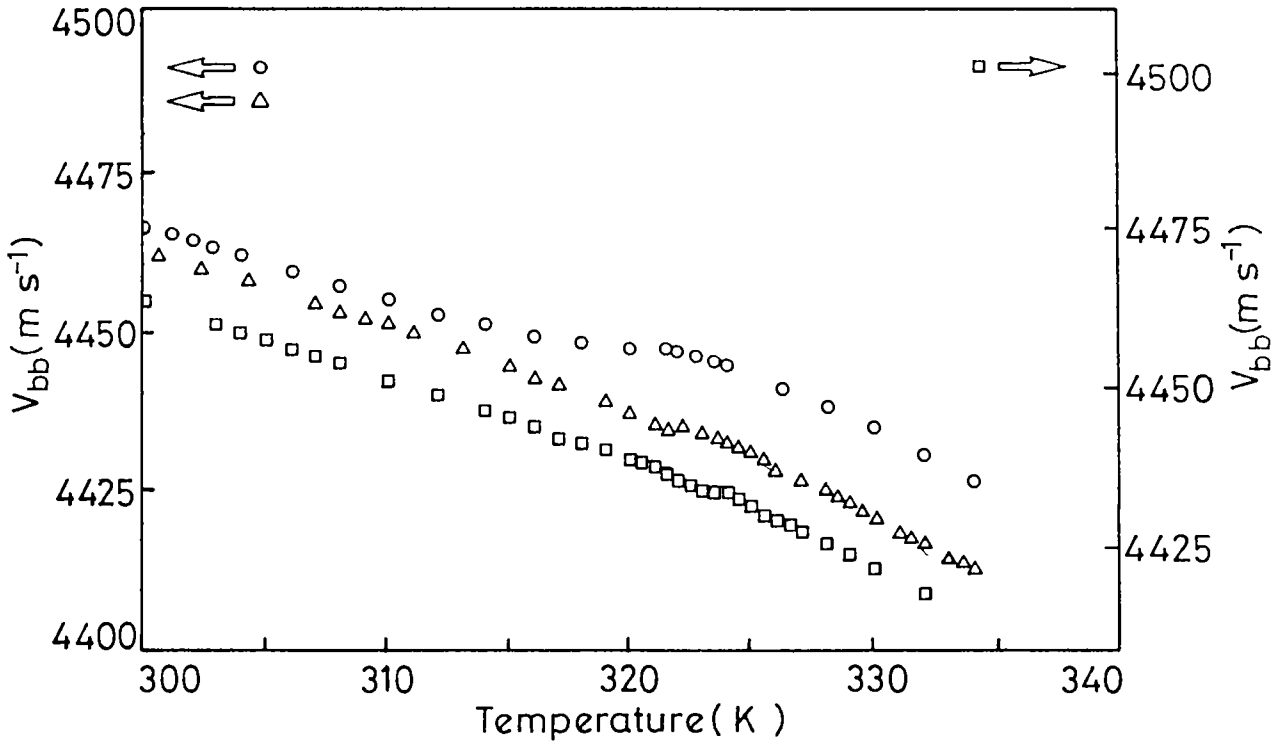

Fig.6.4 Variation of longitudinal velocity (V_{bb}) along the b-axis with temperature.

(O) - pure TGS

(△) - TGS(0.75)P(0.25)

(□) - TGS(0.50)P(0.50)

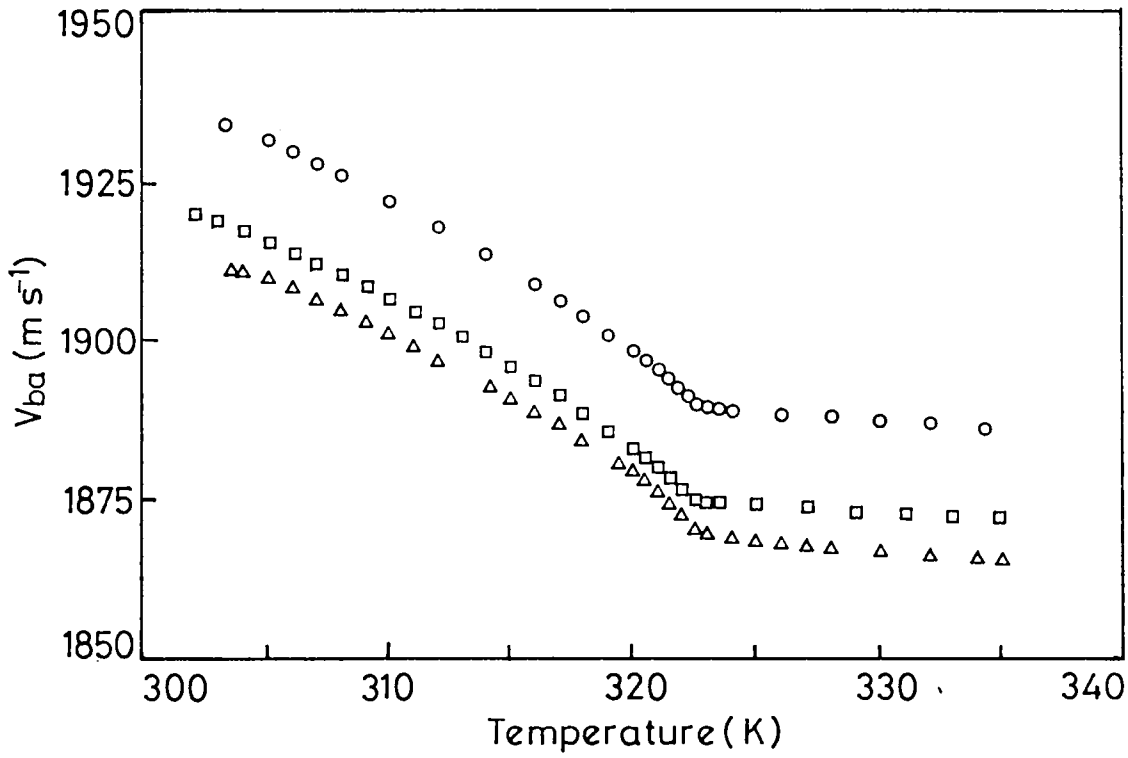

Fig.6.5 Variation of transverse velocity (V_{ba}) along the b-axis with wave polarisation in the [100] direction with temperature.

(O) - pure TGS

(Δ) - TGS(0.75)P(0.25)

(□) - TGS(0.50)P(0.50)

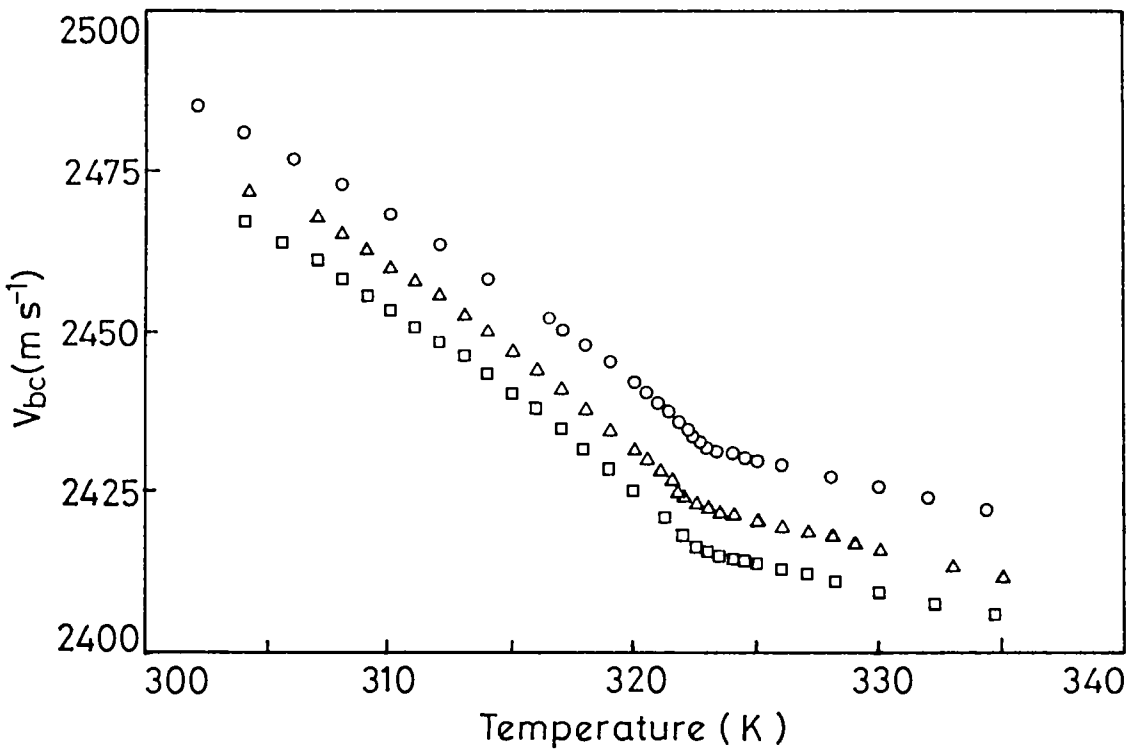

Fig.6.6 Variation of transverse velocity along the b-axis with wave polarisation in the [001] direction V_{bc} with temperature.

(O) - pure TGS

(△) - TGS(0.75)P(0.25)

(□) - TGS(0.50)P(0.50)

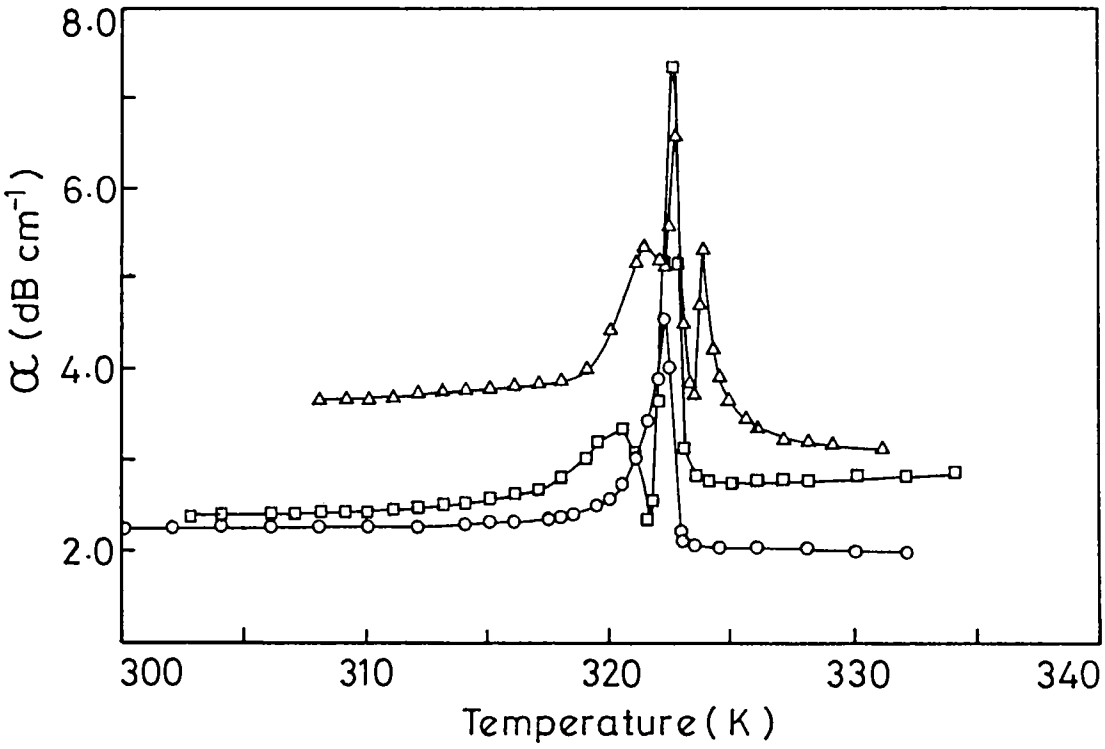

Fig.6.7 Variation of ultrasonic attenuation for the longitudinal wave propagating along the c-axis with temperature.

(o) - pure TGS

(Δ) - TGS(0.75)P(0.25)

(□) - TGS(0.50)P(0.50)

difference upon doping. From the figures it is evident that the largest anomaly in velocity is observed for wave propagating with its wave vector perpendicular to the polar axis *i.e.*, V_{cc} and V_{ca} (Figs.6.1 & 6.2). For pure TGS these figures show a decrease in velocity towards Tc and then a sharp jump to a higher value, which is in good agreement with the Landau - Khalatnikov theory. But for the doped samples the discontinuity in velocity is smoothened out. Eventhough the anomaly in V_{cb} is not much prominent, it also shows the same kind of smoothening effect at the transition point. But in the case of waves propagating along the b-axis, which is the polar axis, the temperature variation of velocities show only very weak anomaly at the transition point (Figs.6.4 - 6.6). Again in Figs.6.1 & 6.2 we can see that the smoothening is more for TGS(0.75)P(0.25) compared to TGS(0.50)P(0.50). A careful comparison of the curves shown in Figs.6.1 & 6.2 indicates that there is an optimum phosphate doping level at which the transition is broadest or the transition width is maximum. Our results show that this maximum is around 25% phosphate doping.

Based on the theories proposed by earlier workers in this field, we can attribute this smoothening to the presence of a strong internal electric field developed in the sample due to doping [21,23]. Our experimental data shown in Figs.6.1 to 6.3 show that the internal electric field is higher in TGS(0.75)P(0.25) than in TGS(0.50)P(0.50) and that at low and high doping levels the internal field is smaller and a maximum electric field is in the sample with an x value around 0.25. On the other hand if the defect centres discussed by Levanyuk *et al.* [25] is the main mechanism for the smoothening in the transition, the sample with higher concentration of phosphate must show more broadening than that having a lesser concentration. As has been observed in several samples by previous workers, defects do contribute to broadening of the transition. Our results on TGSP samples show that contribution from defects is not the prime reason for broadening because

the transition curve for TGS(0.75)P(0.25) is more broadened than that for TGS(0.50)P(0.50). We attribute the broadening to internal field created in the sample due to polarization effects. The generated internal field is higher for TGS(0.75)P(0.25) than for TGS(0.50)P(0.50) due to the critical number of phosphorous atoms replacing sulphur atoms. Consequently transition is broader for TGS(0.75)P(0.25) sample. Similar effects have been reported by Fang *et al.* [13] in their dielectric and pyroelectric coefficient measurements in phosphate doped TGS samples. They have measured the pyroelectric coefficient of samples with three levels of doping with the ratio H_3PO_4/H_2SO_4 = 1/5, 1/2 and 1 and they have reported that the dielectric and pyroelectric behaviour of TGSP with low phosphorous content *i.e.*, ratio 1/5 shows no significant improvement over pure TGS ; while the crystal with high phosphorous content (ratio 1) exhibits very low ferroelectricity; hence only a very low pyroelectric coefficient is achieved. Only crystals with an intermediate level of phosphate doping (H_3PO_4/H_2SO_4 = 1/2) exhibits excellent dielectric and pyroelectric properties. These crystals have a Curie point of 51°C and the pyroelectric coefficient at room temperature of about 6 - $7x10^{-4}$ C/Km^2 which is more than twice that of pure TGS (2 - $3.5x10^{-4}$ C/Km^2). These results are in good agreement with our results. Again from the fact that there is no variation for the curve for the waves travelling along the b-axis we can infer that this increased internal field is in the direction of the polar axis. The field must be along the polar axis for observing the anomaly as has been assumed by Strukov [23] in his theoretical treatment.

Coming to the temperature dependence of attenuation of longitudinal waves plotted in Fig.6.7, we can see similar effects. The attenuation increases sharply at Tc for all the three samples. But it is found that for doped samples multiple

peaks are obtained. Also in the case of pure TGS and TGS(0.75)P(0.25) the attenuation in the high temperature phase is lower than that in the low temperature phase. But in the case of TGS(0.50)P(0.50) the attenuation in the high temperature phase with respect to the low temperature phase is higher compared to the other two samples. Moreover, the peak height is also increased. This may be due to the fact that in the case of third sample there is a contribution from defects according to Levanyuk *et al.* [25] who predicted an increase in attenuation in the symmetric phase which increases towards Tc. The multiple peaks obtained in the doped samples at transition point may be due to the existence of two types of domains present in the sample as suggested by Chynoweth [38] who reported a double maximum in the pyroelectric coefficient caused by the existence of two types of domains in TGS crystals and that may get resolved as the phase transition is broadened. Another reason may be that it is due to the different types of domain structures localized on one impurity or other. No notable attenuation anomaly is observed for the wave propagating along the polar b-axis.

6.4 Conclusions

TGS crystals with different phosphate doping levels are grown and ultrasonic studies have been carried out on them. The advantage of phosphate doping is that for certain doping levels the pyroelectric properties are found to improve. The doping can enhance the [010] face which is very advantageous from a technological point of view.

There is no substantial variation in the absolute velocity values in TGS on phosphate doping due to the fact that the H_3PO_4 getting incorporated into the crystal is much lower than the mole fraction in the solution. But in the critical region it shows marked differences. The sharp increase in velocity obtained at Tc for pure TGS is broadened in doped samples and this broadening is large for the sample

with lower doping level. This may be due to the fact that at low doping levels (for TGS(0.75)P(0.25)) there are effects due to the internal field as well as the defect centres produced upon doping, or the effect of internal field alone. For higher doping level (for TGS(0.50)P(0.50)) the internal field may be reduced and there the dominant effect may be the one due to defect centres alone. The reported dielectric and pyroelectric measurements are in close agreement with this. The attenuation curve also is in agreement with this in which the peak height as well as attenuation in symmetric phase are found to increase in the sample with x = 0.50.

References

1. B.T.Matthias, C.E.Miller and J.P.Remeika, *Phys. Rev.* **104**, 646 (1954).

2. E.A.Wood and A.N.Holden, *Acta Cryst.* **10,** 145 (1957).

3. S.Hoshino, Y. Okaya and R.Pepinsky, *Phys. Rev.* **115**, 323 (1959).

4. T.Ikeda, Y.Tanaka and H.Toyodo, *Jpn. J. Appl. Phys.* **1**, 13 (1962).

5. J.A.Gonzalo, *Phys. Rev.***B1**, 3125 (1970).

6. K.Deguchi and E.Nakamura, *Phys. Rev.* **B5**, 1072 (1972).

7. B.A.Strukov, K.A.Minaeva, N.M.Shirina, V.I.Telesheviskii and S.K.Khanna, *Izv. Akad. Nauk. SSSR, Ser.Fiz.* **39**, 180 (1975).

8. B.A.Strukov, *Ferroelectrics* **12,** 97 (1976).

9. L.D.Landau and I.M.Khalatnikov, *Dokl. Akad. Nauk. SSSR,* **96,** 469 (1954).

10. C.W. Garland in *Physical Acoustics,* Vol.**VII** , 52 (Eds. W.P.Mason and R.N.Thurston) Academic Press, New York (1970).

11. T.Krajewski and T.Breczewski, *Ferroelectrics* **25**, 547 (1980).

12. P.J.Lock, *Appl. Phys. Lett.* **19**, 390 (1971).

13. C.S.Fang, Yao Xi, A.S.Bhalla and L.E.Cross, *Ferroelectrics* **51**, 9 (1983).

14. A.S.Bhalla, C.S.Fang, L.E.Cross and Yao Xi, *Ferroelectrics* **54**, 151 (1984).

15. M.A.Gaffar, A.Abu El-Fadl and S.A.Mansour, *Ind. J. Phys.* **62A**, 479 (1988).

16. M.A.Gaffar and A.Abu El-Fadl, *Ind. J. Pure and Appl. Phys.* **26**, 28 (1988).

17. M.A.Gaffar, A.Abu El-Fadl and S.A.Mansour, *J. Phys. D: Appl. Phys.* **22**, 327 (1989).

18. H.Wolniewicz, *Mat. Sci.* **XI**, 27 (1985).

19. H.Wolniewicz, *Mat. Sci.* **XI**, 77 (1985).

20. H.Wolniewicz, *Mat. Sci.* **XI**, 35 (1985).

21. Kh.M.Mirzoakhmedov, N.N.Khromova, V.A.Shutilov, Z.Vartevig and V.Vindsh, *Sov. Phys. Solid State* **23,** 389 (1981).

22. V.Vindsh, I.Rakhimov, V.M.Sarnatskil, E.V.Charnaya and V.A.Schutilov, *Sov. Phys. Solid State* **27**, 1005 (1985).

23. B.A.Strukov, T.P.Spiridonov, K.A.Minaeva, V.A.Fedorikhin and A.V.Davtyan, *Sov. Phys. Cryst.* **27,** 190 (1982).

24. E.V.Charnaya and I.Rakhimov, *Ferroelectrics* **112**, 45 (1990).

25. A.P.Levanyuk, A.V.Osipov, A.S.Sigov and A.A.Sobyanin, *Sov. Phys. JETP*, **49**, 176 (1979).

26. B.A.Strukov, K.A.Minaevasa, S.A.Taraskin and V.A.Fedorikhin, *Ferroelectrics* **24**, 309 (1980).

27. B.A.Strukov, A.S. Sigov, V.A.Fedorikhin and S.A.Taraskin, *JETP Lett.* **31**, 169 (1980).

28. T.R.Volk, I.Rakhimov, V.M.Sarnatskil, E.V.Charnaya, L.A.Shuvalov and V.A.Shutilov, *Sov. Phys. Solid State* **27**, 2176 (1986).

29. V.P.Konstantinova, I.M.Silverstrova and K.S.Aleksandrov, *Sov. Phys. Cryst.* **4**, 63 (1960).

30. Y.Luspin and G.Hauret, *Ferroelectrics* **15**, 43 (1977).

31. Z.Tylczynski, *Physica* **111B**, 267 (1981).

32. A.Dunk and G.A.Saunders, *J. Mater. Sci.* **19**, 125 (1984).

33. S.Haussuhl and L.Albers, *Ferroelectrics* **15**, 73 (1977).

34. K.S.Aleksandrov, *Sov. Phys. Cryst.* **3**, 630 (1958).

35. H.B.Huntington, S.G.Grangoli and J.L.Mills, *J. Chem. Phys.* **50**, 3844 (1969).

36. K.Hiroshi, Y.Ishabaghi and Y.Takgi, *J. Phy. Soc. Jpn.* **35**, 1450 (1973).

37. K.A.Minaeva, E.V.Baryshnikova, B.A.Strukov and V.M.Varikash, *Sov. Phys. Cryst.* **23**, 361 (1978).

38. A.G.Chynoweth, *Phys. Rev.* **117**, 1235 (1960).

Chapter 7
SUMMARY AND CONCLUSIONS

The present thesis is a result of our attempts to probe the elastic properties of selected solid materials by measuring ultrsonic velocity and attenuation in them. Temperature dependence of velocity and attenuation have been measured in all the samples investigated. The materials investigated are the high Tc superconductors Bi-Sr-Ca-Cu-O and Ag-doped Gd-Ba-Cu-O, Y-Ba-Zr-O which is a substrate material for coating 1-2-3 superconductor thin films and the ferroelectric crystal TGS with different levels of phosphate doping. Considerable amount of effort has been put into setup the instrumentation required to undertake these studies. Ultrasonics is an excellent tool to study elastic properties and it is the most effective technique to investigate phase transitions in solids. The results presented in this thesis reconfirm this.

Ultrasonic studies have been carried out in the high temperature superconductors Bi-Sr-Ca-Cu-O and Ag-doped Gd-Ba-Cu-O. In the case of the former a Pb doped sample has been used since addition of Pb stabilizes the Bi2223 phase. Temperature variation of longitudinal velocity of 10MHz wave has been determined. It shows a phase transition like anomaly in the vicinity of Tc which can be attributed to a structural change occuring in the sample prior to the superconductive phase transition. Small velocity maxima are observed in the region above Tc which can be attributed to a second order phase transition occuring in the sample. Ultrasonic velocity and attenuation studies have also been carried out in the superconductor $GdBa_2(Cu_{1-x}Ag_x)_3O_{7-\delta}$ with x = 0, 0.01, 0.02, 0.03 and 0.05. The temperature dependent velocity curve in the pure sample shows a broad peak at 207K and a sharp slop change at Tc. The peak at 207K in the case of the pure sample gets

shifted to high temperature side with Ag doping. This can be correlated to the oxygen ordering occuring in the one-dimensional Cu-O chain due to the metastability of the 1-2-3 system. Room temperature resistivity and Tc measurements are found to agree with this result. Ultrasonic attenuation curves also show a similar type of behaviour.

Details of the study of ultrasonic as well as thermal properties of a new substrate material YBa_2ZrO_6 (YBZO) for the preparation of 1-2-3 superconducting thin films and the results obtained form a part of the thesis. From a technological point of view, high Tc superconducting materials prepared in the thin film form are very important and it is necessary to have a suitable material as the substrate to prepare thin films. Since YBCO reacts with almost all materials, conventional substrates are unsuitable for preparing thin films. Moreover, it should have stable elastic and thermal properties while the temperature is varied. The results of the measurement of the temperature dependence of the elastic constants of YBZO is discussed. In addition to the elastic properties, the thermal properties like specific heat and thermal conductivity of this material have also been measured. The specific heat measurements have been carried out by ratio method with a DSC. The thermal conductivity data have been obtained by combining thermal diffusivity data obtained from photoacoustic measurements with the specific heat data. The nonreactivity of the material has been checked by X-ray analysis.

Ultrasonic studies have been carried out on Triglycine Sulphate (TGS) single crystals which is an important ferroelectric material. It is also important from application point of view due to its pyroelectric nature which enables it to be used as IR detectors. Replacement of the sulphate groups in TGS by phosphate groups is very advantageous both from crystallographic and technological points of view. Ultrasonic studies have been carried out in

three samples with different phosphate doping levels. The samples are TGS, TGS(0.75)P(0.25) and TGS(0.50)P(0.50). The samples are prepared by solution growth technique. Results of ultrasonic velocity and attenuation as a function of temperature around the ferroelectric-paraelectric transition point as well as doping levels are discussed in detail.

The overall goal of this thesis work has been to study the elastic properties and phase transitions in selected solids using ultrasonic technique as has been mentioned already. Our studies show that ultrasonics is a sensitive probe to bring out minute variations in the elastic properties of complex systems such as high Tc ceramic superconductors. The effect of doping on oxygen ordering in high Tc superconductors, which is difficult to study using other techniques, clearly show up in the acoustic response of the material. The only thing is that ultrasonic investigations are not so easy to carry out and the experiments are time consuming. The effect of phosphate doping on the phase transition width in TGS is rather small but it clearly shows up in our measurements. One has to undertake very systematic and comprehensive experiments to bring out such minute effects and features. Providing the correct interpretation to the experimental results is another difficult task. Comparison with other experimental results often become necessary to give the correct interpretation to ultrasound results.

There is lot of scope for carrying out further investigations of the above type. It would be very interesting to measure the individual elastic constants of single crystals of high Tc superconductors and their variations through the transition point. Lack of good quality, large size single crystals of these materials has prevented us from doing this. There are a very large number of complex materials whose individual elastic constants are still unknown and ultrasonics can be used to measure them when sample preparation techniques improve to provide good quality, large size single crystals.

Many of these, like high Tc superconductors, have very interesting phase transitions as the temperature is varied and ultrasonics is the ideal tool to bring out changes in elastic properties taking place with changes in temperature.

Eventhough ultrasonics has been a widely used technique to study features of phase transitions near critical points, there is lot of scope for doing a great deal of further work in this direction. Ultrasonics is the most powerful technique to investigate phase transitions in which the order parameter is coupled to the internal strain. Using Landau theory it can be shown that in the case of bilinear coupling between strain and the order parameter there is an elastic instability and the corresponding phonon modes become soft. It gets reflected in ultrasonic measurements with the appropriate elastic constants $C_{ij} \rightarrow 0$ at Tc and attenuation tending to infinity. If strain is not directly coupled to the order parameter the anomaly around Tc may not be so prominent but it will be reflected in the measurements. There are a number of solids which undergo phase transitions but have not been explored with ultrasonics.

Only very few systems which undergo incommensurate phase transitions have been studied using ultrasonics. In such modulated or lock-in transitions, the system is characterised by amplitudon and phason modes and ultrasonics is a very powerful technique to investigate the features of such transitions. Due to the difficulties involved in growing large size samples for ultrasonics work, only limited studies have been reported. There is ample scope for doing frontline physics in this area.

Another interesting study one can take up in this line is the measurement of the variations in ultrasonic velocities with external pressure in different samples. Such measurements done for different modes will lead to the determination of higher order elastic constants. So far only third order elastic constants have been measured, that too

only in a few systems belonging to cubic symmetry. Measurement of third order elastic constants is essential to describe nonlinear elastic properties of solids. The variation of third order elastic constants near phase transitions is still unknown in literature. There remain a large number of very interesting problems to be solved in this area. It would be very interesting to persue work in this direction.